SO-199 CHRISP

Christmas Island Seamount Province and the Investigator Ridge: Age and Causes of Intraplate Volcanism and Geodynamic Evolution of the South-Eastern Indian Ocean

Abschlussbericht

- 03G0199A -

Berichtszeitraum: 01. Mai 2008 bis 30. Juni 2010

K. Hoernle und F. Hauff (IFM-GEOMAR)

unter Mitarbeit von

R. Werner, A. Kipf (IFM-GEOMAR), C. Lüter, B. Neuhaus (Museum für Naturkunde Berlin) und U. Barckhausen (BGR)

I.1. Aufgabenstellung

Mit SO199-CHRISP sollten vulkanische Strukturen, magmatische Gesteine, Störungssysteme, magnetische Anomalien und marine Organismen im Whartonbecken und im nordwestlichen Argobecken (südöstlicher indischer Ozean) untersucht werden. Wichtigste Arbeitsgebiete waren die Christmas Island Seamount Provinz, eine großen Intraplatten-Vulkanprovinz (ca. 10° - 15°S und 95° - 114°E), und der Investigatorrücken, eine bei ca. 98° – 99°E in N-S-Richtung verlaufende, 1.700 km lange fossile Störungszone. Die wichtigsten, ineinander greifenden Zielsetzungen und Arbeitsansätze waren:

(1) Durch morphologische, vulkanologische, petrologische, geochemische, geochronologische und strukturgeologische Untersuchungen sollten der Ursprung sowie die zeitlich-räumliche und magmatische Entwicklung der bisher weitgehend unerforschten Christmas Island Seamount Provinz rekonstruiert werden, die nicht allein mit den herkömmlichen Modellen zu den Ursachen von Intraplattenvulkanismus erklärt werden kann. Damit sollte auch ein Beitrag zur „Great Plume Debate“ geleistet werden.

(2) Anhand einer systematischen Beprobung des quer durch die Christmas Island Seamount Provinz verlaufenden Investigatorrückens sollte die zeitliche und geochemische Entwicklung der Ozeankruste und des oberen Mantels in diesem Bereich des Indik von ca. 50 bis 130 Ma charakterisiert werden und so u.a. neue Erkenntnisse über die Entwicklung der „Indian Mantle Domain“ gewonnen werden.

(3) Anhand von Fächerecholotkartierungen und Parasoundprofilen sollen ältere und rezente Deformationsstrukturen im Whartonbecken charakterisiert und damit neue Informationen über die interne Deformation von ozeanischen Platten gewonnen werden.

(4) Mit magnetischen Messungen sollte über die Identifizierung von Ozeanbodenspreizungs-Anomalien das Alter der ozeanischen Kruste im östlichen Whartonbecken und im nördlichen Argobecken bestimmt werden. Mit der Vervollständigung und/oder Revision der Bestimmung der Krustenalter in dieser Region sollten im Verbund mit den oben genannten Untersuchungen neue plattentektonische Modelle für die Evolution des östlichen Indischen Ozeans überprüft werden.

(5) Durch biologische Beprobungen sollte die Biodiversität tiefseebewohnender, bodenlebender Organismen des Investigatorrückens und Whartonbeckens erfasst und mit den Ergebnissen der früheren Ausfahrten z.B. zum Hikurangiplateau (SO168) und zum Manihikiplateau (SO193) verglichen werden, um die biogeographische Einbindung des Tiefseebenthos des ostindischen Ozeans in den Komplex der Faunenprovinzen Indik/Indo-Westpazifik/Pazifik besser zu verstehen.

I.2. Voraussetzungen

Vor SO199-CHRISP existierten nur sehr wenige Basementproben von den submarinen Strukturen der Christmas Island Seamount Province, die ausschließlich aus dem Bereich westlich und südwestlich der Weihnachtsinsel stammten. Die Gebiete westlich von 102°E und östlich von 106°E (und damit der größte Teil der Seamountprovinz) waren gänzlich unbeprobt. Abgesehen von einigen wenigen Schiffstracks lagen auch keine hochauflösenden bathymetrischen Daten aus diesem Bereich vor. Gleiches gilt für den Investigatorrücken, der vor SO199 nur an einer Lokalität nahe seines südlichen Endes beprobt worden war. Mit den wenigen vorhandenen Daten und Basementproben war es nicht möglich, Ursprung, Entwicklung und Bedeutung dieser Strukturen zu rekonstruieren. Auch hatte es im östlichen Whartonbecken und im nördlichen Argobecken vor SO199 bisher nur wenige gezielte Magnetik-Surveys gegeben, die überwiegend schon sehr alt waren. Ferner lag bisher kaum Probenmaterial vom Tiefseebenthos aus diesen Gebieten vor. Das wenige vorhandene Proben- und Datenmaterial aus den Arbeitsgebieten wurde im Antrag zu dem Forschungsvorhaben SO199-CHRISP ausführlich beschrieben. Soweit zugänglich wurde uns dieses Material von unseren Kooperationspartnern zur Verfügung gestellt und in das Forschungsvorhaben mit einbezogen. Die überaus meisten für das Vorhaben notwendigen Daten und Proben wurden auf der Ausfahrt SO199 mit dem F.S. “Sonne” gewonnen. Der sehr erfolgreiche Verlauf von SO199, die Expertise und die apparative Ausstattung aller beteiligten Institutionen und Arbeitsgruppen sowie die finanzielle Unterstützung durch das

BMBF bildeten die Voraussetzungen für den erfolgreichen Abschluss des Forschungsprojektes SO199-CHRISP.

I.3. Planung und Ablauf des Vorhabens

Der Ablauf des Vorhabens entsprach im wesentlichen der von uns im Antrag vorgeschlagenen Arbeits- und Zeitplanung.
Die Vermessungs- und Beprobungsarbeiten auf der Ausfahrt SO199 (02.08.2008 – 22.09.2008) verliefen ausserordentlich erfolgreich. Insgesamt wurden neben 5.694 nm Profilfahrten (SIMRAD EM120/Parasound), davon 2.787 nm zusätzlich mit Magnetometersensoren, 70 Dredgezüge, 13 TV-Greifereinsätze, und 9 Multicorereinsätze in einer durchschnittlichen Wassertiefe von 3.901 m durchgeführt. Dreiundsechzig dieser Geräteeinsätze erbrachten magmatische Gesteine (Laven und Intrusiva), 41 Vulkaniklastika, 27 sedimentäre Gesteine und 13 Mn-Fe-Oxide. Für die Biologie erbrachten 50 Geräteeinsätze Makrofauna und 75 unverfestigte Sedimente. Damit gelang während SO199 u.a. die erste umfassende Beprobung der Christmas Island Seamount Provinz und des Investigatorrückens. Die Ergebnisse der Schiffsexpedition sind im Fahrtbericht (Werner, Hauff & Hoernle 2009, http://www.ifm-geomar.de/index.php?id=publikationen) detailliert dargestellt.
Die Präparation und petrographische und geochemische Analytik der Gesteinproben wurde zwischen Herbst 2008 und Spätsommer 2010 am IFM-GEOMAR und in Laboren unserer Kooperationspartner durchgeführt (s.a. Abschnitt I.5.). Die analytischen Arbeiten sollten nach der im Antrag vorgeschlagenen Arbeits- und Zeitplanung bereits Ende 2009 abgeschlossen werden und erstreckten sich somit über einen etwas längeren Zeitraum als ursprünglich geplant. Grund hierfür waren die unerwartet große Menge an Gesteinsproben, die auf der Ausfahrt gewonnen und im Labor bearbeitet wurden (so wurden z.B. statt der ursprünglich geplanten 180 insgesamt 455 Dünnschliffe angefertigt und ausgewertet), und die mit der Abschaffung des IFM-GEOMAR-eigenen RFA-Labors verbundenen Umstellung auf externe Hauptelementanalytik. Alle Magnetikprofile von SO199 wurden an der Bundesanstalt für Geowissenschaften und Rohstoffe (BGR) 2009 einem vollständigen Gradiometerprozessing unterzogen und die Magnetikkartierung SO199 wurde mit geeigneten Fremdprofilen ergänzt, die ebenfalls vollständig neu prozessiert und gefiltert wurden. Weiterhin wurde die Interpretation des Krustenalters aus Seafloor-Spreading-Anomalien überarbeitet und in die Altersdaten aus Ar/Ar-Datierungen von Gesteinsproben eingehängt. Das auf den Ausfahrten gewonnene biologische Material wurde unter Federführung des Leibniz-Instituts für Evolutions- und Biodiversitätsforschung Berlin untersucht, ein Teil dieses Probenmaterials wurde Spezialisten an anderen Instituten zur Auswertung übergeben (s.a. Abschnitt I.5.). Ferner wurden 16 Gesteinsproben von der Weihnachtsinsel in das Projekt mit einbezogen, die im Rahmen einer inzwischen vor dem Abschluss stehenden Diplomarbeit von Frau Sarah Conrad (Christian-Albrechts-Universität Kiel) bearbeitet wurden. Ein Teil der bathymetrischen und der Parasounddaten wurde von Frau Carolin Bartsch und Frau Elisabeth Seidel (Ernst Moritz Arndt Universität Greifswald, EMAU) im Rahmen einer Bachelorarbeit ausgewertet.
Insgesamt bildete das auf der Expedition gewonnene Daten- und Probenmaterial eine hervorragende Grundlage für die verschiedenen weiterführenden, im Projektantrag umfassend dargestellten Laborarbeiten und Analysemethoden, aus denen die in Abschnitt II.1. vorgestellten Ergebnisse resultierten.

I.4. Wissenschaftlich-technischer Stand (an den angeknüpft wurde)

Der wissenschaftlich-technische Stand wurde im Antrag zu dem Forschungsvorhaben SO199-CHRISP ausführlich beschrieben.

I.5. Zusammenarbeit mit anderen Stellen

Während der Laufzeit des Vorhabens wurde mit verschiedenen Stellen im In- und Ausland intensiv und erfolgreich zusammengearbeitet. Diese Kooperationen, die zukünftig im Rahmen anderer Projekte fortgeführt werden sollen, erbrachten zahlreiche Ergebnisse, die in Abschnitt II.1. dargestellt sind und die teilweise bereits in Manuskripte eingeflossen sind. Unsere wichtigsten Kooperationspartner sind (in alphabetischer Reihenfolge der Institute):

Bundesanstalt für Geowissenschaften und Rohstoffe (Hannover)
Dr. U. Barckhausen (Magnetik)

Christian-Albrechts-Universität (Kiel)
Dr. D. Garbe-Schönberg (ICP-MS-Analytik)

Cornell University (U.S.A)
Prof. Dr. J. Phipps Morgan (Tektonik)

Ernst Moritz Arndt Universität (Greifswald)
Prof. Dr. M. Meschede, C. Bartsch, E. Seidel (Strukturgeologie und Neotektonik des Investigatorrückens)

Geoscience Australia
Dr. Andrew Heap, Dr. R. Mleczko (Bathymetrie, Sedimente)

Institut de Physique du Globe de Paris (Frankreich)
Dr. J. Dyment (Kretazische magnetische Anomalien)

Institute of Marine Sciences, University of Sydney (Australien)
Prof. Dr. R.D. Müller, A. Gibbons (Interpretation magnetischer Anomalien und tektonische Modelle)

Museum für Naturkunde Berlin
Dr. C. Lüter, Dr. B. Neuhaus (Leitung der biologischen Untersuchungen), Dr. U. Struck (Sedimentanalysen)

Universität Graz (Österreich)
Dr. B. Berning (Analyse der Bryozoen)

University of Modena (Italien)
Prof. Dr. M.A. Todaro (Systematik und Biogeographie der Gastrotricha)

University of Otago (New Zealand)
Dr. J. White (Vulkanologie)

University of Rio de Janeiro (Brasilien)
Dr. E. Hajdu (Analyse der Schwämme aus der Gattung *Asbestopluma* und Verwandte)

Zoological Museum, University of Copenhagen (Dänemark):
Prof. R. M. Kristensen (Systematik und Biogeographie der Loricifera)
J. G. Hansen (Systematik und Biogeographie der Tardigrada)

II.1. Darstellung der erzielten Ergebnisse

II.1.1. Publizierte oder in Manuskripten vorliegende Ergebnisse

Die meisten der Ergebnisse von SO199-CHRISP resultieren aus einer sehr aufwendigen und langwierigen Analytik (u.a. Geochemie, radiometrische Alterdatierungen). Viele dieser Analysemethoden können nicht zeitparallel durchführt werden, sondern müssen nacheinander vorgenommen werden. So werden zum Beispiel auf Basis der Ergebnisse der Hauptelementanalytik geeignete Proben für die Spurenelementanalytik ausgewählt, während die Spurenelementdaten wiederum die Basis für die Isotopenanalytik bilden. Aufgrund der großen Menge an zu analysierenden Proben (s. Abschnitt I.3.) und des langen analytischen „Vorlaufs" liegen zum Zeitpunkt der Abgabe diese Abschlussberichts noch keine Artikel vor, die

bereits in Fachzeitschriften publiziert sind („Sonderdrucke“). Aus SO199-CHRISP werden jedoch mehrere Publikationen in Fachzeitschriften resultieren, die wir dem PtJ nach ihrem Erscheinen umgehend zusenden werden.

Ein Teil der wissenschaftlich-technischen Ergebnisse von SO199-CHRISP ist bereits in eine Reihe von Manuskripten eingeflossen, die zur Publikation eingereicht werden sollen. Diese Ergebnisse werden hier nicht detaillierter erläutert. Stattdessen sind die im folgenden aufgelisteten Manuskripte dem Schlußbericht im Anhang beigelegt:

(a) Hoernle K, Hauff F, Werner R, Bogaard PvD, Kipf A, Conrad S, Gibbons A, Barckhausen U, Müller RD, Garbe-Schönberg D, Conrad S (in Vorb.) The Investigator Ridge and Christmas Island Seamount Province, Indian Ocean: Evidence for the Recycling of Continental Lithosphere During Gondwana Breakup. Earth and Planetary Science Letters

In dieser Arbeit werden die Haupt- und Spurenelement- sowie Isotopenzusammensetzungen und Ar/Ar-Alter der Proben aus der Christmas Island Seamount Provinz und vom Investigatorrücken vorgestellt. Es wird gezeigt, dass die geochemisch angereichtere Signatur des Mantel unter dem Indik („Indian Mantle Domain“) seit dem späten Jura existiert. Die Bildung der Christmas Island Seamount Provinz wird auf subkontinentalen lithosphärischen Mantel zurückgeführt, der während des Gondwanaaufbruchs delaminierte, und basierend auf einem neuen plattentektonischen Modell in den oberen Mantel des Whartonbeckens eingebracht wurde. Die Beimischung von subkontinentaler Lithosphäre in den indischen Mantel könnte auch die „Indian Mantle Domain“ erklären. Ein Vorabdruck dieser Arbeit liegt diesem Bericht in Anlage 2 bei.

(b) Barckhausen U, Hoernle K, Werner R, Hauff F, van den Bogaard P, Gibbons A (in Vorb.) Crustal ages along the Investigator Ridge and tectonic implications. Geophysical Journal International

In dieser Studie wird aus Ar/Ar-Altersdaten von Gesteinsproben in Kombination mit Altersbestimmung der ozeanischen Kruste aus identifizierten magnetischen Lineationen ein tektonisches Modell für die Entwicklung des Investigatorrückens abgeleitet. Ein Vorabdruck dieser Arbeit liegt dem Bericht in Anlage 3 bei.

(c) Neuhaus B (in Vorb.) *Semnoderes paucispinosus* sp. nov. (Kinorhyncha, Cyclorhagida) from the deep sea around Christmas Island, Indian Ocean. Helgoland Marine Research

In dieser Arbeit wird die neue Art der Kinorhyncha *Semnoderes paucispinosus* sp. nov. aus dem Sandlückensystem der Tiefsee im Bereich der Weihnachtsinsel beschrieben und von bekannten Arten derselben Gattung abgegrenzt. Erstmals finden sich Hinweise darauf, dass Kinorhyncha möglicherweise ein subadultes Stadium aufweisen ähnlich den nahe verwandten Loricifera. Ein Vorabdruck dieser Arbeit liegt diesem Bericht in Anlage 4 bei.

II.1.2. Ergebnisse aus Bachelor- und Diplomarbeiten

Im Rahmen von SO199-CHRISP wurden bzw. werden eine Bachelorarbeit und eine Diplomarbeit angefertigt. Die bereits abgeschlossene Bachelorarbeit ist aufgrund ihres beträchtlichen Umfangs dem Abschlussbericht nicht beigelegt. Stattdessen ist ihr Inhalt hier kurz zusammengefasst.

(a) Carolin Bartsch und Elisabeth Seidel (2009) "Die strukturelle Untersuchung des Investigatorrückens und der Christmas Island Seamount Provinz im nordöstlichen Indischen Ozean anhand von Bathymetrie und Parasound". Bachelorarbeit; Betreuer: Prof. Meschede (EMAU Greifswald) und Dr. Barckhausen (BGR)

An ausgewählten Beispielen wird das Ergebnis der Messungen mit Fächerecholot und Parasound entlang des Investigatorrückens und im östlichen Whartonbecken gezeigt. Diesen Vermessungen werden stets die Ergebnisse von satellitenbasierten Messungen gegenübergestellt, die bei weit geringerer Auflösung lückenlos das gesamte Messgebiet überdecken. Die Ausschnitte zeigen sehr verschiedene Strukturen entlang des Rückensystems und geben dabei gleichzeitig auch einen Überblick über die Möglichkeiten der kombinierten Nutzung von schiffsgestützten und satellitenbasierten Wassertiefendaten. Auf den Parasound-Profilen werden Abschnitte mit Anzeichen für rezente Tektonik und kleineren Fluid- bzw. Gasaufstiegszonen vorgestellt. Auch die Auswertung der Bathymetrie

deutet auf rezente Tektonik und linkslaterale Verschiebungen im Gebiet der Christmas Island Seamount Provinz und des Investigatorrückens hin. Einige Ergebnisse dieser Arbeit werden im Abschnitt II.1.3. (Deformation/Neotektonik) detaillierter erläutert.

(b) Sarah Conrad (in Vorb., Abschluss voraussichtlich 2011) „Temporal and compositional evolution of Christmas Island" (Arbeitstitel). Diplomarbeit; Betreuer: Prof. Hoernle und Dr. Hauff (IFM-GEOMAR).

Anhand der Haupt- und Spurenelement- sowie Isotopenzusammensetzung von 16 Lavaproben von der Weihnachtsinsel soll in Kombination mit den Altersdatierungen (s. Manuskript Hoernle et al.) der Ursprung und die magmatische Entwicklung der Weihnachtsinsel rekonstruiert werden. Die Weihnachtsinsel ist durch 2 Phasen vulkanischer Aktivität gekennzechnet und weist offenbar als einzige Struktur innerhalb der Christmas Island Seamount Provinz eine junge, pliozäne Aktivitätsphase auf. Diese Arbeit ist noch nicht abgeschlossen, derzeit geplanter Abgabetermin ist April 2011.

II.1.3. Weitere Ergebnisse

Darüber hinaus wird noch an einigen Teilaspekten der Daten gearbeitet, weitere Publikationen sind in Vorbereitung. Einige Ergebnisse von SO199-CHRISP, die nicht in den beiliegenden Manuskripten publiziert werden, sind im Folgenden kurz zusammengefasst.

A. Deformation/Neotektonik

Im Gegensatz zu der herkömmlichen Vorstellung, dass sich (ozeanische) Platten rigide verhalten und nur an ihren Rändern deformiert werden, wurde im Norden des Whartonbeckens rezente interne Deformation der indo-australischen Platte nachgewiesen (z.B. Deplus et al. 1998, Deplus 2001). Anhand umfangreicher Fächer- und Sedimentecholotprofilierungen sollte dieser Prozess im Rahmen von SO199-CHRISP genauer charakterisiert werden. So sollte u.a. festgestellt werden, inwieweit Neotektonik und rezenter Vulkanismus im Bereich der Christmas Island Seamount Provinz und am Investigatorrücken auftreten. Während rezenter oder „anomal“ junger Vulkanismus dort nicht nachgewiesen werden konnte, fanden sich jedoch im nahezu gesamten Arbeitsgebiet deutliche Hinweise auf rezente Tektonik und die Reaktivierung von alten Störungszonen. Im Folgenden werden zunächst 4 ausgewählte Beispiele hierfür kurz beschrieben und anschließend einige Schlußfolgerungen aus diesen Beobachtungen vorgestellt.

I. <u>Investigatorrücken</u>

Während SO199 wurde der Investigatorrücken von ca. 6°S bis 18°S (= ca. 1.300 km) nahezu vollständig auskartiert. Im Norden wird die Investiagtor Bruchzone von zwei parallelen Rücken gebildet, die durch ein Tal getrennt sind. Weiter südlich wird der höher aufragende, östliche Teil des Rückens durch einen steilen Hang vom seinem flacheren, westlichen Teil getrennt. In seinem zentralen und südlichen Teil (ab ca. 8°S) ist das Tal zwischen beiden Seiten des Investigatorrückens nicht mehr deutlich ausgeprägt und der westliche Teil bildet ein flaches Plateau. Eines der auffallendsten morphologischen Merkmale des Rückens ist jedoch, dass der dominante östliche Teil entlang der gesamten Länge des Investigatorrücken einen asymmentrischen Querschnitt besitzt mit einem sehr steilen, nach Westen gewandten Hang und einem deutlich flacheren Osthang (Abb. A1).

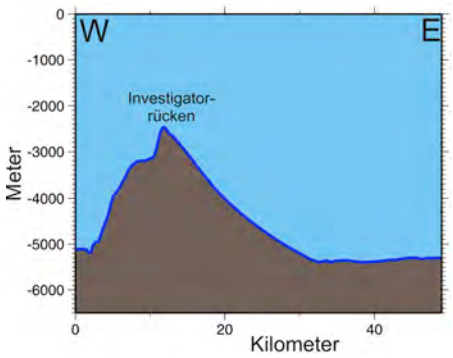

Abb. A1: *Profil durch den Investigatorrücken bei 11°15´N (aus Bartsch und Seidel 2009). Der asymmetrische Querschnitt mit einem steilen Westhang und einen flacheren Osthang ist für den gesamten Investigatorrücken charakteristisch und wird durch eine Reaktivierung der Investiagtor-Störungszone erklärt.*

Unserer Interpretation nach entstand der steile Westhang durch eine Reaktivierung der Investigator-Störungszone. Diese Hypothese wird durch Dredgezüge gestützt, die von diesem Westhang ein extrem weites Spektrum an Gesteinen erbrachten, dass mit Sedimenten, Pillowlaven, „sheeted dike“ Fragmenten, Intrusiva und Serpentiniten quasi einen Querschnitt durch die ozeanische Lithosphäre repräsentiert (z.B. DR 6 bei 9°S, DR 10 bei 11°S, DR 11 bei 12°S oder DR 28 bei 16°S). Eine solche Ansammlung von Gesteinen aus unterschiedlichen Stockwerken der Lithosphäre auf derart engem Raum (wenige 100 m Dredgezug) deutet auf eine intensive Tektonik hin. Häufig sind diese Gesteine nur gering alteriert und es gab keine Anzeichen für eine signifikante Sedimentbedeckung. Hieraus schließen wir, dass die Tektonik am Investigatorrücken zumindest teilweise rezent ist. Dies ist konsistent mit der Hypothese der Biologiearbeitsgruppe, die das völlige Fehlen festwachsender Filtrierer auf Hangschutt, der an der Westflanke des Rückens gedredged wurde, mit einer häufigen Bewegung dieser Gesteine erklärt (s. Abschnitt B dieses Kapitels). Da es entlang des gesamten Investigatorrückens morphologische Hinweise auf linkslaterale Bewegungen gibt (Abb. A2), gehen wir von einer rezenten, linkslateralen Reaktivierung der Investigator-Störungszone aus.

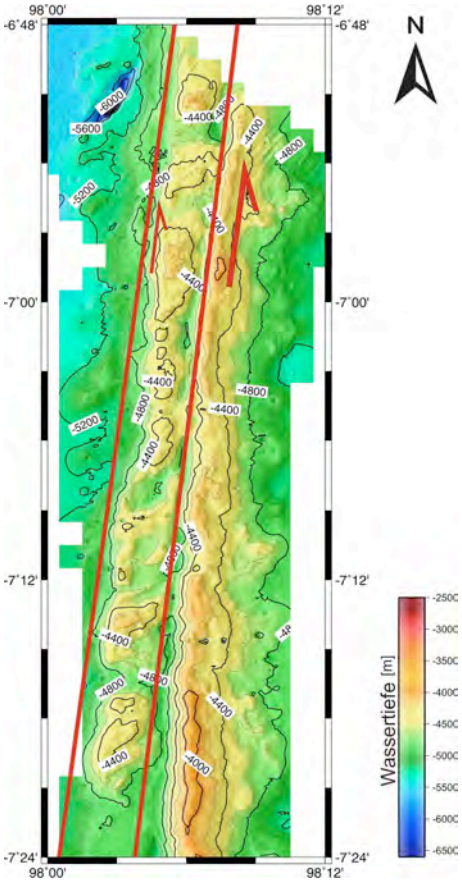

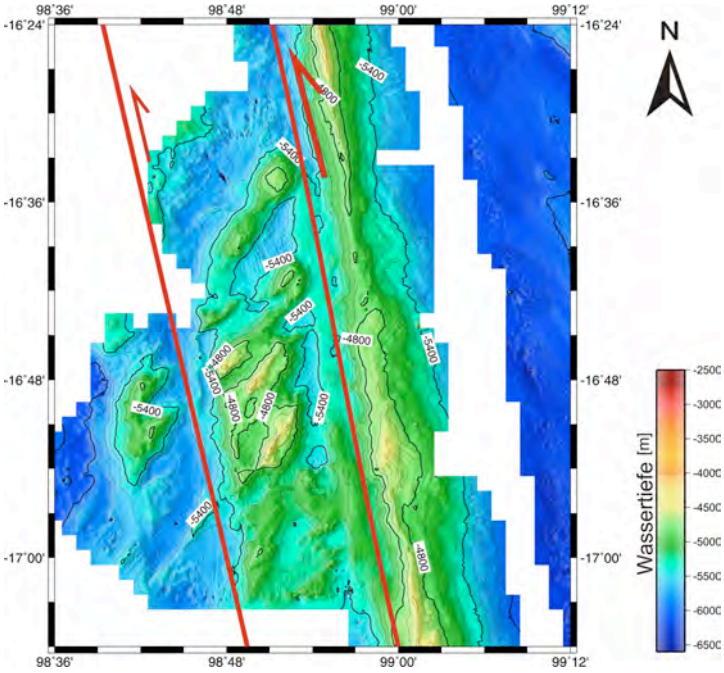

Abb. A2: *Beispiele für linkslaterale Versätze im Norden (links) und im Süden (oben) des Investigatorrückens. Die Größe der Pfeile entspricht dem Versatz entlang der Störungen (aus Bartsch und Seidel 2009).*

II. <u>Östlich und westlich an den Investigatorrücken angrenzende Gebiete</u>

Bereits Liu et al. (1983) beschrieben basierend auf Magnetikdaten parallel zum Investigatorrücken verlaufende Bruchzonen. Während SO199 aufgezeichnete Fächerecholotdaten vom Ozeanboden zwischen dem Investigatorrücken und dem „Outsider Seamount“ (s.u., ca. 6°00´ - 7°00´S und 97°20´ - 98°10´E) sowie zwischen dem Investigatorrücken und den Cocos/Keeling Atollen (ca. 12°20’ - 13°40’S und 96°50´ - 98°20´E, Abb. A3) zeigen einen ca. 15 km breiten, N-S verlaufenden Trog in 35 bis 50 km Entfernung vom Investigatorrücken, der durch einen sehr steilen westlichen Rand gekennzeichnet ist. Nach den auf Satellitenaltimetrie basierenden Karten scheint dieser Trog sub-parallel zum Investigatorrücken über dessen gesamte Länge zu verlaufen. Aufgrund des ungewöhnlich steilen Westhangs des Trogs gehen wir davon aus, dass es sich auch hierbei um eine reaktivierte (N-S-verlaufende) Bruchzone handelt. Diese Interpretation wird durch

Magnetikdaten von SO199 gestützt, da die hier generell Ost-West verlaufenden Ozeanbodenspreizungsanomalien an der Westflanke des Trogs schlagartig abbrechen (Abb. A3).

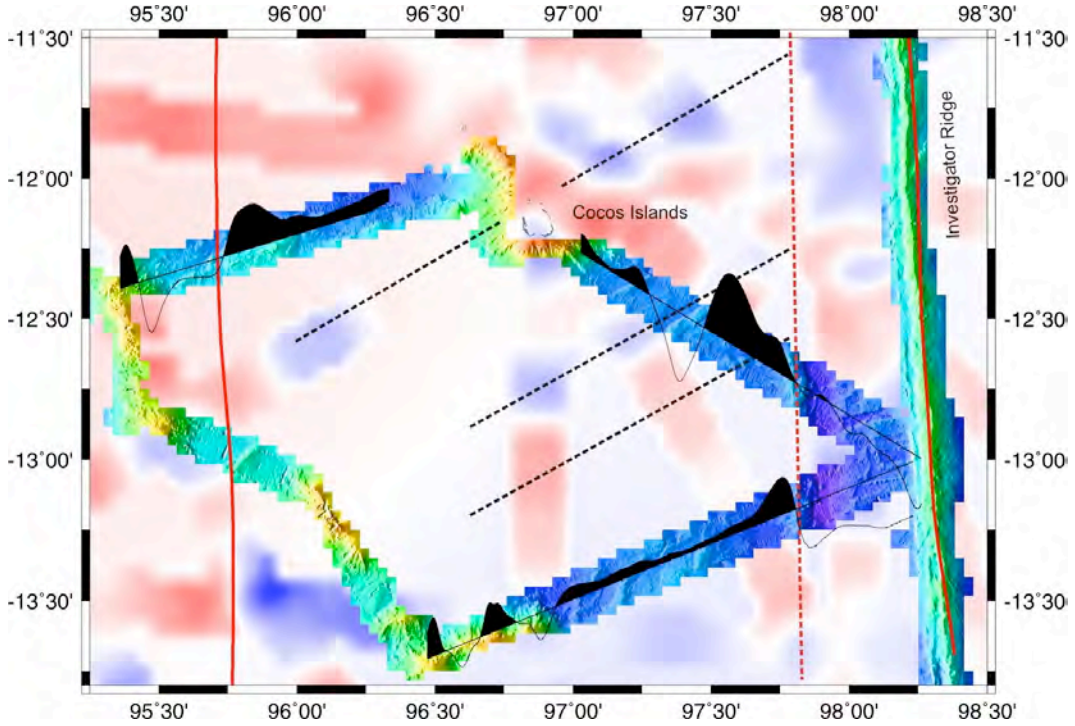

Abb. A3: *Zusammenstellung von Magnetikdaten und Fächerecholotbathymerie aus dem Gebiet der Cocos-Keeling Volcanic Province westlich des Investigatorrückens. Durchgezogene rote Linien kennzeichnen Bruchzonen nach Liu et al. (1983), die gepunktete rote Linie die während SO199 neu identifizierte Bruchzone. Die vermutliche Ausrichtung der Ozeanbodenspreizungsanomalien ist durch gepunktete schwarze Linien dargestellt (Abb. aus Barckhausen et al. 2009).*

Ein Parasoundprofil, das östlich der Cocos-Keeling Atolle aufgezeichnet wurde, zeigt deformierte Beckensedimente und vertikale Störungen, die teilweise bis an die Sedimentoberfläche reichen. Auch ein weiteres, ca. 15 km östlich des Investiagtorrückens auf ca. 8°S gelegenes Parasoundprofil zeigt eine vertikale Diskontinuität, die fast bis an die Sedimentoberfläche reicht, sowie asymmetrische Strukturen (Bartsch und Seidel 2009). Die Tatsache, dass in diesen Gebiete auch die jüngsten Sedimente gestört sind, lässt auch hier auf rezente Tektonik schließen. Ferner deuten Magnetikanomaliedaten von SO199 darauf hin, dass östlich des Investigatorrückens bisher nicht identifizierte Bruchzonen existieren, die sub-paralell zum Rücken verlaufen. Die im Rahmen von SO199 CHRISP durchgeführten Profilierungen im Bereich des Investigatorrückens deuten somit auf intensive (Neo)Tektonik mit einer rezenten Reaktivierung N-S-verlaufender Bruchzonen in diesem Gebiet hin.

III. <u>„Outsider“ Seamount</u>

Etwa 80 km westlich des Investigaterrückens befindet sich bei ca. 6°14´S und 97°24´E ein N-S-gestreckter, ca. 2.300 m hoher Seamount, der von den SO199 Fahrtteilnehmern aufgrund seiner abgelegenen Lage „Outsider Seamount“ genannt wurde. Seine langgestreckte Form ist höchst wahrscheinlich darauf zurückzuführen, dass er entlang eines alten, N-S streichenden, Krustenlineaments entstand (möglicherweise durch eine Spalteneruptionen). Wahrscheinlich handelt es sich dabei um eine alte Bruchzone, bei deren Reaktivierung es zu vulkanischer Aktivität kam. Auffallend an diesem Seamount ist, dass seine Süd- und andeutungsweise auch seine Nordflanke von einer N-S-verlaufenden Schlucht durchzogen sind und die östliche Hälfte seines Tops relativ zur Westlichen um gut 1 km nach Norden versetzt ist (Abb. A4). Offenbar kam es nach Bildung des „Outsider“ Seamounts zu einer linkslateralen Bewegung entlang der alten Bruchzone, die zur Ausbildung der Schluchten und des Versatzes führte.

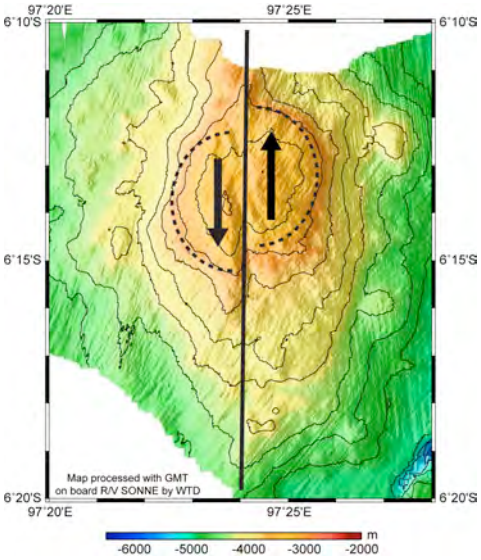

Abb. A4: *Linkslateraler Versatz in der Mitte des „Outsider“ Seamounts, der höchstwahrscheinlich auf die Reaktivierung einer alten, N-S-verlaufenden Bruchzone (= schwarze Linie) zurückzuführen ist.*

VI. Östliche Arbeitsgebiete

In der Arbeit von Bartsch und Seidel (2009) wurden neben den oben erwähnten Parasoundprofilen vier weitere aus dem zentralen und östlichen Bereich der Christmas Island Seamount Provinz sowie zwei aus dem Randbereich des Argobeckens ausgewertet. Die meisten dieser Profile sind durch Versätze und Störungen gekennzeichnet, die auch die obersten Sedimentschichten ± vertikal durchziehen und somit auf rezente Tektonik hindeuten (Abb. A5). Einige dieser Profile zeigen auch Pockmarks und diapirartige Strukturen, die wahrscheinlich Gas- oder Fluidaustritte repräsentieren.

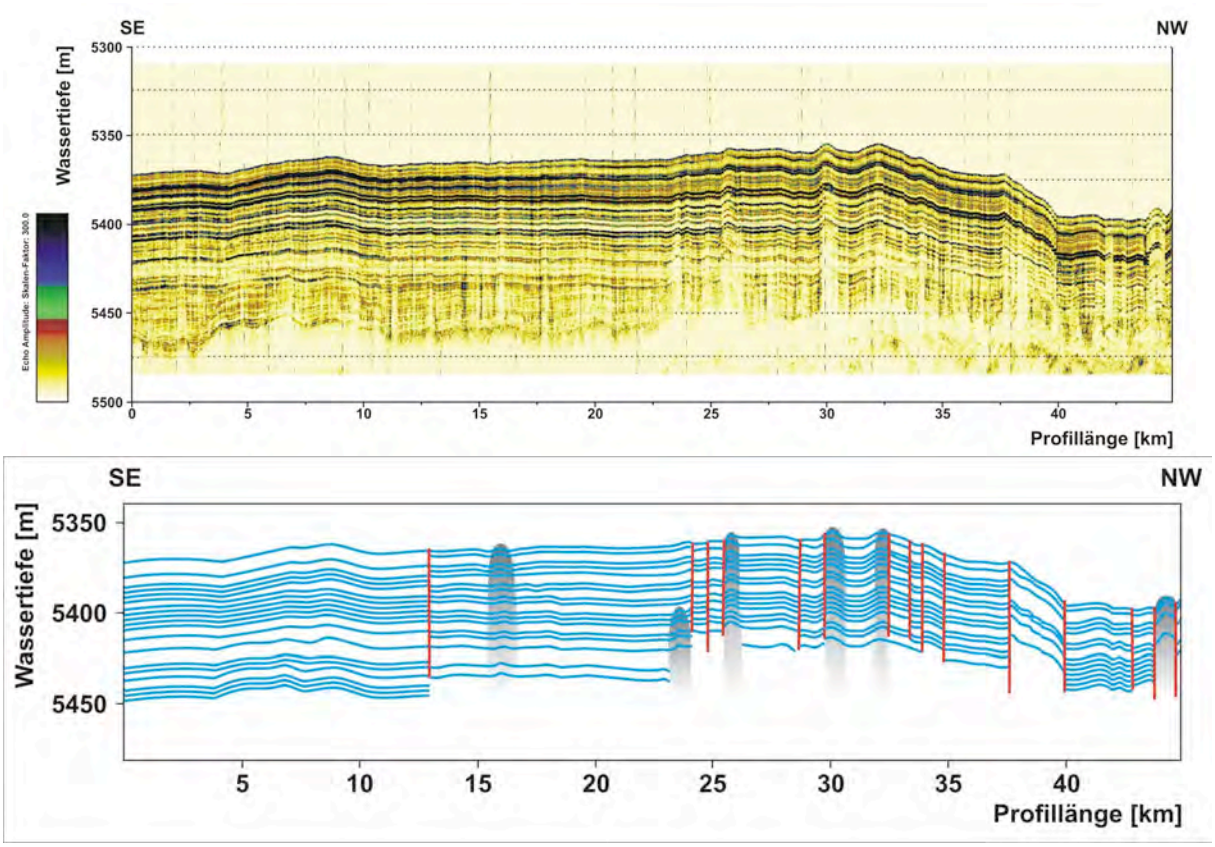

Abb. A5: *Parasoundprofil aus dem Randbereich des Argobeckens (oben) und Interpretation (unten). Die rote Linien repräsentieren Störungszonen, grau unterlegte Bereiche diapirartige Aufstiegszonen (aus Bartsch und Seidel 2009).*

V. Schlussfolgerungen

SO199-CHRISP hat gezeigt, dass sich die von Deplus et al. (1998) für den Norden des Whartonbeckens beschriebene Neotektonik entlang N-S verlaufender Bruchstrukturen und die rezente Deformation der indo-australischen Platte nach Süden hin kontinuierlich fortsetzt. Weiterhin fanden sich Hinweise auf eine sehr aktive Tektonik auch im Osten der Christmas Island Seamount Provinz und im westlichen Randbereich des Argobeckens. Insgesamt dominieren insbesondere im Bereich des Investigatorrückens und der westlichen Christmas Island Seamount Provinz linkslaterale Bewegungen entlang N-S-streichender, älterer Störungszonen. Diese linkslaterale, zumindest teilweise rezente Reaktivierung von Störungszonen ist konsistent mit dem regionalen tektonischen Konzept, dass diese Gegend Teil einer diffusen, sich entwickelnden Plattengrenze zwischen den östlichen (Australien) und den westlichen (Indien) Teilen der indo-australischen Platte ist. Durch die Kollison von Indien mit Asien kann sich der westliche Teil der Platte (etwa westlich des Ninety East Ridge) nicht weiter nach Norden bewegen, während die Bewegung nach Norden des östlichen Teils durch die nach Norden gerichtete Subduktion kontinuierlich anhält (Abb. A6). Die Bewegung zwischen beiden Hälften der Platten ereignete sich offenbar in einem (noch) diffusen Bereich im Osten des Ninety East Ridge entang Nord-Süd-streichender Störungszonen, die als linkslaterale „strike slip faults“ reaktiviert wurden bzw. werden. Dieser Prozess ist sicherlich auch die Ursache für die starken Intraplattenbeben in diesem Bereich. So ereignete sich z.B. am 18. Juni 2000 mit einer Magnitude von 7.8 eines der größten Intraplattenbeben der Geschichte an der Schnittstelle zwischen dem Investigatorrücken und der Christmas Island Seamount Provinz. Aufgrund der intensiven rezenten Tektonik und der oben geschilderten Prozesse ist mit großer Wahrscheinlichkeit davon auszugehen, dass die Erdbebentätigkeit hier anhalten wird.

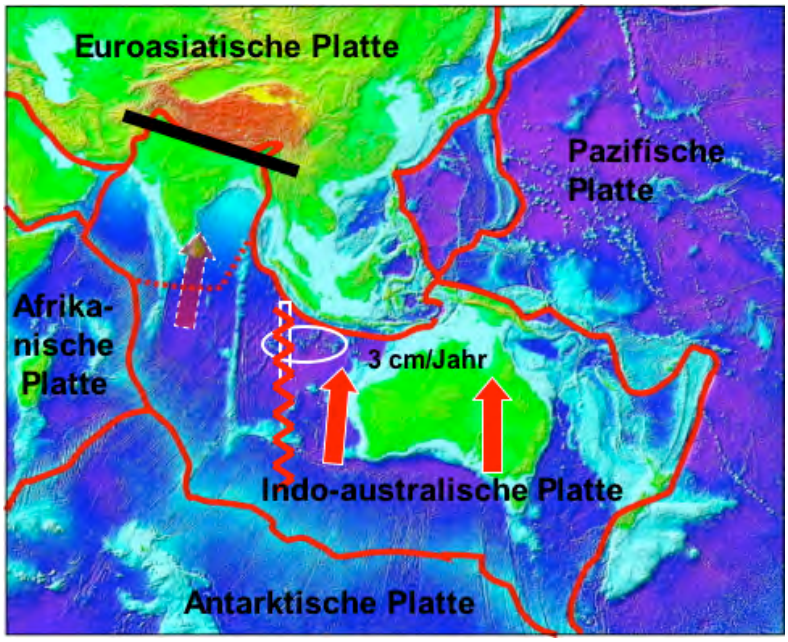

Abb. A6: *Modellvorstellung zu einer diffusen, sich entwicklenden Plattengrenze (= rote Zickzacklinie) innerhalb der indo-australischen Platte im Bereich des Investigator-rückens (weisses Rechteck, weisser Kreis = Christmas Island Seamount Provinz). Die roten Pfeile kennzeichnen die nach Norden gerichtete Bewegung des östlichen Teils der indo-australischen Platte, während sich deren westlicher Teil durch die Kollision mit der eurasichen Platte nicht weiter nach Norden bewegen kann.*

Zitierte Literatur

Barckhausen U, Gibbons A, Zeibig M. (2009) Magnetic. In: Werner R, Hauff F, Hoernle K (eds) RV Sonne Fahrtbericht / Cruise Report SO199 CHRISP: Christmas Island Seamount Province and the Investigator Ridge: Age and Causes of Intraplate Volcanism and Geodynamic Evolution of the South-Eastern Indian Ocean. IFM-GEOMAR Report 25: http://www.ifm-geomar.de/index.php?id=publikationen

Bartsch C, Seidel E (2009) "Die strukturelle Untersuchung des Investigatorrückens und der Christmas Island Seamount Provinz im nordöstlichen Indischen Ozean anhand von Bathymetrie und Parasound" Bachelorarbeit an der EMAU Greifswald. 1 - 78

Deplus C (2001) Indian Ocean actively deforms. Science 292: 1850-1851

Deplus C, Diament M, Hebert H, Bertrand G, Dominguez S, Dubois J, Malod J, Patriat P, Pontoise B, Sibilla J-J (1998) Direct evidence of active deformation in the eastern Indian oceanic plate. Geology 26: 131-134

Liu C-L, Curray JR, McDonald JM (1983) New constraints on the tectonic evolution of the eastern Indian Ocean. Earth Planet Sci Lett 65: 331-342

B. Biologie (C. Lüter, B. Neuhaus et al.)

Die Analysen der Sedimente von 5 MUC-Stationen und 2 TV-Greifern ergaben für Tiefseeböden durchschnittliche Werte (0,6%) hinsichtlich des organischen Kohlenstoffgehalts (TOC), was darauf schließen lässt, dass die geringe Dichte der auf den geborgenen Steinen aufwachsenden Makrofauna nicht auf Nährstoffarmut in der Wassersäule zurückzuführen ist. Im Gegenteil konnten zum z.B. an Station TVG 47 in ca. 2.000 m Tiefe Gärten aus Oktokorallen (Gorgonaria) und vor allem gestielten Seelilien (Crinoida) beobachtet werden. Auf einem Transekt von ca. 300 m wurden etwa 50 Individuen aus zwei verschiedenen Arten dieser urtümlich anmutenden Stachelhäuter beobachtet (Videodokumentation). Die Tiere ernähren sich als mikrophage Filtrierer, was für eine eher hohe Konzentration an Detritus und Plankton (und damit Nährstoffen) in der Wassersäule spricht. Auffällig war, dass insbesondere am Investigatorrücken, aber auch an den beprobten Seamounts die Häufung von Makrofauna-Organismen immer an der Ostflanke der Erhebungen zu beobachten war. Dies spricht für ein Strömungsbild in der Tiefe, das in etwa dem der Meeresoberfläche gleicht, wo durch die Vorzugswindrichtung von Ost nach West die Strömung in entsprechender Richtung verläuft. Für filtrierende Organismen ist das Wachstum in der Strömung ideal, weil dadurch maximale Mengen sauerstoff- und nährstoffreichen Wassers von den Organismen genutzt werden können. Gerade diese Ähnlichkeit des Strömungsbildes an der Oberfläche und in der Tiefe machte die Probenahme allerdings schwierig, denn ein Dredgezug, der immer hangaufwärts (vom Tiefen ins Flache) betrieben wird, geschieht in der Regel auf derjenigen Seite eines untermeerischen Höhenzuges oder Berges, die abgewandt von der Windrichtung und damit der Oberflächenströmung liegt. Dadurch wurden bevorzugt die Teile der Seamounts mit der geologischen Dredge beprobt, die im Strömungsschatten lagen und entsprechend ungünstige Lebensbedingungen für große Filtrierergemeinschaften boten. Das erklärt das Auffinden von nur wenigen, sehr kleinen Organismen in zudem sehr geringer Dichte auf den Dredge-Proben über weite Teile der Expedition.

Der zunächst in N-S-Richtung beprobte Investigatorrücken zeigte zudem das Phänomen, dass seine Westflanken häufig mit abgerundeten Steinen bedeckt waren, deren Oberflächen wenig Schutz und Versteckmöglichkeiten für aufwachsende Organismen boten. Außerdem machten die Dredge-Proben hier häufig den Eindruck eines Gerölls oder Hangschutts, das in ständiger Bewegung ist und dadurch keine permanente Besiedlung durch festwachsende Filtrierer ermöglicht.

Dominiert wurden die auf den Dredge-Proben vorgefunden Faunen von hexactinelliden Schwämmen, sedentären Polychaeten und Bryozoen. Daneben wurden auch Hornschwämme, einige errante Polychaeten, Hydrozoen-Kolonien, Polypen coronater Scheibenquallen (Scyphozoa) und Tunicaten gefunden. Entgegen den Erwartungen konnte nicht ein einziger Vertreter der Brachiopoda in den Aufsammlungen entdeckt werden.

Besonders interessant erscheinen die Schwämme der Gattung *Asbestopluma* (Demospongiae, Cladorhizidae), von denen an vielen Stationen Exemplare geborgen werden konnten. Diese Schwämme sind "fleischfressende" Organismen, d.h. sie ernähren sich nicht durch das Filtrieren Detritus-reichen Wassers, denn ihnen fehlt normalerweise ein Lakunensystem. Ihre Taxonomie und Stammesgeschichte sind weitgehend unbekannt, und wird zur Zeit von unseren Kooperationspartnern noch ausgewertet.

Gleiches gilt für die während der Ausfahrt gesammelten Bryozoa. Auch hier gibt es (leider) noch keine abschließende Publikation. Unsere Kooperationspartner arbeiten nach wie vor an dem Material. Da genetische und morphologische (rasterelektronenmikroskopische) Untersuchungen unternommen werden, die anschließend zusammengeführt werden sollen, ist das Prozedere forschungsintensiv und zeitaufwendig.

Hinsichtlich der Makrofauna gab es ein entscheidendes, technisches Problem während der Ausfahrt: Wie sich trotz intensiver Fehlersuche durch die Bordelektroniker erst im Nachhinein herausstellte, war der TV-Greifer während einer Überholung vor der Ausfahrt mit fehlerhaften Kabeln ausgestattet worden, was zu häufigen Ausfällen der Datenleitung ab einer bestimmten Wassertiefe führte. Da davon auch die Übertragung des Kamerasignals betroffen war, mussten die Einsätze nach Auftreten des Fehlers sofort abgebrochen werden. Von insgesamt 12 Einsätzen des TV-Greifers konnten nur 3 erfolgreich abgeschlossen werden, was zu einer erheblichen Minderung der Makrofauna-Ausbeute beigetragen hat.

II.2. Voraussichtlicher Nutzen, Verwertbarkeit

Durch den erfolgreichen Verlauf des Forschungsvorhabens SO199-CHRISP haben wir u.a. neue Erkenntnisse über Intraplattenvulkanismus, den Mantel unter dem indischen Ozean und plattentektonische Prozesse sowie die Benthosfauna in diesem Bereich gewonnen. Damit wird u.a. zu einem besseren Verständnis von Aufschmelzprozessen im Erdmantel, zur erdgeschichtlichen Entwicklung und der Biodiversität und Biogeographie des Indik beigetragen. Dies sind wichtige Grundlagen für weiterführende wissenschaftliche, aber auch umweltpolitische oder wirtschaftliche Programme. Somit können die Ergebnisse von SO199-CHRISP in nationale und internationale Forschungsprojekte bzw. -programme einfließen. Ergebnisse aus SO199-CHRISP wurden auf Tagungen und in Berichten bzw. Artikeln vorgestellt bzw. werden demnächst zur Publikation eingereicht (s. Abschnitt II.1.), die Publikation weiterer Ergebnisse ist in Vorbereitung. Ferner konnte im Rahmen von SO199-CHRISP die Zusammenarbeit mit Kollegen u.a. aus Australien intensiviert werden. Weiterhin wurden Proben und/oder Daten aus diesem Forschungsvorhaben nationalen (u.a. BSH, Pangaea) und internationalen Stellen (u.a. Geoscience Australia) zur Verfügung gestellt. Unter anderem wurden während SO199 auf Bitte von Geoscience Australia Teile der Basis der Weihnachtsinsel auskartiert. Die dabei generierten Daten und Karten, die u.a. eine Gefährdung der Insel durch Hangrutschungen offenbarten, wurden an Geoscience Australia übergeben. Weiterhin wurden Geoscience Australia während SO199 gewonnene Sedimentproben zur Verfügung gestellt. Ergebnisse, Daten und Proben von SO199-CHRISP können somit zu Fragen der Seerechtskonvention, für die zukünftige Abschätzung mineralischer Rohstoffe, für Fragen des Umweltschutzes und für Risikoanalysen (Vulkanismus, Erdbeben, Hangrutschungen, Klimaänderung) von den dafür zuständigen nationalen und internationalen Stellen genutzt werden. Das auf SO199 gewonnene zoologische Material einschließlich des Typenmaterials wird nach der wissenschaftlichen Auswertung in die Sammlungen des Museums für Naturkunde (Berlin) integriert. Die Ergebnisse zu den Kinorhyncha werden in die Weltartenliste der Kinorhyncha im Unesco-IOC Register of Marine Organisms Eingang finden. Über die vom BMBF geförderte Sammlungsdatenerfassung im Museum für Naturkunde im Rahmen der "Global Biodiversity Information Facility" (GBIF) werden alle Biodiversitätsdaten aus dem Projekt über Datenbanken international verfügbar sein.
Insgesamt sind somit aus diesem Forschungsvorhaben mittel- und langfristig verschiedene potentielle Nutzungen zu erwarten. Auch können aus dem Vorhaben Kooperationen mit der Wirtschaft (Exploration auf Rohstoffe, Risikoabschätzungen durch Versicherungsgesellschaften, biologische Wirkstoffe) hervorgehen. Wissenschaftlich ergaben sind intensivere Kooperationen mit nationalen und internationalen Einrichtungen, die im Rahmen zukünftiger Projekte fortgesetzt und weiter ausgebaut werden sollen. Die Veröffentlichung der Ergebnisse in der Fachliteratur hat zudem auch einen Werbeeffekt für die deutsche Meeresforschung, aus dem Nachfrage nach Expertise, Verfahren und Instrumenten erwachsen mag.

II.3. Fortschritt bei anderen Stellen

Die Fortschritte bei anderen Stellen sind unter Abschnitt II.1. “Darstellung der Ergebnisse” zusammengefasst.

II.4. Erfolgte und geplante Publikationen der Ergebnisse

Artikel (peer-reviewed)

Barckhausen U, Hoernle K, Werner R, Hauff F, van den Bogaard P, Gibbons A, (in Vorb.) Crustal ages along the Investigator Ridge and tectonic implications. Geophysical Journal International

Hoernle K, Hauff F, Werner R, Bogaard PvD, Kipf A, Conrad S, Gibbons A, Barckhausen U, Müller RD, Garbe-Schönberg D, Conrad S (in Vorb.) The Investigator Ridge and Christmas Island Seamount Province, Indian Ocean: Evidence for the Recycling of Continental Lithosphere During Gondwana Breakup. Earth and Planetary Science Letters

Neuhaus B (in Vorb.) *Semnoderes paucispinosus* sp. nov. (Kinorhyncha, Cyclorhagida) from the deep sea around Christmas Island, Indian Ocean. Helgoland Marine Research

Weitere Pubilkationen über die in Abschnitt II.1.3. kurz zusammengefassten Ergebnisse sind in Vorbereitung. Ferner ist eine Arbeit von Gibbons et al. über Krustenalter und die plattentektonische Entwicklung im Argobecken in Vorbereitung. Die Auswertung und Interpretation der während SO199 im Argobecken aufgezeichneten Magnetikdaten wird zur Zeit von unseren Kooperationspartnern an der University of Sydney durchgeführt.

Berichte, polulärwissenschaftliche Artikel, Diplomarbeiten etc.

Werner R, Hauff F, Hoernle K (eds) (2009) RV Sonne Fahrtbericht / Cruise Report SO199 CHRISP: Christmas Island Seamount Province and the Investigator Ridge: Age and Causes of Intraplate Volcanism and Geodynamic Evolution of the South-Eastern Indian Ocean. IFM-GEOMAR Report 25: http://www.ifm-geomar.de/index.php?id=publikationen

Bartsch C, Seidel E (2009) "Die strukturelle Untersuchung des Investigatorrückens und der Christmas Island Seamount Provinz im nordöstlichen Indischen Ozean anhand von Bathymetrie und Parasound" Bachelorarbeit an der EMAU Greifswald. 1 - 78

Hoernle K, Hauff F, Werner R, Barckhhausen U (2010) Bruchzonen: Urpsprung für große Erdbeben und Archiv der Geschichte des Ozeanbodens. In: Mit der Sonne die Erde erforschen, RF Forschungsschiffahrt, Bremen: 44-47 *(dieser Artikel ist auch in Englisch erschienen)*

Werner R, Hauff F, Hoernle K (2010) Marine Supervulkane. In: Mit der Sonne die Erde erforschen, RF Forschungsschiffahrt, Bremen: 39-43 *(dieser Artikel ist auch in Englisch erschienen)*

Conrad S (in Vorb.) „Temporal and compositional evolution of Christmas Island" (Arbeitstitel). Diplomarbeit an der CAU Kiel

Vorträge und Poster auf Tagungen

Werner R, Hoernle K, Hauff F, Heydolph K, Barckhausen U, SO199 Scientific Party (2008) R/V Sonne Cruise SO199 CHRISP: New Insights Into the Geodynamic History of northern Wharton Basin (South-East Indian Ocean) AGU Fall Meeting, San Francisco, California, USA, Eos Transactions, Poster

Barckhausen U, Gibbons A, Hoernle K, Werner R, Hauff F, Mueller RD (2008): Seafloor Spreading Anomalies of the South-Eastern Indian Ocean Revisited. AGU Fall Meeting, San Francisco, California, USA, Eos Transactions, Vortrag

Werner R, Hoernle K, Hauff F, Barckhausen U, Heydolph K, SO199 Fahrtteilnehmer (2009) Hintergrund und erste Ergebnisse von SO199 CHRISP (Christmas Island Seamount Provinz und der Investigatorrücken): Alter und Ursachen von Intraplattenvulkanismus sowie die geodynamische Entwicklung des südöstlichen Indischen Ozeans. Tagungsband SONNE Statusseminar, 12-13 Februar, Bremerhaven, p27-30, Vortrag

Neuhaus B (2009) Untersuchungen zur Biodiversität und zum Lebenszyklus der Meiofauna des Manihiki Plateaus, Investigator Rückens und Wharton Beckens (Ausfahrten SO 193, SO 199). Tagungsband SONNE Statusseminar, 12-13 Februar, Bremerhaven, p49-53, Vortrag

Hauff F, Hoernle K, Bogaard Pvd, Werner R, Kipf A, Conrad S, Garbe-Schönberg D, Barckhausen U (2011) SO199 CHRISP (Christmas Island Seamount Provinz und der Investigatorrücken): Alter und Geochemie einer enigmatischen Seamountsprovinz. Tagungsband SONNE Statusseminar, 09-10 Februar, Hannover, Vortrag

Danksagung

Wir danken dem BMBF für die gewährte Unterstützung und dem Projektträger PtJ-Warnemünde für die unbürokratische administrative Abwicklung. Unser besonderer Dank gilt Kapitän Mallon sowie der Besatzung des F.S. “Sonne” für ihre hervorragende Kooperation während der Ausfahrt. Sehr dankbar sind wir auch R.D. Müller und C. Heine, die uns teilweise unveröffentliche Daten sowie viele andere wertvolle Informationen für SO199 CHRISP zur Verfügung gestellt haben. Darüber hinaus danken wir Geoscience Australia, die uns bathymetrische Daten von früheren Ausfahrten im Arbeitsgebiet von SO199 zur Verfügung stellten. Weiterer Dank gilt dem Auswärtigen Amt in Berlin und der deutschen Botschaft in Canberra, die uns bei der Beantragung der Forschungsgenehmigungen in hervorragender Weise unterstützten. Die Teilnahme von A. Gibbons an SO199 wurde durch die University of Sydney finanziert, die biologischen Untersuchungen wurden durch die “Freunde und Förderer des Museums für Naturkunde e.V.”, die “Johanna und Fritz Buch Gedächtnis-Stiftung” und die “Thermo Electron Corporation” unterstützt.

Verzeichnis der Anlagen

- Anlage 1: Erfolgsprotokollbericht
- Anlage 2: Vorabdruck der Arbeit Hoernle et al.
- Anlage 3: Vorabdruck der Arbeit Barckhausen et al.
- Anlage 4: Vorabdruck der Arbeit Neuhaus
- Anlage 5: Bescheinigungen BSH und Pangaea

Anlage 1

Erfolgsprotokollbericht

1. Beitrag der Ergebnisse zu den förderpolitischen Zielen des Förderprogramms

Das Forschungsvorhaben SO199-CHRISP war eingebettet in das Meeresforschungsprogramm des BMBF und berührt vor allem unter “Marine Geowissenschaftliche Forschung” genannte Aufgaben (… der Beschaffenheit der ozeanischen Kruste, …. den Prozessen bei der Sediment- und Lagerstättenbildung sowie dem Stoffaustausch an der Grenzfläche des Meeresbodens). So wurden u.a. neue Erkenntnisse über die Morphologie des Ozeanbodens, über Aufschmelzprozesse im oberen Erdmantel und die Ursachen von Intraplattenvulkanismus im ozeanischen Bereich sowie plattentektonische Prozesse gewonnen, die nicht nur in der geowissenschaftlichen Grundlagenforschung eine hohe Priorität besitzen (u.a. im Integrated Ocean Drilling Program oder bei “Great Plume Debate”), sondern auch umweltpolitische und wirtschaftliche Relevanz haben. Die im Rahmen von SO199-CHRISP untersuchten magmatischen Prozesse waren bzw. sind ursächlich für submarine Vulkanausbrüche und Fluidaustritte, die z.B. einen erheblichen Einfluss auf chemische und physikalische Eigenschaften des Meerwassers haben. Um dessen Bedeutung und Folgen für die (marine) Umwelt besser zu erfassen, ist die Kenntnis der vulkanischen und hydrothermalen Aktivität zugrundeliegenden Prozesse essentiell. Ferner ergaben die während SO199-CRISP durchgeführten Untersuchungen Hinweise auf rezente Tektonik im Whartonbecken, die höchstwahrscheinlich mit einer internen Deformation der indo-australischen Platte im Zusammenhang steht. Diese Beobachtungen und Daten sind für die Erstellung von Risikoanalysen (hier: Intraplattenbeben) bedeutsam. Auch die bei SO199-CHRISP durchgeführten biologischen Untersuchungen sind von hohem Interesse, denn es muß z.B. vor dem Isolieren neuer pflanzlicher oder tierischer Wirkstoffe bekannt sein, welche Art den interessierenden Stoff produziert. Weiterhin lassen sich Organismen nur dann als Teile eines Ökosystems verstehen und es kann nur dann ein langfristiges Monitoring von Organismen durchgeführt sowie Veränderungen erkannt werden (Stichwort: Global Change), wenn man die Lebewesen auch identifizieren kann, deren Ansprüche an die Umwelt man erkennen möchte. Die Erfassung und das Monitoring mariner Biodiversität erfüllt eine der Hauptaufgaben im Sinne der "Convention on Biological Diversity" (CBD), die durch die Bundesregierung 1993 ratifiziert wurde. Dies gilt umso mehr vor dem Hintergrund bisher nicht genutzter, möglicher Resourcen biogener Wirkstoffe, die in diesem Vorhaben in Form der Bryozoen/Mikroorganismen-Assoziationen untersucht werden.

Unsere Arbeitsansätze tragen somit hinsichtlich der meereswissenschaftlichen Grundlagenforschung, aber auch hinsichtlich der angewandten Forschung zu den förderpolitischen Zielen des BMBF bzw. der Bundesregierung bei. Die Veröffentlichung der Ergebnisse in der Fachliteratur hat zudem auch einen Werbeeffekt für die deutsche Meeresforschung, aus dem Nachfrage nach Expertise, Verfahren und Instrumenten erwachsen mag.

2. Wissenschaftlich-technische Ergebnisse des Vorhabens

Die wissenschaftlichen Ergebnisse von SO199-CHRISP sind in Abschnitt II.1. des Schlussberichts und in den dem Schlussbericht beigelegten Manuskripten sowie im Fahrtbericht ausführlich beschrieben. Auf Tagungen wurde über das Projekt berichtet und weitere Arbeiten, die auf den vorgelegten Ergebnissen aufbauen, sind in Planung. Einige der wichtigsten Ergebnisse sind:

- die Alter der Vulkane der Christmas Island Seamount Provinz (ohne Weihnachtsinsel) reichen von 136 bis 47 Mill. Jahren und zeigen eine grobe Ost-West-Altersprogression,
- plattentektonische Rekonstruktionen sind nicht konsistent mit der Bildung der Christmas Island Seamount Provinz über einem einzigen, ortstabilen Hotspot,

- die geochemische Zusammensetzung der Vulkane der Christmas Island Seamount Provinz reicht von angereichteren mittellozeanischen Rückenbasalt (MORB) bis zu sehr stark angereicherten Zusammensetzungen, die eher für kontinentalen Vulkanismus typisch sind,
- die Bildung der (meisten) Vulkane der Christmas Island Seamount Provinz wird auf subkontinentalen lithosphärischen Mantel (und eventuell untere Kruste) zurückgeführt, der während des Gondwanaaufbruchs delaminierte,
- die analysierten Gesteine vom Investigatorrücken sind 153 bis 62 Mill. Jahre alt, weisen alle angereichertere geochemische Signaturen auf als atlantischer oder pazifischer MORB und ähneln in ihrer Zusammensetzung dem heutigen indischen MORB,
- die geochemisch angereichtere Signatur des Mantel unter dem Indik („Indian Mantle Domain") existiert demnach wahrscheinlich seit dem späten Jura,
- die Beimischung von subkontinentaler Lithosphäre in den indischen Mantel kann die „Indian Mantle Domain" erklären,
- in großen Teilen des Arbeitsgebietes von SO-199 CHRISP gibt es Hinweise auf rezente Tektonik, besondere ausgeprägt mit der linkslateralen Reaktivierung von Bruchzonen im Bereich des Investigatorrückens und seiner benachbarten Gebiete,
- im Bereich zwischen dem Investigatorrücken und dem Ninety East Ridge deutet die linkslaterale Reaktivierung von Bruchzonen auf eine diffuse, sich entwickelnde Plattengrenze hin, an der die indo-australische Platte auseinander bricht,
- im Bereich dieser sich entwickelnden Plattengranze sind weitere (Intraplatten)beben zu erwarten,
- östlich des nördlichem Teils des Investigatorrückens wurden die Anomalien 33n und 33r identifiziert,
- am südlichen Investigatorrücken wurden jurassische magnetische Anomalien identifiziert,
- eine Abfolge jurassischer und kretazischer Anomalien mit einem Sprung der Rückenachse im Argobecken wurde identifiziert,
- die Tiefsee-Sedimente im Arbeitsgebiet von SO199-CHRISP weisen einen typischem Gehalt an organischem Kohlenstoff auf,
- die strömungszugewandten Ostflanken der Seamounts/Rücken weisen eine sehr diverse Benthosfauna auf,
- eine diverse Meiofauna mit neuen Merkmalen im Lebenszyklus der Kinorhyncha und Loricifera wurde identifiziert.

3. Einhaltung der Zeit- und Ausgabenplanung

Der im Antrag vorgestellte Finanzierungs- und Zeitplan wurde weitestgehend eingehalten. Die einzigen wesentlichen Abweichungen waren:

(1) Die unter den Positionen 0842 und 0845 bewilligten Mittel für die An- und Abreise zur SO199-Expedition wurden nicht vollständig benötigt. Diese Einsparung ergab sich vor allem daraus, dass etwas günstigere Flüge gebucht werden konnten als dies zum Zeitpunkt der Antragstellung (Herbst 2007) zu erwarten war.

(2) Wie im Abschlussbericht erläutert erstreckte sich die Aufbereitung und Analytik der während SO199 gewonnenen Hartgesteine über einen längeren Zeitraum als urprünglich geplant und konnte erst im Spätsommer 2010 abgeschlossen werden (Planung: Ende 2009). Grund hierfür war neben mit der Abschaffung des IFM-GEOMAR-eigenen RFA-Labors verbundenen Umstellung auf externe Hauptelement-Analytik vor allem, dass während SO199 mehr Gesteinsproben gewonnen wurden als von uns ursprünglich erwartet worden war. Um diesen einzigartigen Probensatz umfassend zu nutzen bzw. auszuwerten, wurden erheblich mehr Gesteinsdünnschliffe angefertigt bzw. ausgewertet und Ar/Ar-Datierungen durchgeführt als für SO199 beantragt worden sind. Auch die Anzahl der geochemischen Analysen übersteigt bei den meisten Methoden die im Antrag genannten Zahlen. Der Großteil der über das Antragsvolumen hinaus angefertigten Dünnschliffe, Datierungen und Analysen sowie die Analytik der Proben von der Weihnachtsinsel (Diplomarbeit Conrad) wurde durch Eigenmittel

des IFM-GEOMAR finanziert, einer kleiner Teil dieser Kosten im Rahmen der 20% Überziehung einzelner Position. (s. Punkt 3).
(3) Die in der Position 0845 für 2009 bewilligte Reise zur AGU-Herbsttagung in San Francisco wurde nicht angetreten, da erste Ergebnisse von SO199-CHRISP bereits auf der AGU-Herbsttagung 2008 vorgestellt worden sind (Beiträge von Barckhausen et al. und Werner et al.) und Endergebnisse später dort präsentiert werden sollen (finanziert aus Eigenmitteln). Die für die AGU-Herbsttagung 2009 bewilligten Mittel wurden im Rahmen der 20% Überziehung einzelner Position für die Analytik verwandt.

4. Verwertbarkeit der Ergebnisse

Durch den erfolgreichen Verlauf des Forschungsvorhabens SO199-CHRISP liegt ein umfassender Datensatz vor, der zu einem besseren Verständnis von den Ursachen von Intraplattenvulkanismus, der geodynamischen Entwicklung des Südost-Indiks und der Biodiversität und Biogeographie in diesem Bereich beiträgt. Die Ergebnisse werden in der internationalen Fachliteratur publiziert und damit allgemein zugänglich gemacht. Sie bilden nicht nur wichtige Grundlagen für laufende Projekte, sondern stellen auch die Basis für weiterführende Programme dar. Dabei handelt es sich vornehmlich um rein wissenschaftliche Zielsetzungen, die jedoch auch eine umweltpolitische und wirtschaftliche Relevanz haben. Weiterhin wurden Daten und Ergebnisse, soweit sinnvoll (z. B. Bathymetrie, Biologie [s.u.]), an die internationalen Datenbanken transferiert. Auch wurden Proben und Daten Anrainerstaaten direkt zur Verfügung gestellt, u.a. wurde auf Bitte von Geoscience Australia Teile der Basis der Weihnachtsinsel auskartiert und Sedimentproben zur Verfügung gestellt. Die bei SO199-CHRISP gewonnenen Ergebnisse, Daten und Proben können somit zu Fragen der Seerechtskonvention, für die zukünftige Abschätzung mineralischer und biologischer Rohstoffe, für Fragen des Umweltschutzes und für Risikoanalysen (Vulkanismus, Erdbeben, Hangrutschungen, Klimaänderung) von den dafür zuständigen nationalen und internationalen Stellen genutzt werden.
Das zoologische Material der SO199-Expedition wird in die über 22 Millionen zoologische Individuen umfassenden Sammlungen des größten deutschen naturkundlichen Forschungsmuseums, des Museums für Naturkunde Berlin, integriert werden. Das bedeutet, dass die neuen Arten und ihr Verbleib über die Originalpublikationen und eine Datenbank recherchierbar sein werden und damit der internationalen Wissenschaftlergemeinschaft zur Verfügung stehen. Diese Verfügbarkeit wird zudem für neu beschriebene Arten zwingend durch die 4. Fassung des *International Code of Zoological Nomenclature* vorgeschrieben. Die Ergebnisse zu den Kinorhyncha werden in die Weltartenliste der Kinorhyncha im UNESCO-IOC *Register of Marine Organisms* eingetragen. Das gleiche gilt für die europäische Artenliste des von der EU im MAST III (Marine Science and Technology) Programm geförderten *A register of marine species in Europe to facilitate marine biodiversity research and management* (= *European Registry of Marine Species*).

5. Erfindungen, Schutzrechtsanmeldungen und erteilte Schutzrechte

Erfindungen und Schutzrechtsanmeldungen wurden im Rahmen des Projektes SO199-CHRISP nicht gemacht, es wurden auch keine Schutzrechte erteilt.

6. Arbeiten, die zu keiner Lösung geführt haben

Die im Projektantrag formulierten Zielsetzungen des Vorhabens konnten weitestgehend erreicht werden. Aus den gewonnenen Daten und Ergebnissen haben sich aber einige neue Fragestellungen ergeben, deren Bearbeitung Gegenstand zukünftiger Forschungsvorhaben sein wird.

Anlage 2

The Investigator Ridge and Christmas Island Seamount Province, Indian Ocean: Evidence for the Recycling of Continental Lithosphere during Gondwana Breakup

K. Hoernle, F. Hauff, R. Werner, P. van den Bogaard, A. Kipf, U. Barckhausen, A. Gibbons, D. Müller, D. Garbe-Schönberg and S. Conrad

Abstract

A fundamental question is the extent and origin of heterogeneity in the Earth's upper mantle, in particular why Indian and South Atlantic mid ocean ridge basalts (MORB) have more enriched compositions (referred to as DUPAL anomaly) than those from the Pacific and North Atlantic mid ocean ridges. In order to address this question, we sampled the north-south-trending Indian Ocean Floor along the Investigator Ridge (Fracture Zone) from 10-17°S and the east-west-trending Christmas Island Seamount Province (CHRISP) in the northeastern Indian Ocean, extending from the Argo Basin to Christmas Island and the Vening Meinez Seamounts to the seamounts surrounding Cocos/Keeling Island in the Wharton Basin on the R/V SONNE 199 CHRISP cruise. Here we report the first age (Ar/Ar) and geochemical (major and trace element and Sr-Nd-Hf-Pb DS isotopic) data from a continuous sequence of Jurassic to Eocene Indian MORB crust (with age dates ranging from 153-62 Ma) and from the CHRISP seamount chain (136-4 Ma). The Investigator ridge volcanic and plutonic samples have incompatible element characteristics and Sr-Nd-Pb-Hf isotopic compositions more enriched than present-day North Atlantic or Pacific MORB but are similar to more enriched present-day Indian MORB, suggesting that the Indian upper mantle has had its distinct composition since the late Jurassic. The seamount samples show a crude age decrease from the Argo Basin (136 Ma), to the Eastern Wharton Basin (115-94 Ma) to the Central Wharton Basin (96-64 Ma) to the Cocos-Keeling seamounts (56-47 Ma) in the western Wharton Basin. Samples from Christmas Island and its flanks, located between the Eastern and Central Wharton Basin provinces, yielded significantly younger ages of 44-37 and 4.4 Ma, not consistent with an age progression. The samples from the seamounts and Christmas Island range from basalt to trachyte and basanite to tephri-phonolite and have incompatible element characteristics similar to ocean island basalts (OIB). The isotopic compositions (e.g. 206Pb/204Pb = 17.3-19.3; 207Pb/204Pb = 15.49-15.67; 143Nd/144Nd = 0.51220-0.51295; 176Hf/177Hf = 0.28246-0.28319) range from enriched MORB (or the common "C" component) to very enriched compositions more typical of continental than oceanic volcanism. Lamproitic rocks from western Australia, India and other continental areas, derived from metasomatized lithospheric mantle, could serve as the enriched endmember. Despite the crude east to west age progression, plate tectonic reconstructions are not consistent with the formation of Christmas Island seamount province with a single fixed hotspot. The highly enriched compositions of the Eastern and Central Wharton Basin volcanic provinces and their formation on young seafloor formed shortly after the separation of Greater India from Australia and Antarctica suggest that these volcanic rocks are derived from subcontinental lithospheric mantle and/or lower crust delaminated during the Gondwana breakup. Incorporation of subcontinental lithosphere into the Indian upper mantle could also explain the more enriched composition of Indian MORB compared to Pacific and North Atlantic MORB.

Introduction

The geochemistry of oceanic basalts from mid-ocean ridges and volcanic islands and seamounts provide important insights into the composition of the Earth's mantle (e.g. Hofmann et al., 1997). It is commonly believed that mid-ocean ridges sample the upper mantle, whereas volcanic chains on the seafloor, with an age progression in the direction of plate motion, bring material from a deep boundary layer, such as the upper/lower mantle or core/mantle boundary, to the Earth's surface. Isolated seamounts and chains of volcanoes that don't show age progressions in the direction of plate motion can also provide information about upper mantle heterogeneity (e.g. Hirano et al., 2006; Geldmacher et al., 2008).

Based on the composition of mid ocean ridge basalts (MORB), the upper mantle beneath the Indian and South Atlantic Oceans are enriched compared to that beneath the Pacific and North Atlantic Oceans (e.g. Dupre and Allegre, 1983; Storey et al., 1989). Compared to North Atlantic and Pacific MORB, Indian and South Atlantic MORB require enriched components with low 206Pb/204Pb, 143Nd/144Nd and 176Hf/177Hf but higher 207Pb/204Pb, 208Pb/204Pb and 87Sr/86Sr isotope ratios (Escrig et al., 2004). The more enriched composition of Indian and South Atlantic MORB are often referred to as the DUPAL anomaly (e.g. Hart, 1984). A variety of models have been proposed to explain the origin of the DUPAL isotopic signature in Indian MORB. These include contamination of the Indian upper mantle by 1) ancient subduction processes (Kempton et al., 2002; Rehkämper and Hofmann, 1997), 2) a plume, such as the Kerguelen plume (Storey et al., 1989), and 3) subcontinental lithospheric mantle (SCLM) or lower crust delaminated/detached during the breakup of Gondwana (e.g. Mahoney et al., 1996; Escrig et al., 2004; Hanan et al., 2004; Geldmacher et al., 2008). Determining the origin of the enriched signature (DUPAL anomaly) in the Indian upper mantle is essential for understanding upper mantle heterogeneity, one of the major goals of chemical geodynamics (e.g. Escrig et al., 2004). One of the major goals of our study was to investigate the composition of Jurassic to Eocene Indian oceanic crust in the Wharton Basin, northeastern Indian Ocean, sampled along the Investigator Ridge during the R/V SONNE (SO199) CHRISP expedition, to see how far back the DUPAL isotopic signature can be traced in Indian MORB.

The Christmas Island Seamount Province (CHRISP) is located between ~ 10°S and ~ 15°S and ~ 95°E and ~ 109°E and extends from the Argo Basin in the east through the Wharton Basin and across the Investigator ridge, covering ~1,000,000 square kilometers (Fig. 1). The Seamount Province extends in an E-W direction and therefore orthogonally to the NNE-direction of present plate motion (~75 mm/yr) in the Wharton Basin, which is not consistent with an origin by a "classical" fixed mantle plume. Plate motion in the past, as evidenced by the bend in the strike of the Investigator Ridge towards the south, was however more east-west and therefore age data and good tectonic reconstructions are essential for determining the origin of these seamounts. Although faults through the ocean crust may have facilitated the rise of some magmas to the surface, it is unlikely that the existence and evolution of the Seamount Province is exclusively controlled by the faults and fracture zones, since all recognizable faults and fracture zones (e.g., Investigator Ridge) have a N-S strike in the northeast Indian Ocean. A second major goal of this study was to determine the origin of this seamount province and to determine if the sources of the seamounts could have affected the chemistry of the Indian upper mantle. Combining geochemical and age data from samples obtained on the SO199 expedition with magnetic data and plate tectonic reconstructions, we propose a non-plume model for the formation of this volcanic chain. This model can also explain the enriched composition of the Indian upper mantle.

Geological Overview

The Investigator Ridge is a ~1,700 km long, roughly N-S striking bathymetric high (Fig 1) that extends from ~2°S, where it is being subducted beneath Sumatra, to ~18°S, where it curves to the east towards Australia. The ridge represents the most prominent of the numerous N-S to NNW-SSE striking faults in the ocean crust of the Wharton Basin. Due to different histories for the seafloor on both sides of the Investigator Ridge, the ridge is thought to represent a fracture zone. Ar/Ar age dating shows that the crust on the western side of the ridge ranges in age from Eocene in the north and increases systematically to Jurassic in the south, formed by continuous, slow spreading (c. 11 mm/yr; Barckhausen et al., in prep.). Magnetic data from the ocean crust on the eastern side of the Investigator Ridge indicates that the crust formed over a similar age range as the crust on the western side but appears to have

formed by faster spreading with several ridge jumps. Samples in this study come primarily from the western side of the Investigator Ridge and thus appear to come from the western side of the original transform fault between ~7-18°S. The samples from the western Investigator Ridge crust range in age from 153 Ma at about 17°S to 62 Ma at ~10°S. The samples to the north of 10°S are expected to be younger than 62 Ma and may extend into the Eocene. Sushchevskaya et al. (2000) discuss the geochemistry of basalts dredged at one site at the southern Investigator Ridge and a second site on the ocean crust somewhat to the west. These samples range in composition from MORB-type tholeiites to alkali basalts and show enriched lead isotope ratios. To our knowledge, further rock samples or detailed bathymetric data from the Investigator Ridge have not been published.

The CHRISP is characterized by approximately 50 large, up to 4,500 m high seamounts (including Cocos/Keeling Atoll, Muirfield Seamount, Vening-Meinesz Seamounts and Christmas Island) and numerous smaller submarine volcanic and tectonic features. Before the SO199 cruise, there was almost nothing known about the morphology, age, chemical composition and origin of this huge seamount province. Based on seafloor morphology, we have divided the Christmas Island Seamount Province (CHRISP) into four sub provinces or groups (Fig. 1): 1) Argo Basin Volcanic Province (AP), located in the Argo Basin in the easternmost part of the northeast Indian Ocean, 2) Eastern Wharton Basin Volcanic Province (EWP), located in the eastern Wharton Basin to the southwest of Christmas Island, 3) Central Wharton Basin Volcanic Province (CWP), which includes the Vening Meinesz seamounts and is located to the southeast of Christmas Island but east of the Investigator Rise, and 4) the Cocos-Keeling Volcanic Province (CKP), which is located in the western Wharton Basin to the west of the Investigator Rise. Not included in these sub-provinces is Christmas Island, which lies between the EWP and CWP and slightly further north. It is the closest volcanic structure to the Java trench on the outer rise of the incoming Indo-Australian plate. Outsider Seamount is also not included in the sub provinces, because it is about 5° to the north of the CKP, also west of the Investigator Rise.

The most information to date about the CHRISP comes from Christmas Island. This island has undergone substantial uplift as evidenced by the thick subaerially-exposed carbonate sequences. The uplift is presumably related to the flexure of the Indo-Australian plate outboard the Java trench (Woodroffe ,1988). On Christmas

Island two volcanic successions have been identified (Woodroffe ,1988). The „lower series“, consists of a lower unit (andesites to trachybasalts), intercalated with Upper Eocene limestones of the Lower Carbonate Series, and an upper unit (basalts to andesites and trachybasalts), intercalated and overlain by Late Oligocene and Miocene limestones of the Upper Carbonate Series (e.g., Trueman 1965, Woodroffe 1988). Based on Ar/Ar age dating (Falloon, written communication; this study), we identify a younger Pliocene volcanic event also, which appears to have been included in the upper unit of Trueman (1965).

In contrast to Christmas Island, the Cocos/Keeling Atolls, located ~900 km to the west, are subsiding. Charles Darwin visited these islands in 1836 when he developed his well-known theory of atoll formation (Darwin, 1842), which has gained wide acceptance. He proposed that the growth of coral reefs continues during and after the subsidence of the seamount. The thickness of the corals underlying the Cocos/Keeling Atolls is not known, but dredging of basaltic rocks in local waters suggest that it is on the order of 500 – 1,000 m (Pulu Keeling National Park Plan of Management, 1999, http://www.environment.gov.au/parks/publications/cocos/management-plan.html).

Only a few of the submarine structures of the Christmas Island Seamount province had been sampled before the SO199 CHRISP cruise. Dredging on the RV Argo (1 dredge according to Exon et al., 1993), RV Vityaz (Bezrukov and Andrushenko, 1974), RV Franklin (Fallon et al., 1989) and RV Rig Seismic (Exon et al., 1993) yielded alkali basaltic and trachytic lavas as well as various volcaniclastic rocks from the base of Christmas Island and adjacent seamounts. However, many of these samples have not been analyzed or the data have not yet been published. During DSDP Leg 22, three sites were drilled into the ocean crust in the area of the Christmas Island Seamount Province. Site 211 is located to the northwest of Christmas Island and yielded amphibole-bearing basalts overlain by Campanian (?) sediments. K/Ar dating of doleritic sills, which penetrated these sediments, yielded an age of 71±2 Ma (McDougall, 1974). Site 212 to the south and Site 213 to the west of Christmas Island yielded altered pillow basalts with Indian mid ocean ridge basalt (MORB) type compositions (Hekinian, 1974). Prior to the SO199 CHRISP expedition, the sample and data set for the CHRISP was not adequate to enable the reconstruction of the origin and evolution of this huge submarine volcanic province.

During the R/V SO199 CHRISP Expedition, 54 seamounts were at least partially mapped with the Simrad EM 120 multi-beam echosounding system on board the Sonne and 38 were sampled via dredging. Multi-beam mapping revealed a broad variety of seamount morphologies within the CHRISP. The most abundant volcanic structures are large guyots, uneroded circular or oval-shaped seamounts, and volcanic ridges. Guyots represent former ocean island volcanoes that were eroded to sea level and subsequently subsided beneath sea level. Guyots or guyot-like structures occur in all CHRISP sub-provinces. They measure up to 50 x 70 km at their base and rise up to 4,500 m above the surrounding sea floor. The water depth of their erosional platforms varies between 1,200 m and 3,000 m, but do not show any clear regional systematics. Notably, uneroded volcanic cones on the guyot platforms are common, indicating revival of volcanic activity after subsidence of the guyots below sea level. Uneroded seamounts range from small, isolated cones, measuring only a few kilometer in diameter and ~100 m in height, up to 4,500 m high volcanoes with more than ~50 km basal diameter. The ridge-like structures are up to ~100 km long and mainly alongated in a roughly N-S direction. Many of the ridges appear to consist of two or more seamounts that merged during their formation. Another morphological structure are large plateau-like features with an uneven surface, which cover an area of up to ~15,000 km^2 (according to predicted bathymetry) and rise from ~5,500 m up to 1,500 – 2,000 m above the surrounding ocean floor. These "plateaus" are restricted to the Central Wharton Basin Volcanic Province. In summary, the CHRISP comprises very diverse volcanic structures including (former) volcanic islands similar in size to the recent Canary Islands. The volcanic cones on the guyot platforms, uneroded seamounts that are higher than nearby guyots, the varying depth of the erosional platforms, and the variety of morphologies suggest a complex, long-lasting history of the CHRISP sub-provinces with several phases of volcanic activity. As pointed out above for the orientation and width of the CHRISP, these morphological observations are also inconsistent with an origin by a "classical" fixed mantle plume.

Methods

40Ar/39Ar age dating

125 mineral and matrix separates from 80 dredged rock samples (SO199-DR-1 to –DR-87) and 13 land samples (Christmas Island; SO199-CH1 to –CH13) were

analyzed by 40Ar/39Ar laser step-heating. Crystals (plagioclase, K-feldspar, hornblende) matrix and glass particles were hand-picked from crushed and sieved splits (250-500µm). Feldspar separates were etched in 15% hydrofluoric acid for 5 minutes in order to remove alteration surfaces and adhering matrix material. All samples were washed and cleaned using an ultrasonic disintegrator.

Separates were irradiated in aluminum trays and cans lined by cadmium foil at the 5-MW reactor of the GKSS Research Center (Helmholtz-Zentrum Geesthacht, Germany). The neutron flux was monitored using Taylor Creek Rhyolite Sanidine (TCR-2: 27.87 ± 0.04 Ma; Lanphere and Dalrymple, 2000). 40Ar/39Ar laser step-heating analyses were carried out at the IFM-GEOMAR Geochronology Lab using a 20W SpectraPhysics Argon-Ion laser and an MAP 216 series noble gas mass spectrometer. Ar Isotope ratios from mass spectrometry were corrected for mass discrimination, background and blank values, J-value gradients, and interfering neutron reactions on Ca and K.

The step-heating data are evaluated in age spectra (apparent age and error vs cumulative 39Ar) trying to detect plateaus (>3 consecutive steps comprising >50% of the 39Ar released, with ages overlapping within 2Sigma errors), plateau ages representing the inverse-variance weighted mean of the plateau step ages and errors. The MSWD (mean square weighted deviates; should be <<3) and POF (probability of fit; should be >0.05 at 2 Sigma / 95% confidence levels) are calculated to test the statistical robustness of the plateaus and plateau ages (Baksi, 1999). Because many of the SO199 marine and land samples are variably strongly altered, the degree of alteration was monitored critically by calculating alteration indices based on the measured 36Ar/37Ar ratios (plagioclase, hornblende, matrix, basaltic glass) or measured 36Ar/39Ar ratios (K-feldspar) following the methods established by Baksi (2007).

Consequently, the results of 75 step-heating analyses which yielded scattered age spectra, too small plateaus (39Ar<<50%), statistically invalid plateaus (POF<<0.05), or large-error pseudo-plateaus were rejected. All of these exhibit excessively high alteration indices (36Ar/37Ar) throughout the age spectra, reflecting a significant uptake of (atmospheric) 36Ar during alteration, and indicating variable violations of the “closed system” assumption, such as gain or loss of the parent/daughter after formation/closure.

Fifty step-heating analyses yield statistically valid plateau ages and plateau range alteration indices around and close to the cut-off values for fresh sample material suggested by Baksi (2007). Low-temperature heating steps generally yield 10 to 100 times higher alteration indices, but are not included in the plateau age calculation. Results are summarized in Table 1.

Major and trace element and isotope geochemistry

Samples selected for geochemistry were first crushed to small pieces, then washed in de-ionized water and carefully handpicked under a binocular microscope. Whole rock powders were then made using an agate mortar and swing mill. Major elements of most whole rock samples were determined on fused beads using a Phillips X'Unique PW1480 X-ray fluorescence spectrometer (XRF) equipped with a Rh-tube at IFM-GEOMAR. H_2O and CO_2 were analyzed in an infrared photometer (Rosemount CSA 5003). A subset of samples (marked with an asterix (*) were analyzed at AcmeLabs by ICP-OES using a lithium metaborate/tetraborate fusion technique. For analytical details see www.acmelabs.com. The major element data are shown in Supplement Table 1 and the data shown in the plots are normalized to 100% on a volatile free basis. The values obtained for the JB-2, JB-3, JA-2 and JR-1 (N=3) standards on the IFM-GEOMAR XRF and for BIR-1 (N=2), BHVO-2, BCR-2, AGV-2 and SO18 (N=4) standards obtained at Acme Labs are shown in Supplement Table 2. Trace element concentrations were determined by ICP-MS on an Agilent 7500cs ICPMS at the Institute of Geoscience (IfG) of the Kiel University after the methods of Garbe-Schönberg (1993) and are shown in Supplement Table 1. A subset of samples (marked with an asterix (*) were analyzed at Acme Labs by ICPMS following a lithium metaborate/tetraborate fusion technique. Results for the standards (BIR-1 (N=5), BHVO-2 (N=4), BCR-2 (N=3), AGV-2 (N=2) and the Acme in house standard SO18 (N=4) are displayed in Supplement Table 3. A total of 8 samples were replicated by means of separate digestions (Supplement Table 5) and are within 0.1 to 2 % for most elements at the IfG (Kiel) and between 1 to 4% for a single replicate analyses at Acme Labs. Machine reproducibility of the Agilent 7500cs ICPMS was monitored by running multiple analyses of a sample digest over the course of an analytical session (Supplement Table 5) and is found to vary by less than 1% for moderately enriched samples (SO199 DR56-1; OIB) and between 1-3 % for highly depleted material (SO199 DR23-19; MORB-Gabbro).

Sr-Nd-Pb (Double Spike (DS)) isotope analyses were determined on leached rock chips (2N HCl at 70°C for 1 hour and triple rinsed with ultrapure water thereafter). Powders used for Hf isotope analyses were not leached. The element chromatography followed the methods of Hoernle and Tilton (1991) and Hoernle et al. (2008). Sr-Nd-Pb isotopic ratios were analyzed in static multi-collection on the TRITON and MAT262 RPQ2+ thermal ionization mass spectrometers (TIMS) at IFM-GEOMAR. Sr and Nd isotopic ratios are normalized within run to $^{86}Sr/^{88}Sr$= 0.1194 and $^{146}Nd/^{144}Nd$= 0.7219 respectively. All Sr isotope data are reported relative to NBS987 $^{87}Sr/^{86}Sr$= 0.710250 with an external 2s error of ±0.000014 (N=14) for the MAT262 and 2s of ±0.000010 (N=18) for the TRITON. Similarly the Nd isotope data (exclusively determined on the TRITON) are reported relative to La Jolla $^{143}Nd/^{144}Nd$= 0.511850± 0.000006 (N=22). Double Spike corrected NBS 981 values (N=72) gave $^{206}Pb/^{204}Pb$= 16.9417± 0.0033, $^{207}Pb/^{204}Pb$= 15.4998± 0.0032, $^{208}Pb/^{204}Pb$= 36.7250± 0.0083, $^{207}Pb/^{206}Pb$= 0.91489± 0.00004 and $^{208}Pb/^{206}Pb$= 2.16773± 0.00011. These values compare well with published double and triple spike data for NBS981 (Baker et al., 1994; Galer and Abouchami, 1998; Thirlwall, 2000; Thirlwall, 2002; Baker et al., 2005). For details of the Pb-DS technique see Hoernle at al. (accepted with minor revisions). Hf chemistry was carried out following the methods of Blichert-Toft et al. (1997) and isotope ratios were measured in static mode on a VG Elemental AXIOM multi-collector magnetic sector inductively coupled plasma mass spectrometer (MC-ICP-MS) at IFM-GEOMAR. Our in-house SPEX Hf ICP standard solution (Lot #9) yields an averaged, JMC 475-normalized value of $^{176}Hf/^{177}Hf$= 0.282173± 0.000008 (n= 132). A detailed description of the Hf analytical procedures is found in Geldmacher et al. (2006). Total chemistry blanks were <100 pg for Sr, Nd, Hf and Pb and thus considered negligible.

Results

Jurassic to Eocene volcanic and plutonic rock samples from the Investigator Rise between 7-18°S were analyzed for major element, trace element and Sr-Nd-Hf-Pb DS isotopic composition (Supplement Table 1, Table 2). The volcanic samples range from tholeiitic basalts to trachybasalts (Fig. 2) and the plutonic samples are predominantly gabbroic. The Investigator ridge samples have low $(La/Sm)_n$ and $(Sm/Yb)_n$ ratios (generally <2.2), reflecting relatively flat REE and incompatible

element patterns on multi-element diagrams (Fig. 3) and low highly to moderately incompatible element (e.g. (La, Ta, Nb, Th)/(Yb, Y)) ratios (Fig. 4). The Investigator Ridge igneous samples have incompatible element characteristics and Sr-Nd-Pb-Hf isotopic compositions more enriched than present-day North Atlantic or Pacific MORB but overlap with the enriched part of the present-day Indian MORB field (Fig. 5), excluding samples from the Southwest Indian Ridge (SWIR between 39-41°E). On the Pb isotope diagrams, the present-day Indian (excluding SWIR 39-41°E), Pacific and North Atlantic MORB fields and the Investigator samples form positive arrays, but the Investigator array has a slightly shallower slope than the present-day MORB fields. Whereas the fields for present-day Pacific and North Atlantic MORB form negative correlations on diagrams of 206Pb/204Pb vs. 143Nd/144Nd and 176Hf/177Hf isotope ratios, the Jurassic to Eocene Investigator samples form a trend with a slightly positive slope that only overlap these MORB fields at high 206Pb/204Pb but overlap the enriched (with lower Nd and Hf isotopic compositions) part of the Indian MORB field. In summary, all present-day MORB fields (Pacific, North and South Atlantic and Indian) extend from a common "C" type component (Hanan and Graham, 1996) to a depleted (DM) type of component. The present-day Indian and South Atlantic MORB fields also require the presence of an EM1 type of component. In contrast, the Investigator samples extend from the common C component to an enriched type of component.

The CHRISP seamount samples show a crude decrease in age from the Argo Basin (136 Ma), to the Eastern Wharton Basin (115-94 Ma) to the Central Wharton Basin (96-64 Ma) to the Cocos-Keeling seamounts (47-56 Ma) in the western Wharton Basin (Fig. 1; Table 1). Outsider seamount to the north of the Cocos-Keeling seamounts was dated at 53 Ma, yielding a similar age to the Cocos-Keeling seamounts. Samples from Christmas Island and its flanks, located between the Eastern and Central Wharton Basin provinces, yielded significantly younger ages of 44-37 Ma and 4.5-4.3 Ma, not consistent with the crude age progression formed by the seamounts.

The samples from the seamounts and Christmas Island are primarily alkalic, ranging from alkali basalt to trachyte and basanite to tephri-phonolite, but there are also some tholeiitic samples from the Eastern and Central Wharton Basin and from Outsider Seamount (Fig. 2). The seamount samples generally have high $(La/Sm)_n$ and $(Sm/Yb)_n$ ratios (from 1-6 and 1-9 respectively), reflecting steep REE and

incompatible element patterns on multi-element diagrams with negative slopes (Fig. 3) and high highly to moderately incompatible element ratios (e.g. (La, Ta, Nb, Th)/(Yb, Y); Fig. 4) (Supplement Table 1). The seamount samples generally have incompatible element characteristics similar to ocean island basalts (OIB) (Fig. 3 and 4). The isotopic compositions show a large range (e.g. 206Pb/204Pb = 17.3-19.3; 207Pb/204Pb = 15.49-15.67; 143Nd/144Nd = 0.51220-0.51295; 176Hf/177Hf = 0.28246-0.28319) (Table 2) and extend from enriched (E) MORB (or the common "C" component in MORBs), characterized by samples from the Argo Basin and Cocos Keeling seamounts and the Oligocene volcanic rocks on Christmas Island, to very enriched (EM1) type compositions, characterized by samples from the eastern and central Wharton Basin volcanic provinces and the Pliocene volcanic rocks from Christmas Island (Fig. 5). The EWP and CWP form elongated arrays on isotope correlation diagrams, indicating mixing between the E-MORB (C) and the EM1-type components. The volcanic rocks from Christmas Island also require the presence of both C (Oligocene volcanic rocks) and EM1 (Pliocene volcanic rocks) components. Lamproitic rocks from western Australia, India and other continental areas, generally interpreted to originate from ancient metasomatized lithospheric mantle, extend to very low 206Pb/204Pb but elevated and very variable 87Sr/86Sr, 207Pb/204Pb and 208Pb/204Pb and low but variable 143Nd/144Nd and 176Hf/177Hf and could serve as the enriched endmembers.

Discussion

The Evolution of the Indian Upper Mantle from Jurassic to Eocene Samples from the Investigator Fracture Zone

The tholeiitic compositions, the low $(La/Sm)_n$ and $(Sm/Yb)_n$ ratios (generally <2.2) and the low highly to moderately incompatible element (e.g. (La, Ta, Nb, Th)/(Yb, Y)) ratios are consistent with large degrees of melting at shallow depths, consistent with an origin of these samples at a mid ocean ridge spreading center. Therefore, the Investigator Ridge samples provide us with the first continuous record of Indian MORB composition from the Jurassic to Eocene – the oldest crust yet sampled in the Indian Ocean Basin.

The isotopic compositions of the Investigator Ridge samples show higher 207Pb/204Pb, 208Pb/204Pb, 87Sr/86Sr and lower 143Nd/144Nd and 176Hf/177Hf than generally observed in present-day Pacific or North Atlantic MORB but overlap the enriched part of the Indian MORB field extending from the common C component towards an EM1 type component. With the exception of a crude increase in 143Nd/144Nd with decreasing age, there are no systematic variations with age or distance along the Investigator Ridge in trace element or isotopic composition. The Investigator Ridge and present-day MORB fields form arrays which crudely converge at the end of the MORB arrays with radiogenic Pb (e.g. 206Pb/204Pb of ~19.1-19.5) or with a C type composition defined by Hanan and Graham (1996). These authors proposed that the C component represents a ubiquitous reservoir sampled by both MORB and ocean island basalts (OIB) located in the transition zone, containing ocean crust ranging in age from ~300-2000 Ma. With decreasing 206Pb/204Pb, the present-day Pacific and North Atlantic MORB fields trend to more depleted compositions characterized by more radiogenic Nd and Hf isotope ratios and less radiogenic Sr isotope ratios. The Indian and South Atlantic MORBs require both an enriched and depleted endmember at low 206Pb/204Pb. Investigator Ridge array, however, only trends to a more enriched (EM1-type) composition (less radiogenic Nd but more radiogenic 87Sr/86Sr, 207Pb/204Pb and 208Pb/204Pb) with decreasing 206Pb/204Pb isotopic composition. These Investigator Ridge data suggest that the Indian upper mantle may have been more enriched than at the present day with the exception of the part of the mantle being presently sampled by the SWIR between 39-41°E, which may reflect a local heterogeneity in the upper mantle beneath this part of the Indian Ocean. Any model that attempts to explain the origin and evolution of the upper Indian mantle must be able to explain the overall more enriched composition of Jurassic to Eocene Indian MORB compared to present-day Indian MORB, but must also be able to explain more extreme local heterogeneities persisting in the upper mantle until the present.

The Origin of the Christmas Island Seamount Province

The CHRISP form a diffuse volcanic province, which has a general east to west orientation with a length of ~2,200 km and width of up to ~650 km. The province, however, consists of multiple sub-provinces or groups that in part are

spatially separated. For example, the two clusters of seamounts in the Argo Basin (AP) are separated by about 600 km from the Eastern Wharton Basin volcanic seamounts (EWP) with very few seamounts in between. There are also seamounts outside of the CHRISP, such as Outsider Seamount, which has a similar geochemistry to the Central Wharton Basin volcanic seamounts (CWP), but is located 550 km to the northwest. Therefore, although there appears to be a crude east to west age progression from 136 to 47 Ma (excluding Christmas Island), the morphology of this diffuse seamount province is not consistent with formation through a mantle plume, which generally form narrower (100-400 km) and more continuous island/seamount chains. Furthermore, when Christmas Island is included, the age progression disappears, because within 150 km of Christmas Island there are seamounts dated between 107-81 Ma. Based on submarine samples dredged to depths of up to 3600 m and on subaerial samples scattered across the island, the main edifice of the island appears to have formed in the Oligocene between 44-37 Ma. Samples from the end of the western arm of Christmas Island yielded ages of 4.5-4.3 Ma with all four ages being within error of each other. The very low volume Pliocene volcanic event is most likely related to bending, uplift and extensional faulting of the Indo-Australian Plate just outboard the Java trench, allowing small amounts of upwelling of the upper mantle and low degrees of melting of the uppermost mantle by decompression. Nonetheless, in a very restricted area (~150 km across), major volcanism related to the formation of large seafloor volcanoes took place from 107 to 37 Ma or over a time span of ~70 Ma, which is clearly not consistent with the plume hypothesis. Finally, the beginning of the CHRISP is not associated with a flood basalt event, which however is not always required for the initiation of plumes (e.g. Samuel and Farnetani, 2005), and the chain suddenly ends at ~50 Ma. Any model for the origin of this island/seamount belt should be able to explain the aforementioned observations.

Both P and S-wave seismic tomographic images suggest the presence of a low velocity anomaly extending to depths of 1000 km beneath the Cocos/Keeling Volcanic Province (CKP) (Montelli et al., 2006). Nevertheless, the age of four samples from three different locations including the flanks of Cocos/Keeling Island, range from 56-47 Ma. In light of the NNE plate motion of the Indo-Australian Plate at a rate of about 75 mm/yr over the last 50 Ma, the CKP must have been formed between 3500-4000 km further to the SSW and therefore the presence of the seismic anomaly beneath these old seamounts/islands appears to be somewhat fortuitous.

The volcanic rocks from the CHRISP have trace element and isotopic compositions similar to but extending to even more enriched EMI type compositions than ocean island basalts with EMI type compositions, such as Walvis Ridge in the Atlantic and Pitcairn Island in the Pacific, but overlap with the Afanasy-Nikitin rise and seamount in the Indian Ocean south of India (Mahoney et al., 1996, Sushchevskaya et al., 1996, Borisova et al., 2001). The Afanasy-Nikitin rise and seamount (~80 Ma old; Mahoney et al., 1996) are isolated structures on the seafloor that are not clearly associated with a hotspot track or chain of seamounts, ridges and/or islands and therefore are unlikely to have formed by a mantle plume. They, however, appear to have formed on young crust near a mid-ocean ridge spreading center. Borisova et al. (2001) proposed that their anomalous geochemical compositions can be explained by assimilation of granulitic lower crust and thus imply that the Afanasy-Niktin Rise is underlain by continental crust, which may be the reason for this morphological anomaly on the seafloor. The Petit Spot seamounts, which also have EM1 type compositions, formed through bending of the plate outboard the Japan, causing it to extend and crack as it subducts beneath Japan (Hirano et al., 2006). Upwelling under the bending plate resulted in small degrees of decompression melting that can explain the origin of the very small Petit Spot volcanoes. The Pliocene volcanism on Christmas Island could have formed by a similar mechanism. The very small Godzilla seamount, which also has an EM1 type composition, is an isolated feature on the seafloor in the North Atlantic that cannot be related to a hotspot and therefore is interpreted to reflect upwelling and melting of the uppermost mantle, possibly through extension of an extension of the Oceanographer Fracture Zone (Geldmacher et al., 2008). Finally, Christmas Island provides evidence that both C (volcanic edifice) and EMI (Pliocene volcanic rocks) components are located in the shallow mantle, because these volcanic rocks formed long after the volcanism forming the EWP (115-94 Ma) and CWP (96-64 Ma) seamounts. Therefore there is evidence for the presence of enriched EM1 type material in the shallow mantle in all three of the major ocean basins. The question is how it gets there?

The geochemistry of the CHRISP rocks can provide further constraints on the origin of this seamount cluster. The incompatible element and isotopic data show exceptionally large variations compared to most hotspot tracks. The data require at least three distinct components (figure 5): 1) “C” component of Hanan and Graham

(1996) or FOZO component of Hauri et al., (1994), 2) an enriched EMI type component with low 206Pb/204Pb and very low 143Nd/144Nd and 176Hf/177Hf but high 207Pb/204Pb, and 3) an enriched EMI type component with low 206Pb/204Pb and low 207Pb/204Pb, 143Nd/144Nd and 176Hf/177Hf. The C component forms the common endmember for Atlantic, Pacific and Indian MORB and has been interpreted to reflect a reservoir in the transition zone between the upper and lower mantle, which may be where subducted ocean crust is stored. Lamproites have similar and more extreme enriched compositions than the Christmas Island seamounts. Mixing between lamproitic (± lower crustal) melts and melts from the C type material could generate the EWP and CWP arrays. Lamproites show an extremely wide array of compositions and those with low 206Pb/204Pb can be divided into two distinct endmembers, which also serve as endmembers for the CHRISP rocks. The western Australia lamproites from the Kimberly region in northwest Australia form one of the lamproite endmembers with very radiogenic 207Pb/204Pb (15.65 - 15.75) and 87Sr/86Sr (0.711 - 0.721), radiogenic 208Pb/204Pb (37.8 - 38.5), but fairly unradiogenic 206Pb/204Pb (17.2 - 17.6) and very unradiogenic 143Nd/144Nd (0.5117 - 0.5121). They have the necessary endmember composition to explain the compositions of the CWP rocks (Fig. 5). The Smokey Butte lamproites from Montana (U.S.A.), on the other hand, have extremely unradiogenic 206Pb/204Pb (16.0 - 16.6), 207Pb/204Pb (15.19 - 15.27) and 208Pb/204Pb (36.2 - 36.7), fairly unradiogenic 143Nd/144Nd (0.5112 - 0.5115) but radiogenic 87Sr/86Sr (0.7058 - 0.7063), representing the EMI type endmember necessary to explain the compositions of the EWP rocks (Fraser et al., 1985). Although the Krishna lamproites from central India show a very large variation in Pb isotopic composition, those with low 206Pb/204Pb (<17.1) could serve as endmembers for the EWP and CWP rocks (Chakrabarti et al., 2007). Lamproitic rocks have thus far only been found on the continents and are interpreted to originate from subcontinental lithospheric mantle depleted by extraction of continental crust and then re-enriched by an ancient metasomatic event. Lower crustal granultic rocks could also serve as possible endmembers for these enriched rocks and other enriched volcanic rocks sampled in the Indian ocean basin, such as the Aphanasy-Nikitin Rise and seamount lavas (e.g. Borisova et al., 2001). In either case, mixing of a C component with melts from continental lithosphere could explain the geochemistry of the CHRISP. Below we will discuss how continental lithosphere gets into the upper mantle.

Using plate tectonic reconstructions made with Gplates (Boyden et al., 2011), it is not possible to explain the Christmas Island seamount province with a stationary mantle plume or with a mantle plume moving consistently in a single direction albeit at variable rates. Interestingly, however, the plate tectonic reconstructions show that the CHRISP begins forming shortly after breakup and rifting between Australia, Greater India and the Argo block (Fig. 6), suggesting a connection between the breakup and the seamount formation. Continental lithosphere was located above each of these areas during the breakup of Australia from Greater India. Therefore, delamination/detachment of subcontinental lithospheric mantle ± lower crust during the breakup could provide a mechanism for getting enriched continental lithosphere into the upper mantle. In addition, blocks of continental crust can be stranded in the ocean basins during rifting and seafloor spreading (e.g. Borisova et al., 2001; Mortimer et al., 2006; Pilot et al., 1998; Whitmarsch et al., 1991).

The seamounts also appear to have formed on very young ocean crust and thus near a spreading center. Rifting begins between Greater India and Australia at ~154 Ma (Heine et al., 2004) (Fig. 6). At 136 Ma a seamount formed in the southern part of the Argo Basin on ~20 Ma old crust. The crust decreases in age to 134 Ma beneath the northern seamounts in the Argo Basin. The crust beneath the EWP formed between 124 Ma in the southeast and ~105 Ma in the northwest (Liu et al., 1983). The largest age difference between a seamount in this sub province and the crust it formed on is ≤25 Ma. The crust under the CWP ranges from ~100 Ma in the southeast and 78 Ma in the northwest (Liu et al., 1983). The difference in age between the seamount volcanism and underlying crust is ≤25 Ma. Finally the crust beneath the CKP ranges from 67 Ma in the south to 61 Ma in the north (Liu et al., 1983) with a difference in age between seamount/island and the underlying crust of ≤20 Ma. Therefore, all of the seamounts formed on crust that was between ~2-25 Ma old. Formation near a spreading axis suggests that upwelling mantle may have carried delaminated/detached pieces of continental lithosphere upwards, facilitating melting of metasomatized, volatile (H_2O and CO_2) rich portions of the lithospheric mantle and lower crust (if present) by decompression melting (e.g. Finn et al., 2005; Korenaga, 2005). The Aphanasy-Nikitin Ridge and Seamount also appears to have formed on young (<25 Ma) ocean crust when it formed ~80 Ma ago. Therefore, recycled delaminated/detached continental lithosphere may have also contributed to the formation of the Aphanasy-Nikitin volcanism in the Late Cretaceous.

The Origin of the Enriched Component in Indian MORB

A number of models have been proposed to explain the origin of the enriched nature of Indian and South Atlantic MORB (DUPAL anomaly). One possible explanation for the enriched compositions of Indian and South Atlantic MORB compared to Pacific and North Atlantic MORB could be contamination of the Indian and South Atlantic asthenosphere by mantle plumes, such as the Kerguelen-Heard plume (Storey et al., 1989). Although the Kerguelen-Heard plume has similar 143Nd/144Nd and similar and more radiogenic 87Sr/86Sr isotope ratios, the Pb isotopic composition is too radiogenic with 206Pb/204Pb ≥17.9. Other possible hotspots in the area, such as the Marion, Bouvet, Crozet, Reunion-Mauritius, do not have the appropriate Sr, Nd or Pb isotopic composition to be enriched endmember for the SWIR 39-41°E lavas (Mahoney et al., 1992). The Pb isotopic composition of the Walvis Ridge and Pitcairn Islands, the EMI endmembers for possible hotspot volcanism in the South Atlantic and Pacific ocean basins, respectively, is too high to serve as the endmember for the SWIR lavas. Therefore an origin of the DUPAL anomaly in the Indian and South Atlantic through plume contamination of the upper mantle is unlikely. Recycling of subducted sediments and ocean crust has also been proposed as an explanation for the enriched composition observed in the Indian and South Atlantic Oceans. Present-day oceanic pelagic sediments, however, generally have intermediate 206Pb/204Pb isotope ratios between 18.6-19.0, which are too high. Ancient sediments (>1.25 Ga) with low 238U/204Pb, however, could generate enriched compositions with low 206Pb/204Pb (Rehkämper and Hofmann, 1997). Hanan et al. (2004), however, pointed out that both the Indian and the South Atlantic formed contemporaneously with continental rifting and breakup, in contrast to the Pacific, which is surrounded by subduction zones but is characterized by relatively depleted compositions. Therefore it is to be expected that rifting and continental breakup are likely to be responsible for the difference in composition between these ocean basins. As was the case with the CHRISP arrays, lamproites, i.e. melts from subcontinental lithospheric mantle, and/or lower crust delaminated or detached during the breakup of Gondwana could provide a mechanism for introducing continental material into the ocean basins. Metasomatized areas of the lithosphere could melt within millions of years after delamination/detachment exposed inner parts of the

lithosphere and the lithosphere sinks into the hotter asthenosphere and heats up through conduction. Such a mechanism can explain the more enriched compositions observed in Indian MORB and be the explanation for the DUPAL anomaly in both the Indian and South Atlantic Oceans (Hawkesworth et al., 1986; Mahoney et al., 1992; Hanan et al., 2004; Escrig et al., 2004). Upwelling beneath spreading centers could further facilitate melting by decompression. And finally stranded blocks of continental lithosphere could contaminate melts passing through them, for example, as is believed to be the case for the Heard Island lavas on the Kerguelen Plateau. Garnet-bearing geneisses in a conglomerate interbedded with basalt drilled on the Elan Bank provide unequivocal evidence for the presence of continental crust in the Kerguelen Plateau (Frey et al., 2000).

Pacific, Atlantic and Indian MORB require at least three types of components. Pacific, North Atlantic and Indian MORB form arrays on isotope diagrams that converge at E-MORB. This common component in MORBs has been referred to as the C component with 206Pb/204Pb of ~19.5, 207Pb/204Pb of ~15.6, 208Pb/204Pb of ~39.3, 87Sr/86Sr of ~0.7035, 143Nd/144Nd of ~0.5129 and 176Hf/177Hf of ~0.2831. It has been interpreted to reflect a transition zone reservoir containing young recycled oceanic crust ranging from 300-2000 Ma (Hanan and Graham, 1996). As is clear on binary isotope correlation diagrams (Fig. 5), the different MORB fan out from the C component with decreasing 206Pb/204Pb. The MORB data arrays require at least two additional components with low 206Pb/204Pb: 1) a depleted (DM or depleted MORB source mantle) component, characterized by the low 206Pb/204Pb end of the North Atlantic and Pacific MORB arrays, which has unradiogenic 87Sr/86Sr, 207Pb/204Pb and 208Pb/204Pb but radiogenic 143Nd/144Nd and 176Hf/177Hf, and 2) at least one enriched EMI type component with more radiogenic 207Pb/204Pb, 208Pb/204Pb and 87Sr/86Sr but less radiogenic 143Nd/144Nd and 176Hf/177Hf, as characterized by low 206Pb/204Pb end of the main Indian MORB array. The Jurassic to Eocene Indian MORB crust sampled along the Investigator Fracture Zone forms an array also extending from C to a more enriched composition than the MORB array with lavas from the Southwest Indian Ridge (SWIR) between 39-41°E longitudes extending the array to an even more enriched composition. The enriched end of the Investigator + SWIR (39-41°E) array falls between the main MORB arrays and the enriched (low 206Pb/204Pb) EWP and CWP CHRISP arrays, indicating that the seamount source material could reflect the contaminant needed to

explain the enriched compositions of all present-day Indian MORB and Jurassic to Eocene Indian MORB sampled along the Investigator Ridge. Excluding the SWIR lavas between 39-41°E, the Jurassic to Eocene samples from the Investigator Ridge show more enrichment than present-day Indian MORB, consistent with the major introduction of the enriched material into the Indian upper mantle during the breakup of Gondwana and its dispersion and dilution taking place thereafter. The enriched compositions at the SWIR (39-41°E) at the present, however, indicate that there is less diluted enriched material still available in the Indian upper mantle that may be entrained by mantle upwelling beneath spreading centers. In conclusion, we propose that deeper and lower degrees of melting to form off-axis seamounts such as the Christmas Island seamounts will primarily tap the enriched C (young recycled oceanic crust) and EM1 (recycled continental lithosphere) components in the otherwise depleted MORB source upper mantle. The depleted MORB source component is primarily sampled at ridge segments that don't contain the enriched components and through larger degrees of melting at shallower depths beneath spreading centers.

Acknowledgements

We would like to thank the Captain and Crew of the F/S Sonne for their excellent support that contributed directly to the success of the SO199 CHRISP Expedition. Dagmar Rau (XRF), Jan Sticklus (Ar-Ar Laboratory), Jan Fietzke (Axiom MC-ICPMS), Ulrike Westernströer (ICPMS at IfG (Kiel)) and Silke Hauff (TIMS) are gratefully thanked for their continuous support in running these facilities. We also thank the German Ministry of Education and Research (BMBF) for their continued funding of marine research.

References

Baker, J.A., Gamble, J.A., Graham, I.J., 1994. The age, geology and geochemistry of the Tapuaenuku Igneous Complex, Marlborough, New Zealand. New Zealand Journal of Geology and Geophysics 37, 249-268.

Baker, J.A., Peate, D.W., Waight, T.E., Thirlwall, M.F., 2005. Reply to the: Comment on "Pb isotopic analysis of standards and samples using a 207Pb-204Pb double spike and thallium to correct for mass bias with a double focusing MC-ICP-MS" by Baker et al. Chemical Geology 217, 175-179.

Baksi, A.K., 1999. Reevaluation of Plate Motion Models Based on Hotspot Tracks in the Atlantic and Indian Oceans. The Journal of Geology 107, 13-26.

—, 2007. A quantitative tool for detecting alteration in undisturbed rocks and minerals -I: Water, chemical weathering, and atmospheric argon. Geological Society of America Special Papers 430, 285-303.

—, 2007. A quantitative tool for detecting alteration in undisturbed rocks and minerals -II: Application to argon ages related to hotspots. Geological Society of America Special Papers 430, 305-333.

Barckhausen, U., Hoernle, K., Werner, R., Hauff, F., van den Bogaard, P., Gibbons , A., in prep. Crustal ages along the Investigator Ridge and tectonic implications. Geophysical Journal International.

Bezrukov, P.L., Andrushschenko, P.F., 1974. Iron-maganese concretions of the Indian Ocean. International Geology Review 15 (3), 342-356.

Blichert-Toft, J., Chauvel, C., Albarede, F., 1997. Separation of Hf and Lu for high-precision isotope analyses of rock samples by magnetic sector-multiple collector ICP-MS. Contributions Mineralogy Petrology 127, 248-260.

Borisova, A.Y., Belyatsky, B.V., Portnyagin, M.V., Sushchevskaya, N.M., 2001. Petrogenesis of Olivine-phyric Basalts from the Aphanasey Nikitin Rise: Evidence for Contamination by Cratonic Lower Continental Crust. Journal of Petrology 42, 277-319.

Boyden, J.A., Müller, R.D., Gurnis, M., Torsvik, T.H., Clark, J.A., Turner, M., Ivey-Law, H., Watson, R.J., Cannon, J.S., 2011. Next-generation plate-tectonic reconstructions using GPlates. in: Geoinformatics: Cyberinfrastructure for the Solid Earth Sciences, Keller G.R. and Baru, C., eds., Cambridge University Press, in press.

Chakrabarti, R., Basu, A.R., Paul, D.K., 2007. Nd-Hf-Sr-Pb isotopes and trace element geochemistry of Proterozoic lamproites from southern India: Subducted komatiite in the source. Chemical Geology 236, 291-302.

Darwin, C., 1842. The Structure and Distribution of Coral Reefs. Smith, Elder and Co: London.

Dupré, B., Allègre, C.J., 1983. Pb-Sr isotope variation in Indian Ocean basalts and mixing phenomena. Nature 303, 142-146.

Escrig, S., Capmas, F., Dupré, B., Allègre, C.J., 2004. Osmium isotopic constraints on the nature of the DUPAL anomaly from Indian mid-ocean-ridge basalts. Nature 431, 59-63.

Exon, N.F., Graham, T.L., Williams, S.M., Chaproniere, G.C.H., Chudyk, E., Coleman, P.J., Kalinisan, L., Moss , G., Dhafik, S., Group, T.S., 1993. BMR Cruise 107: Seabed morphology and offshore resources around Christmas Island, Indian Ocean. AGSO Record 1993/6, 1-87.

Falloon, T.J., Varne, R., Morris, J.D., Hart, S.R., 1989. Alkaline volcanics from Christmas Island and nearby seamounts; magmatism of the Northeast Indian Ocean. In: Continental magmatism, abstracts. New Mexico Bureau of Mines and Mineral Resources. Socorro, NM, United States, 86.

Farnetani, C.G., Samuel, H., 2005. Beyond the thermal plume paradigm. Geophys. Res. Lett. 32, L07311.

Finn, C.A., Müller, R.D., Panter, K.S., 2005. A Cenozoic diffuse alkaline magmatic province (DAMP) in the southwest Pacific without rift or plume origin. Geochemistry Geophysics Geosystems 6, Q02005, doi:10.1029/2004GC000723.

Fraser, K.J., Hawkesworth, C.J., Erlank, A.J., Mitchell, R.H., Scott-Smith, B.H., 1985. Sr, Nd and Pb isotope and minor element geochemistry of lamproites and kimberlites. Earth and Planetary Science Letters 76, 57-70.

Galer, S.J.G., Abouchami, W., 1998. Practical application of lead triple spiking triple spiking for correction of instrumental mass discrimination. Mineralogical Magazine 62A, 491-492.

Garbe-Schönberg, C.-D., 1993. Simultaneous determination of thirty-seven trace elements in twenty-eight international rock standarts by ICP-MS. Geostandard Newsletter 17, 81-97.

Geldmacher, J., Hoernle, K., Klügel, A., Bogaard, P.v.d., Wombacher, F., Berning, B., 2006. Origin and geochemical evolution of the Madeira-Tore Rise (eastern North Atlantic). Journal Geophysical Research 111, B09206, doi:10.1029/2005JB003931.

Geldmacher, J., Hoernle, K., Klugel, A., van den Bogaard, P., Bindeman, I., 2008. Geochemistry of a new enriched mantle type locality in the northern hemisphere: Implications for the origin of the EM-I source. Earth and Planetary Science Letters 265, 167-182.

Hanan, B.B., Blichert-Toft, J., Pyle, D.G., Christie, D.M., 2004. Contrasting origins of the upper mantle revealed by hafnium and lead isotopes from the Southeast Indian Ridge. Nature 432, 91-94.

Hanan, B.B., Graham, D.W., 1996. Lead and Helium Isotope Evidence from Oceanic Basalts for a Common Deep Source of Mantle plumes. Science 272, 991-995.

Hart, S.R., 1984. A large-scale isotope anomaly in the Southern Hemisphere mantle. Nature 309, 753-757.

Hauri, E.H., Whitehead, J.A., Hart, S.R., 1994. Fluid dynamics and geochemical aspects of entrainment in mantle plumes. Journal Geophysical Research 99, 24275-24300.

Hawkesworth, C.J., Mantovani, M.S.M., Taylor, P.N., Palacz, Z., 1986. Evidence from the Parana of south Brazil for a continental contribution to Dupal basalts. Nature 322, 356-358.

Heine, C., Müller, R.D., Gaina, C., 2004. Reconstructing the Lost Eastern Tethys Ocean Basin: Convergence History of the SE Asian Margin and Marine Gateways, *in* Clift, P., Wang, P., Kuhnt, W., and Hayes, D., eds., Continent - Ocean Interactions Within East Asian Marginal Seas, AGU Geophysical Monograph Series: Volume 149: p. 37-54, Washington, American Geophysical Union.

Hekinian, R., 1974. Petrology of igneous rocks from Leg 22 in the northeastern Indian Ocean. In: von der Borch CC, Sclater JG et al. Init Repts DSDP 22, Washington (US Government Printing Office), 413-448.

Hirano, N., Takahashi, E., Yamamoto, J., Abe, N., Ingle, S.P., Kaneoka, I., Hirata, T., Kimura, J.-I., Ishii, T., Ogawa, Y., Machida, S., Suyehiro, K., 2006. Volcanism in Response to Plate Flexure. Science 313, 1426-1428.

Hoernle, K., Abt, D.L., Fischer, K.M., Nichols, H., Hauff, F., Abers, G.A., van den Bogaard, P., Heydolph, K., Alvarado, G., Protti, M., Strauch, W., 2008. Arc-parallel flow in the mantle wedge beneath Costa Rica and Nicaragua. Nature 451, 1094-1097.

Hoernle, K., Hauff, F., Kokfelt, T.F., Haase, K.M., Garbe-Schönberg, D., Werner, R., accepted with minor revisions. Interaction of a Weak Ascension Plume with the South Mid-Atlantic Ridge and Long-term Evolution of the Plume. Earth and Planetary Science Letters.

Hoernle, K.A., Tilton, G.R., 1991. Sr-Nd-Pb isotope data for Fuerteventura (Canary Islands) basal complex and subaerial volcanics: applications to magma genesis and evolution. Schweiz. Mineral. Petrogr. Mitt. 71, 3-18.

Hofmann, A.W., 1997. Mantle geochemistry: the message from oceanic volcanism. Nature 385, 219-228.

Kempton, P.D., Pearce, J.A., Barry, T.L., Fitton, J.G., Langmuir, C., Christie, D.M., 2002. Sr-Nd-Pb-Hf Isotope Results from ODP Leg 187: Evidence for Mantle Dynamics of the Australian-Antarctic Discordance and Origin of the Indian MORB Source. Geochemistry Geopysics Geosystems 3, 1074, doi:10.1029/2002GC000320.

Korenaga, J., 2005. Firm mantle plumes and the nature of the core-mantle boundary region. Earth and Planetary Science Letters 232, 29-37.

Lanphere, M.A., Dalrymple, G.B., 2000. First-principles calibration of 38Ar tracers: Implications for the ages of 40Ar/39Ar fluence monitors. U.S. Geological Survey Professional Paper 1621, 1-10.

Liu, C.-S., Curray, J.R., McDonald, J.M., 1983. New constraints on the tectonic evolution of the eastern Indian Ocean. Earth and Planetary Science Letters 65, 331-342.

Mahoney, J., LeRoex, A.P., Peng, Z., Fisher, R.L., Natland, J.H., 1992. Southwestern Limits of Indian Ocean Ridge Mantle and the Origin of Low $^{206}Pb/^{204}Pb$ Mid-Ocean Ridge Basalt: Isotope Systematics of the Central Southwest Indian Ridge (17°-50° E). Journal Geophysical Research 97, 19771-19790.

Mahoney, J.J., Frei, R., Tejada, M.L.G., Mo, X.X., Leat, P.T., Nägler, T.F., 1998. Tracing the Indian Ocean mantle Domain through time: Isotopic results from old West Indian, East Tethyan, and South Pacific seafloor. Journal of Petrology 39, 1285-1306.

McDougall, I., 1974. Potassium-Argon ages on basaltic rocks recovered from DSDP, Leg 22, Indian ocean. In: von der Borch CC, Sclater JG et al. Init Repts DSDP 22, Washington (US Government Printing Office), 377-380.

Montelli, R., Nolet, G., Dahlen, F.A., Masters, G., 2006. A catalogue of deep mantle plumes: New results from finite-frequency tomography. Geochem. Geophys. Geosyst. 7, Q11007, doi:10.1029/2006gc001248.

Mortimer, N., Hoernle, K., Hauff, F., Palin, J.M., Dunlap, W.J., Werner, R., Faure, K., 2006. New constraints on the age and evolution of the Wishbone Ridge, southwest Pacific Cretaceous microplates, and Zealandia-West Antarctica breakup. Geology 34, 185-188.

Pilot, J., Werner, C.-D., Haubrich, F., Baumann, N., 1998. Palaeozoic and Proterozoic zircons from the Mid-Atlantic Ridge. Nature 393, 676-679.

Rehkämper, M., Hofmann, A.W., 1997. Recycled ocean crust and sediment in the Indian Ocean MORB. Earth Planetary Science Letters 147, 93-106.

Storey, M., Saunders, A.D., Tarney, J., Gibson, I.L., Norry, M.J., Thirlwall, M.F., Leat, P., Thompson, R.N., Menzies, M.A., 1989. Contamination of Indian Ocean asthenosphere by the Kerguelen-Heard mantle plume. Nature 338, 574-576.

Sushchevskaya, N., Belyatsky, B., Nikulin, V., 2000. Geochemical heterogeneity of the magmatism from the Ninetyeast and Investigator Ridges. Goldschmidt Conference Oxford UK, Journal Conference Abstracts 5 (2), 968-969.

Thirlwall, M.F., 2000. Inter-laboratory and other errors in Pb isotope analyses investigated using a ^{207}Pb-^{204}Pb double spike. Chemical Geology 163, 299-322.

—, 2002. Multicollector ICP-MS analysis of Pb isotopes using a ^{207}Pb-^{204}Pb double spike demonstrates up to 400 ppm/amu systematic errors in Tl-normalization. Chemical Geology 184, 255-279.

Trueman, N.A., 1965. The phosphate, volcanic and carbonate rocks of Christmas Island (Indian Ocean). Journal Geological Society Australia 12, 261-283.
Whitmarsh, R.B., Party, S.S., 1998. Drilling reveals transition from continental breakup to early magmatic crust. EOS Transactions, AGU 79 (14), 173-181.
Woodroffe, C.D., 1988. Vertical movement of isolated oceanic islands at plate margins: evidence from emergent reefs in Tonga (Pacific Ocean), Cayman Islands (Caribbean Sea) and Christmas Island (Indian Ocean). Zeitschrift für Geomorphologie, Neue Folge Suppl.-Bd. 69, 17-37.

Figures

Figure 1. Overview map of the northeast Indian Ocean that shows the Investigator Rise (Fracture Zone) and the Christmas Island Seamount Province (CHRISP). The CHRISP is subdivided into four sub provinces (going from east to west): 1) Argo Basin (136 Ma), 2) Eastern Wharton Basin (94-115 Ma), 3) Central Wharton Basin (64-96 Ma), and 4) the Cocos/Keeling (47-56 Ma) Volcanic Provinces. Also shown are Christmas Island (44-37Ma and 4.4 Ma), between the Eastern and Western Wharton Basin provinces, and Outsider Seamount (53 Ma), west of the Investigator Fracture Zone and north of the Cocos-Keeling seamount province. The inset shows the study area in relation to Indonesia and Australia.

Figure 2. Rock nomenclature diagrams: a) SiO2 vs. the alkalis and b) Ti/100 vs. V.

Figure 3. Multi element diagrams: a) Spider diagram and b) immobile trace elements.

Figure 4. Incompatible element ratio diagrams: a) Th/Yb vs. La/Yb, b) Nb/Y vs. La/Yb, c) La/Nb vs. Th/Nb, and d) La/Ta vs. Th/Ta.

Figure 5. a) 87Sr/86Sr vs 143Nd/144Nd, 206Pb/204Pb vs 207Pb/204 (b), 208Pb/204 (c), 143Nd/144Nd (d), 87Sr/86Sr (e) and f) 143Nd/144Nd vs 176Hf/177Hf.

Figure 6. Model for the rifting apart of the Greater India, Australian and Antarctica. The red star represents the location of a fixed hotspot located beneath the Argo Basin at 136 Ma. The figure is based on a plate tectonic reconstruction created with GPlates (Boyden et al. 2011).

Tables

Table 1. Ar/Ar age data for for the Investigator Ridge, the Christmas Island Seamounts and Christmas Island.
Table 2. Sr-Nd-Pb-Hf Isotope data for the Investigator Ridge, the Christmas Island Seamounts and Christmas Island.

Supplementary Files

Table 1. Major and trace element data for the Investigator Ridge, the Christmas Island Seamounts and Christmas Island.

Table 2. Major and selected trace element data of reference materials obtained by XRF (IFM-GEOMAR) and ICP-OES at Acme Labs.

Table 3. Trace element concentration data of reference materials obtained by ICPMS at the Institute of Geosciences (IfG, Kiel University) and Acme Labs (marked with an asterix *)

Table 4. Results of ICPMS replicate analyses by means of separate sample digests

Table 5. Machine reproducibility of the Agilent 7500cs ICPMS instrument at IfG over the course of an analytical session.

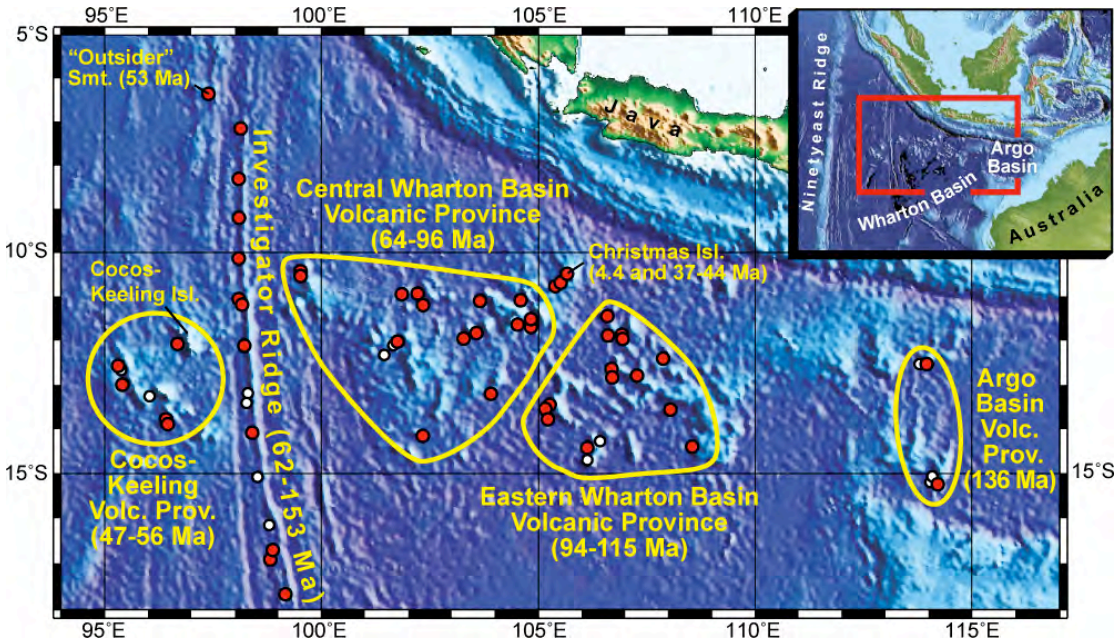
95°E
100°E
105°E
110°E
115°E
5°S
10°S
15°S
"Outsider" Smt. (53 Ma)
Java
Investigator Ridge (62-153 Ma)
Central Wharton Basin Volcanic Province (64-96 Ma)
Christmas Isl. (4.4 and 37-44 Ma)
Cocos-Keeling Isl.
Cocos-Keeling Volc. Prov. (47-56 Ma)
Eastern Wharton Basin Volcanic Province (94-115 Ma)
Argo Basin Volc. Prov. (136 Ma)
Ninetyeast Ridge
Argo Basin
Wharton Basin
Australia

Figure 1

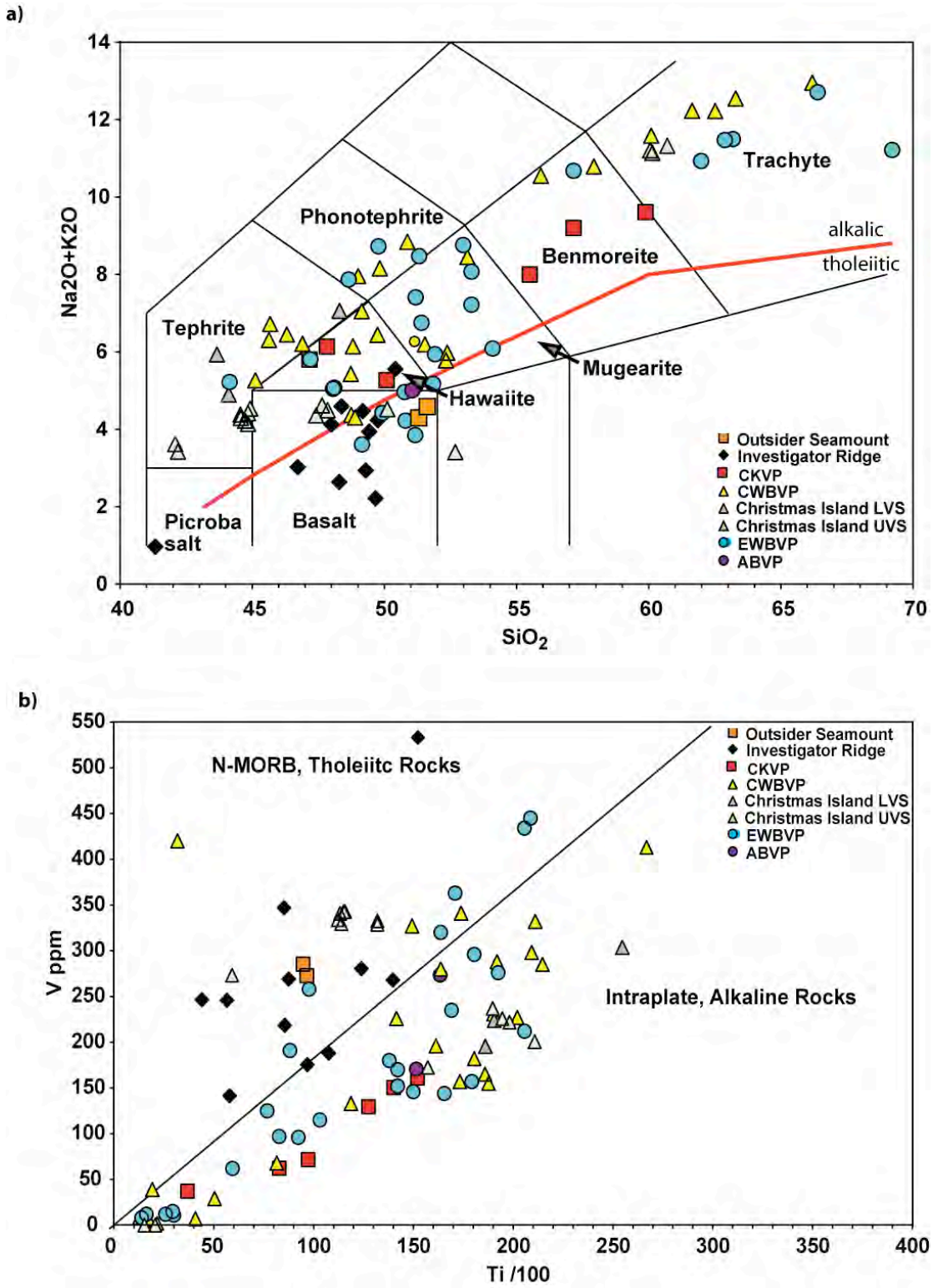
a)
Na2O+K2O
SiO2
Trachyte
Phonotephrite
Benmoreite
alkalic
tholeiitic
Tephrite
Mugearite
Hawaiite
Picroba
salt
Basalt
Outsider Seamount
Investigator Ridge
CKVP
CWBVP
Christmas Island LVS
Christmas Island UVS
EWBVP
ABVP
b)
V ppm
Ti /100
N-MORB, Tholeiitc Rocks
Intraplate, Alkaline Rocks
Outsider Seamount
Investigator Ridge
CKVP
CWBVP
Christmas Island LVS
Christmas Island UVS
EWBVP
ABVP

Figure 2A + B

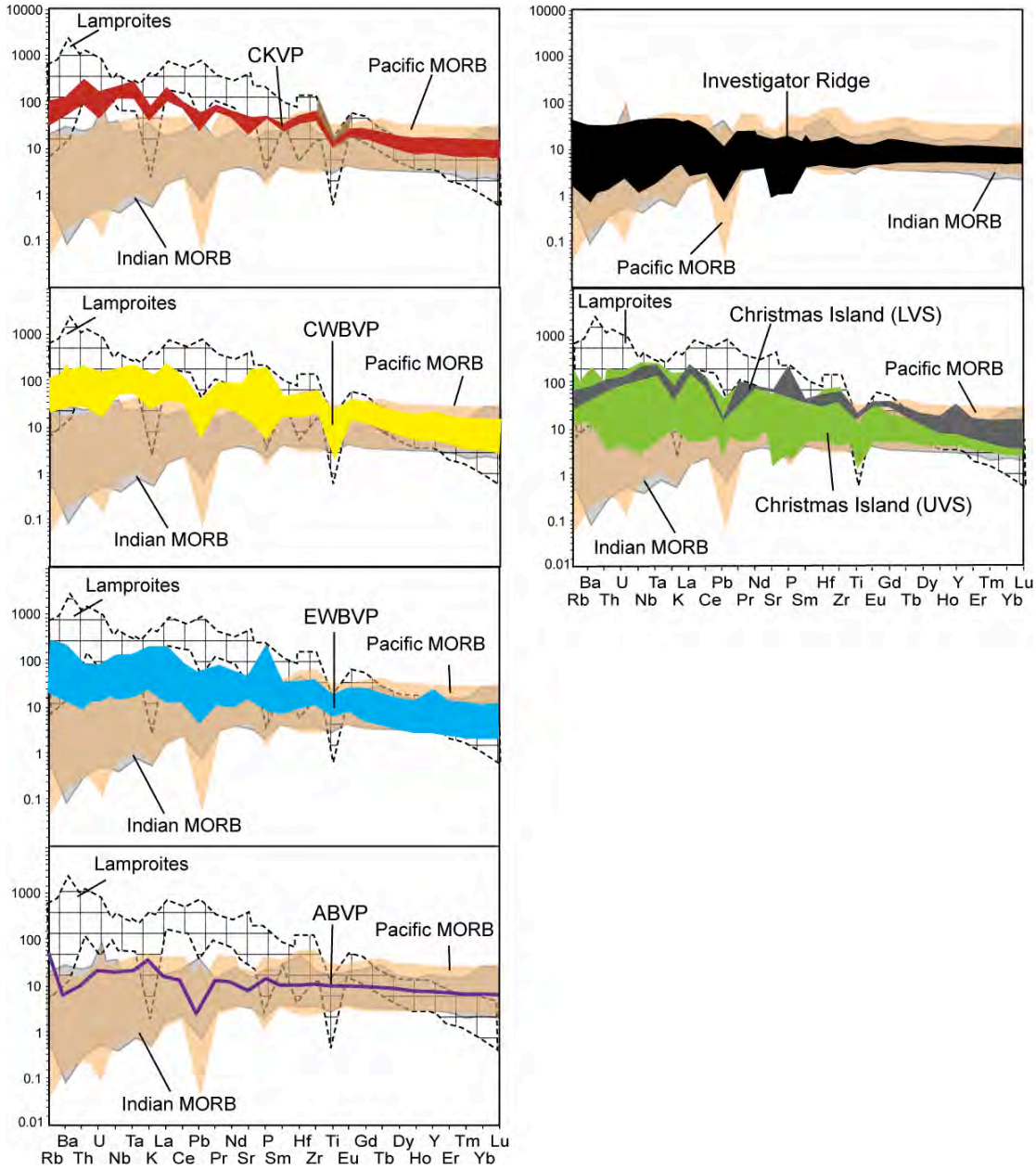
Lamproites
CKVP
Pacific MORB
Indian MORB
Investigator Ridge
Pacific MORB
Indian MORB
Lamproites
CWBVP
Pacific MORB
Indian MORB
Lamproites
Christmas Island (LVS)
Pacific MORB
Christmas Island (UVS)
Indian MORB
Lamproites
EWBVP
Pacific MORB
Indian MORB
Lamproites
ABVP
Pacific MORB
Indian MORB
10000
1000
100
10
1
0.1
0.01
Ba U Ta La Pb Nd P Hf Ti Gd Dy Y Tm Lu
Rb Th Nb K Ce Pr Sr Sm Zr Eu Tb Ho Er Yb

Figure 3A

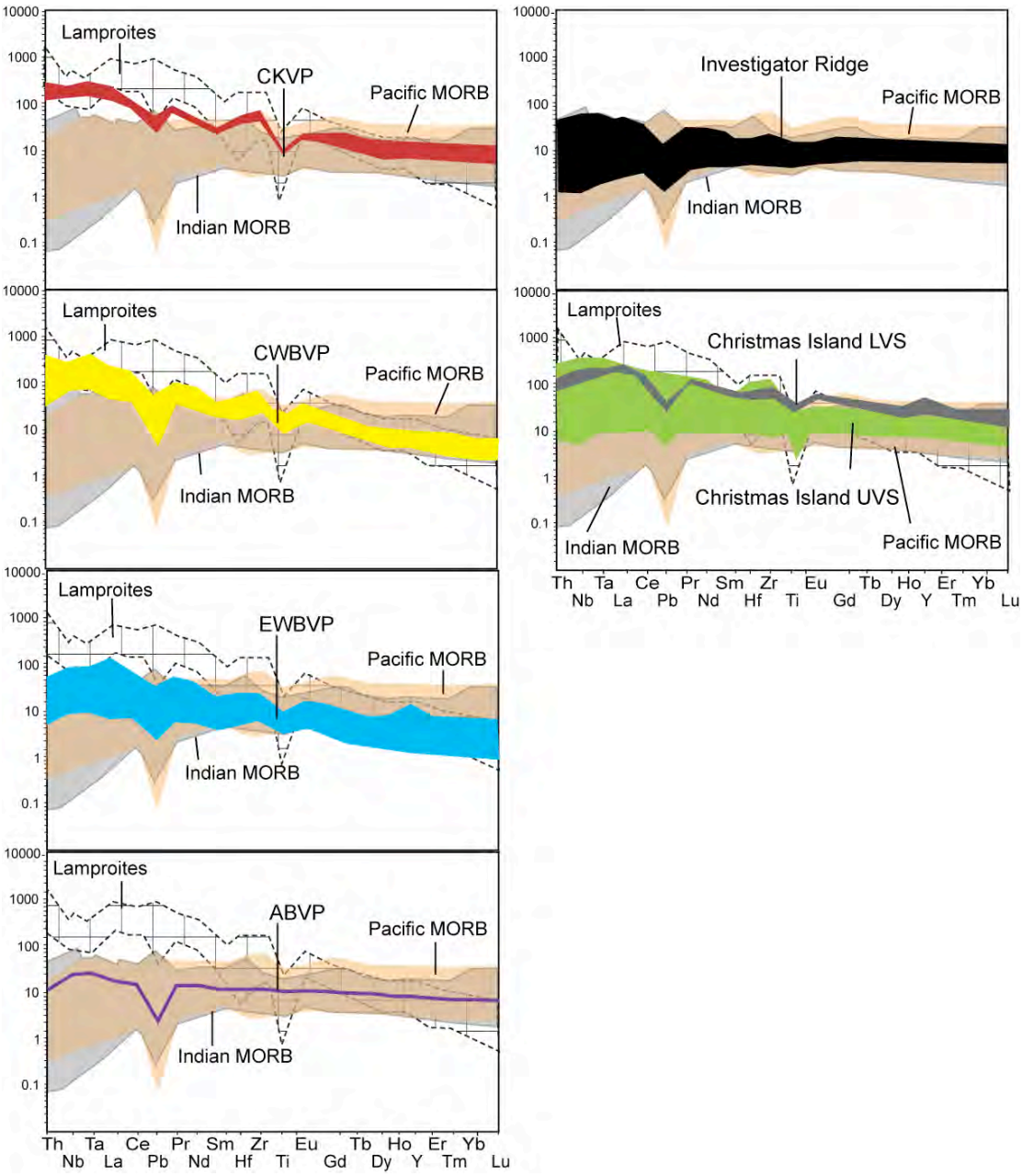
Lamproites
CKVP
Pacific MORB
Indian MORB
Investigator Ridge
Pacific MORB
Indian MORB
Lamproites
CWBVP
Pacific MORB
Indian MORB
Lamproites
Christmas Island LVS
Christmas Island UVS
Indian MORB
Pacific MORB
Lamproites
EWBVP
Pacific MORB
Indian MORB
Lamproites
ABVP
Pacific MORB
Indian MORB
10000
1000
100
10
1
0.1
Th Ta Ce Pr Sm Zr Eu Tb Ho Er Yb
Nb La Pb Nd Hf Ti Gd Dy Y Tm Lu

Figure 3B

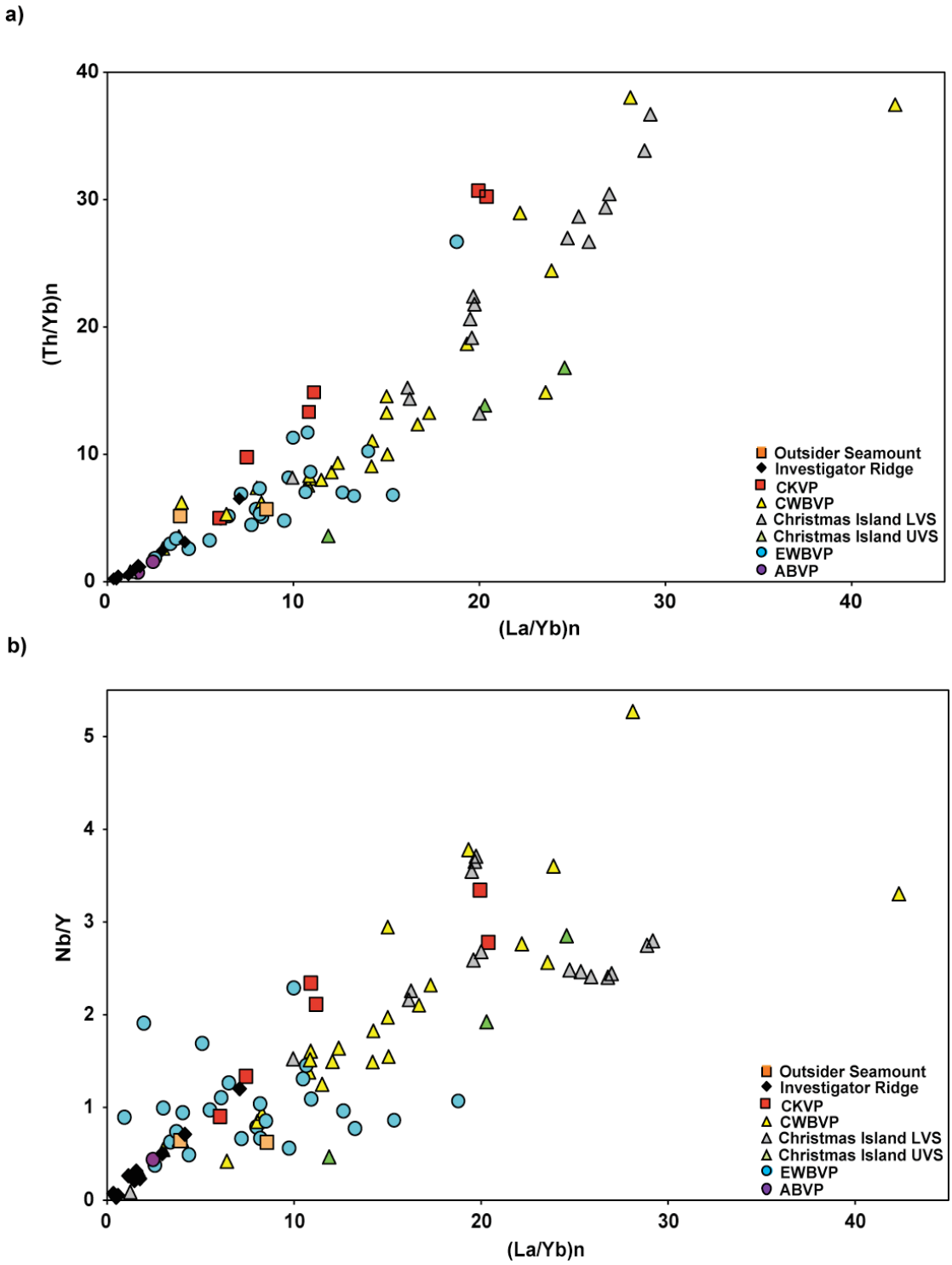
a)
(Th/Yb)n
(La/Yb)n
0
10
20
30
40
Outsider Seamount
Investigator Ridge
CKVP
CWBVP
Christmas Island LVS
Christmas Island UVS
EWBVP
ABVP
b)
Nb/Y
(La/Yb)n
0
1
2
3
4
5
10
20
30
40
Outsider Seamount
Investigator Ridge
CKVP
CWBVP
Christmas Island LVS
Christmas Island UVS
EWBVP
ABVP

Figure 4A + B

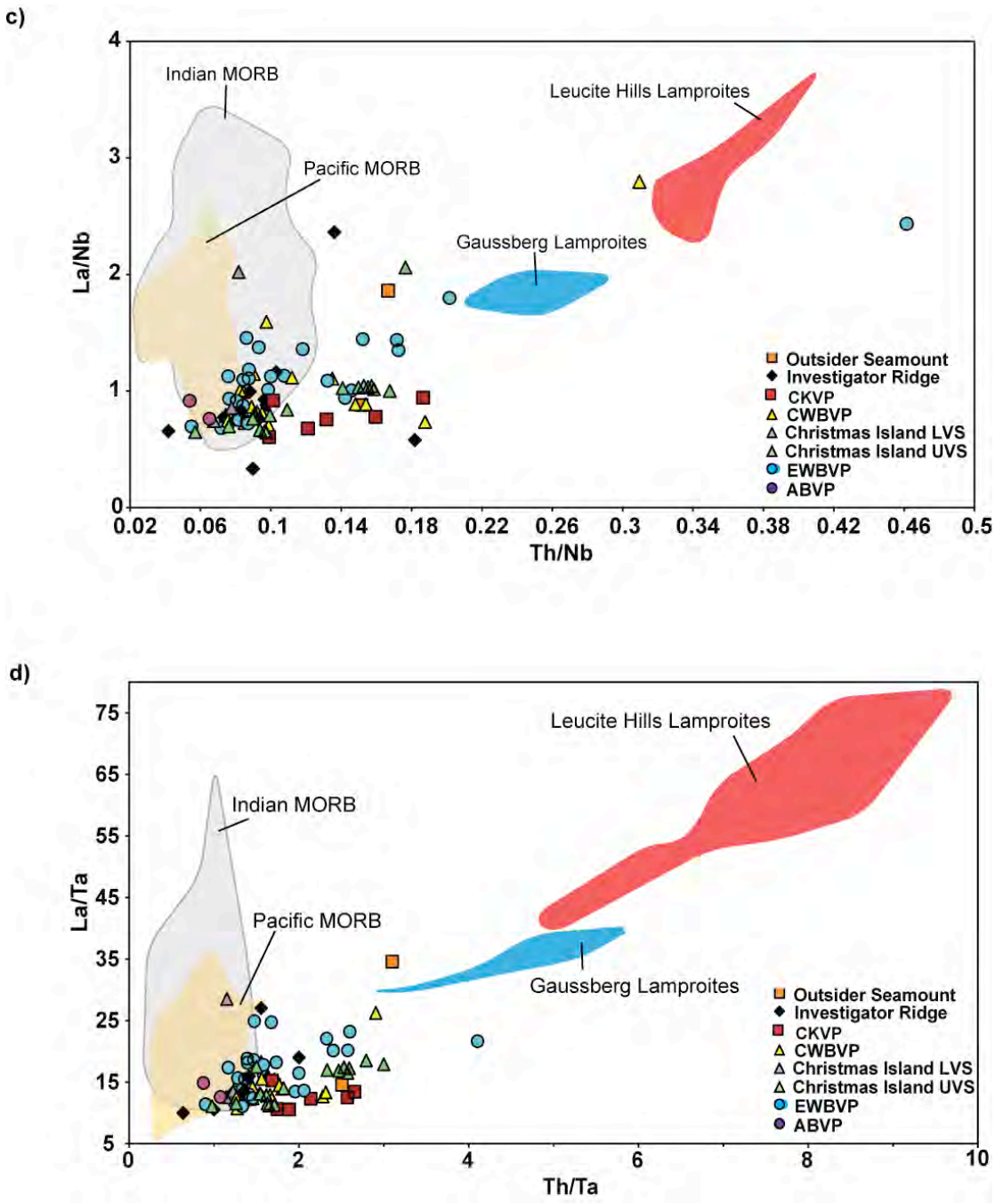
c)
Indian MORB
Pacific MORB
Leucite Hills Lamproites
Gaussberg Lamproites
La/Nb
Th/Nb
Outsider Seamount
Investigator Ridge
CKVP
CWBVP
Christmas Island LVS
Christmas Island UVS
EWBVP
ABVP
d)
Leucite Hills Lamproites
Indian MORB
Pacific MORB
Gaussberg Lamproites
La/Ta
Th/Ta
Outsider Seamount
Investigator Ridge
CKVP
CWBVP
Christmas Island LVS
Christmas Island UVS
EWBVP
ABVP

Figure 4C + D

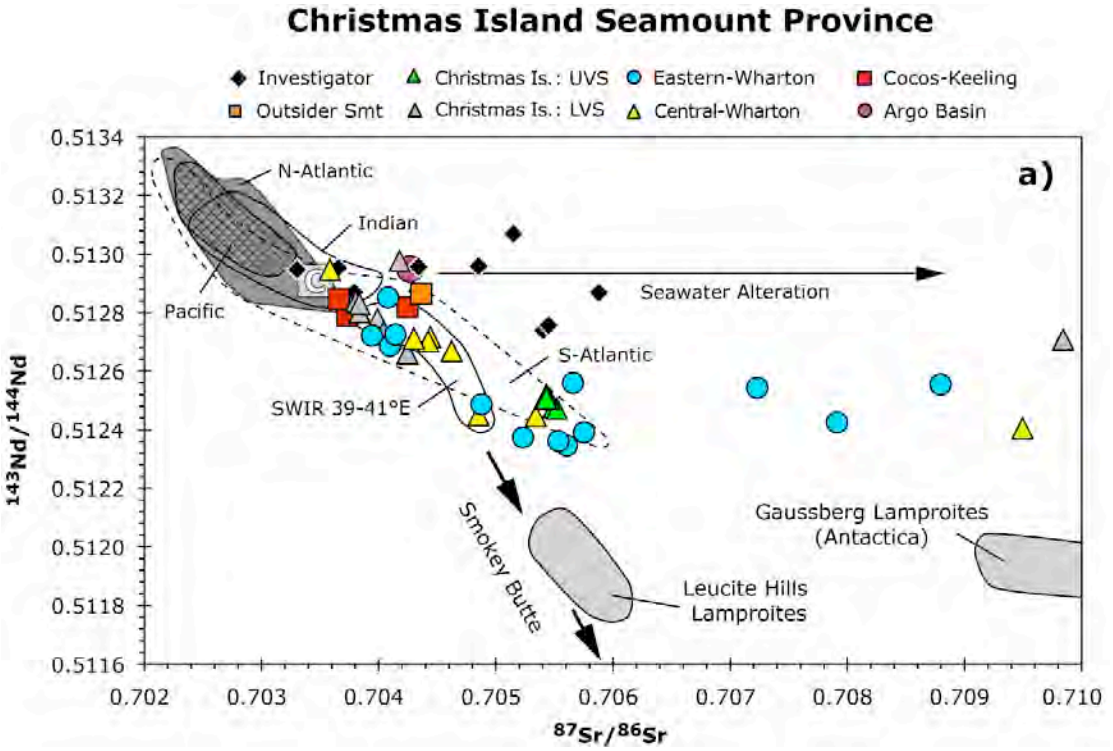
Christmas Island Seamount Province
Investigator
Christmas Is.: UVS
Eastern-Wharton
Cocos-Keeling
Outsider Smt
Christmas Is.: LVS
Central-Wharton
Argo Basin
a)
N-Atlantic
Indian
Pacific
Seawater Alteration
S-Atlantic
SWIR 39-41°E
Smokey Butte
Gaussberg Lamproites
(Antactica)
Leucite Hills
Lamproites
0.5134
0.5132
0.5130
0.5128
0.5126
0.5124
0.5122
0.5120
0.5118
0.5116
0.702
0.703
0.704
0.705
0.706
0.707
0.708
0.709
0.710
143Nd/144Nd
87Sr/86Sr

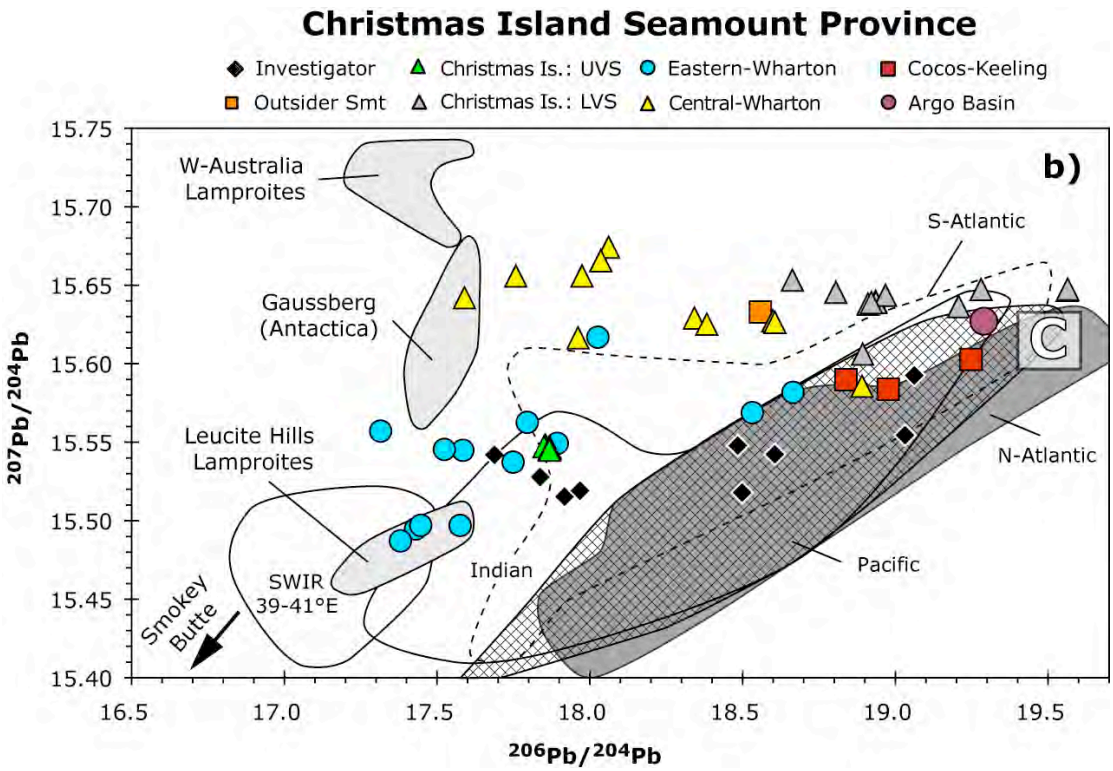
Christmas Island Seamount Province
Investigator
Christmas Is.: UVS
Eastern-Wharton
Cocos-Keeling
Outsider Smt
Christmas Is.: LVS
Central-Wharton
Argo Basin
b)
W-Australia
Lamproites
S-Atlantic
Gaussberg
(Antactica)
Leucite Hills
Lamproites
N-Atlantic
Indian
Pacific
SWIR
39-41°E
Smokey
Butte
15.75
15.70
15.65
15.60
15.55
15.50
15.45
15.40
16.5
17.0
17.5
18.0
18.5
19.0
19.5
207Pb/204Pb
206Pb/204Pb

Figure 5A + B

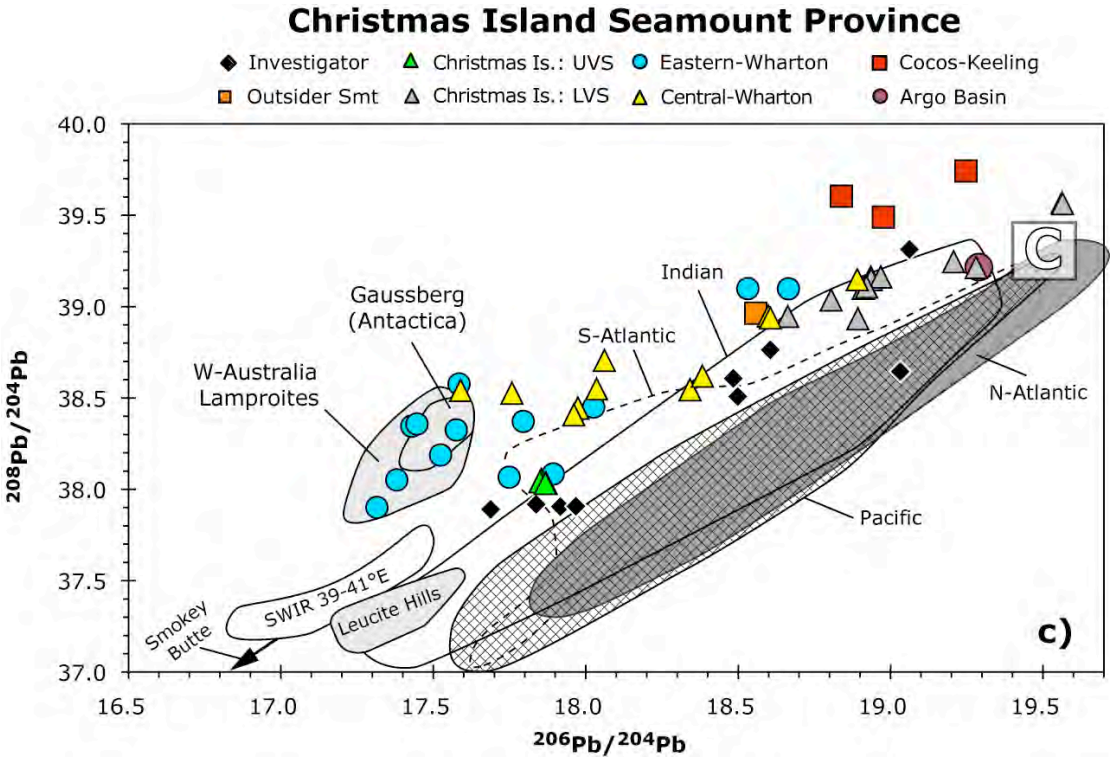
Christmas Island Seamount Province
Investigator
Christmas Is.: UVS
Eastern-Wharton
Cocos-Keeling
Outsider Smt
Christmas Is.: LVS
Central-Wharton
Argo Basin
Gaussberg (Antactica)
W-Australia Lamproites
Indian
S-Atlantic
N-Atlantic
Pacific
SWIR 39-41°E
Leucite Hills
Smokey Butte
C
c)
$^{208}Pb/^{204}Pb$
$^{206}Pb/^{204}Pb$

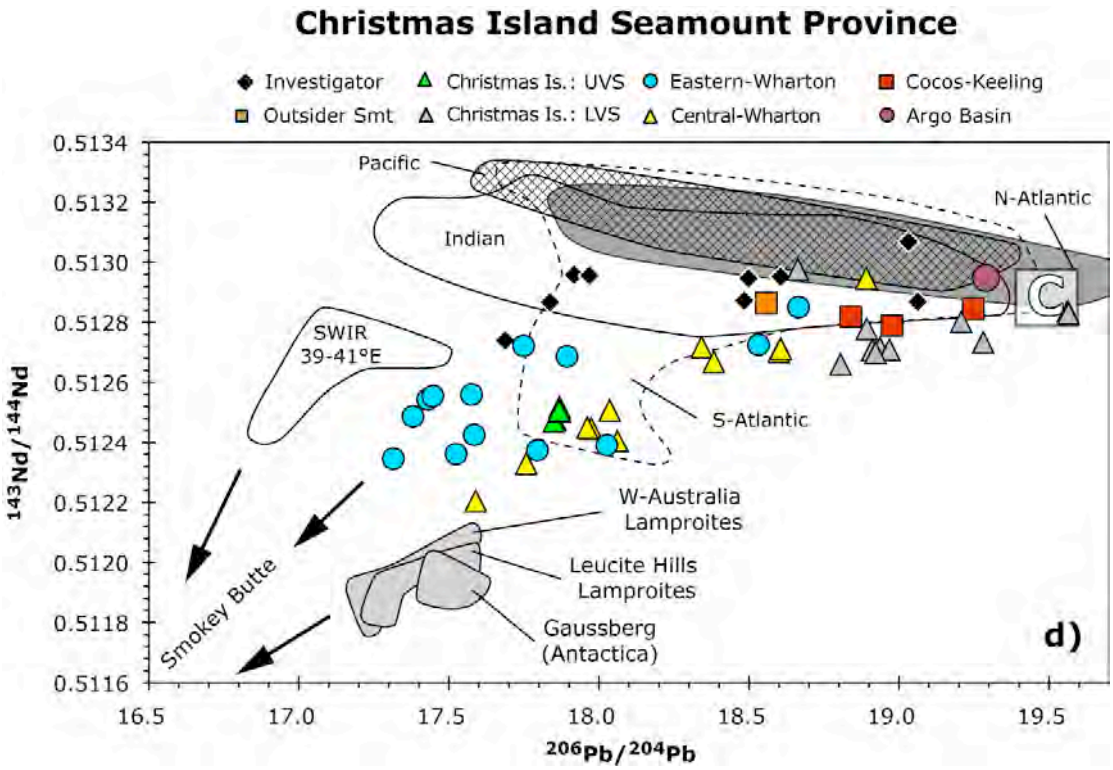
Christmas Island Seamount Province
Investigator
Christmas Is.: UVS
Eastern-Wharton
Cocos-Keeling
Outsider Smt
Christmas Is.: LVS
Central-Wharton
Argo Basin
Pacific
N-Atlantic
Indian
SWIR 39-41°E
S-Atlantic
W-Australia Lamproites
Leucite Hills Lamproites
Gaussberg (Antactica)
Smokey Butte
C
d)
$^{143}Nd/^{144}Nd$
$^{206}Pb/^{204}Pb$

Figure 5C + D

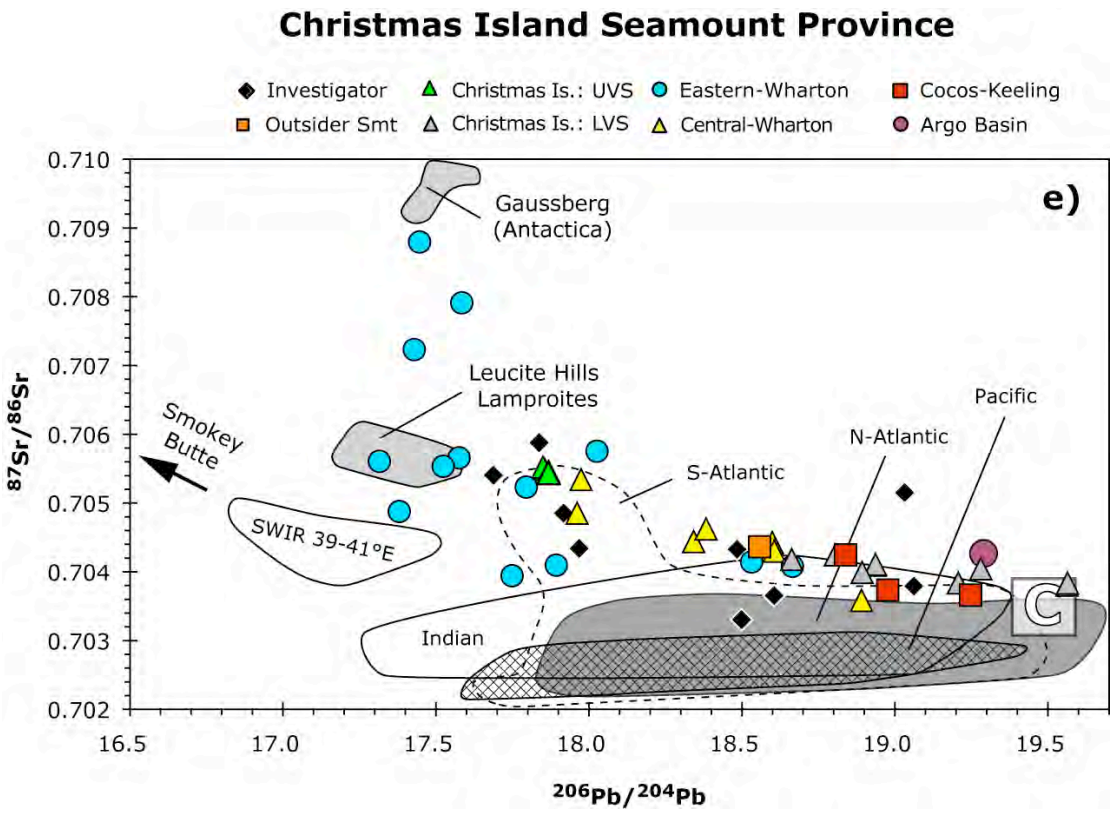
Christmas Island Seamount Province
Investigator
Outsider Smt
Christmas Is.: UVS
Christmas Is.: LVS
Eastern-Wharton
Central-Wharton
Cocos-Keeling
Argo Basin
e)
Gaussberg (Antactica)
Leucite Hills Lamproites
Smokey Butte
SWIR 39-41°E
Indian
S-Atlantic
N-Atlantic
Pacific
C
0.710
0.709
0.708
0.707
0.706
0.705
0.704
0.703
0.702
87Sr/86Sr
16.5
17.0
17.5
18.0
18.5
19.0
19.5
206Pb/204Pb

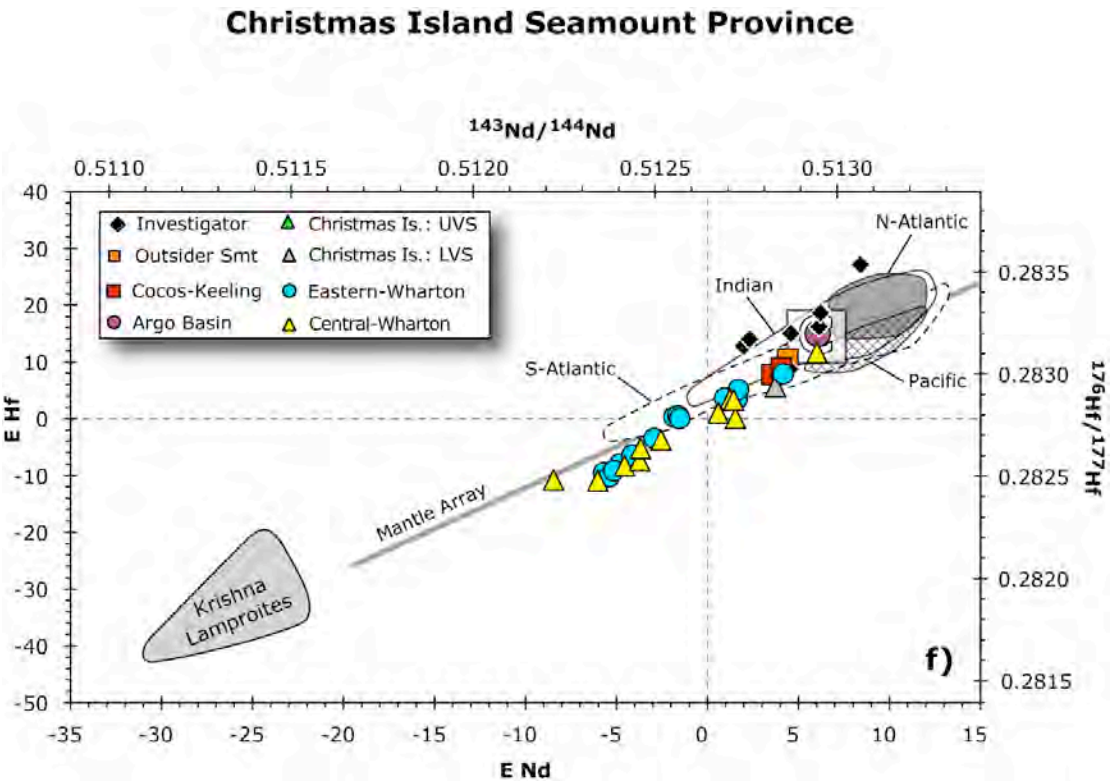
Christmas Island Seamount Province
143Nd/144Nd
0.5110
0.5115
0.5120
0.5125
0.5130
Investigator
Outsider Smt
Cocos-Keeling
Argo Basin
Christmas Is.: UVS
Christmas Is.: LVS
Eastern-Wharton
Central-Wharton
N-Atlantic
Indian
S-Atlantic
Pacific
Mantle Array
Krishna Lamproites
f)
E Hf
40
30
20
10
0
-10
-20
-30
-40
-50
176Hf/177Hf
0.2835
0.2830
0.2825
0.2820
0.2815
-35
-30
-25
-20
-15
-10
-5
0
5
10
15
E Nd

Figure 5E + F

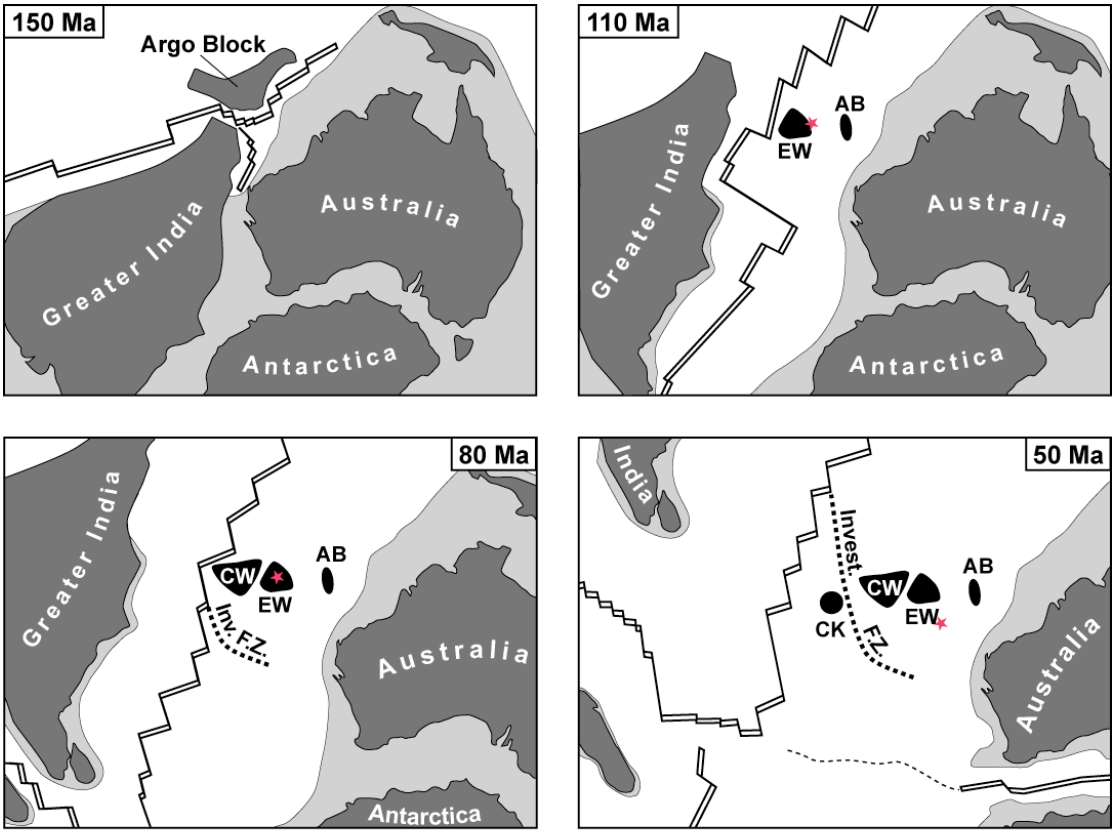
150 Ma
Argo Block
Greater India
Australia
Antarctica
110 Ma
AB
EW
Greater India
Australia
Antarctica
80 Ma
Greater India
CW
EW
AB
Inv. FZ.
Australia
Antarctica
50 Ma
India
Invest.
CW
AB
CK
EW
FZ
Australia

Figure 6

Table 1: 40Ar/39Ar dating results

Sample No	Rock Type	Material Dated	Step-heating plateau data							
			Age (Ma)	±	2s (Ma)	MSWD	Probability	%39Ar	Steps	Alteration Index
Investigator Ridge										
SO199-DR8-5		plagioclase	62,1	±	2,7	1,10	0,35	76,7	5 to 19	0.0004-0.002
SO199-DR10-16	pillow	plagioclase	74,6	±	2,5	1,30	0,22	82,2	8 to 16	0.0002-0.002
SO199-DR11-4	Gabbro	plagioclase	90,6	±	2,1	2,7	0,02	67,5	12 to 17	0.0003-0.002
SO199-DR23-15	Gabbro	plagioclase	102,5	±	2,9	0,7	0,50	53,4	15 to 17	0.0005-0.0008
SO199-DR30-1A	pillow glass	glass	153,1	±	3,3	0,5	0,84	84,5	11 to 18	0.0001-0.0002
Cocos-Keeling Volcanic Province										
SO199-DR13-1	Trachyandesite	plagioclase	56,0	±	0,2	0,81	0,66	97,4	6 to 20	0.0002 - 0.002
SO199-DR13-12C		hornblende	55,6	±	0,2	1,19	0,31	81,2	13 to 18	0.0002 - 0.0003
SO199 DR16-1C	Basalt	hornblende	46,7	±	0,2	0,96	0,47	86,4	8 to 17	0.0002 - 0.0004
SO199-DR21-1		matrix	47,0	±	0,2	0,86	0,56	84,0	8 to 17	0.0002 - 0.0004
Outsider Smt										
SO199-DR1-10		glass	53,4	±	0,3	1,40	0,22	50,0	6 to 10	0.0003 - 0.001
Central Wharton Basin Volcanic Province										
SO199-DR35-1A	Basalt	plagioclase	63,6	±	2,5	1,60	0,10	76,3	7 to 18	0.0001 - 0.001
SO199-DR40-1	Trachybasalt	plagioclase	70,4	±	0,3	0,7	0,60	85,8	15 to 20	0.0001 - 0.0005
SO199-DR40-2	Trachybasalt	plagioclase	69,5	±	0,5	0,8	0,57	81,1	12 to 17	0.0001 - 0.0003
SO199 DR40-3	Trachybasalt	plagioclase	70,1	±	0,4	0,14	0,99	46,7	10 to 16	0.0007 - 0.001
SO199-DR42-1		plagioclase	71,6	±	0,5	0,79	0,58	55,6	11 to 17	0.0002 - 0.0005
SO199 DR42-3	Trachybasalt	plagioclase	70,9	±	0,5	1,09	0,36	52,1	7 to 12	0.0001 - 0.0002
SO199 DR44-1	basaltic Trachyandesite	plagioclase	63,5	±	0,3	0,24	0,98	86,4	8 to 15	0.0001 - 0.0006
SO199-DR45-1	Trachyte	K-feldspar	64,9	±	0,1	1,2	0,31	69,9	13 to 17	0.0001 - 0.0002
SO199-DR49-1	basaltic Trachyandesite	plagioclase	85,0	±	0,4	1,2	0,32	76,8	10 to 14	0.0001 - 0.0002
SO199-DR49-3		plagioclase	84,2	±	0,7	0,53	0,81	82,6	13 to 20	0.0002 - 0.0005
SO199-DR50-1	Phonotephrite	plagioclase	82,1	±	0,2	1,5	0,17	79,5	11 to 17	0.0002 - 0.0006
SO199-DR50-9C		K-feldspar	81,1	±	0,2	1,60	0,15	96,2	1 to 16	0.00003 - 0.0002
SO199-DR87-1	basaltic Trachyandesite	plagioclase	95,6	±	1,4	1,7	0,14	62,3	12 to 17	0.00015 - 0.0003
SO199-DR87-19C		K-feldspar	89,8	±	0,2	0,33	0,86	80,7	16 to 20	0.00002 - 0.00003

Table 1: continued

Sample No	Rock Type	Material Dated	Step-heating plateau data							
			Age (Ma)	±	2s (Ma)	MSWD	Probability	%39Ar	Steps	Alteration Index
Christmas Island (Lower Volcanic Series)										
SO199-DR55-1	Trachybasalt	plagioclase	40,2	±	0,2	1,2	0,31	96,2	7 to 11	0.00015 - 0.00035
SO199-DR55-3		plagioclase	39,6	±	0,4	0,20	0,94	65,3	15 to 19	0.00015 - 0.001
SO199-DR55-3		hornblende	39,3	±	0,4	0,89	0,54	87,5	8 to 17	0.00007 - 0.0004
CH5A		matrix	41,1	±	0,1	1,50	0,10	86,1	5 to 19	0.003 - 0.004
CH9		matrix	37,0	±	0,6	1,70	0,11	52,3	5 to 12	0.004 - 0.08
CH11		matrix	42,6	±	0,4	1,60	0,09	53,1	7 to 18	0.004 - 0.01
CH13		matrix	43,6	±	0,4	2,00	0,02	64,9	6 to 17	0.007 - 0.009
Christmas Island (Upper Volcanic Series)										
CH1A		matrix	4,31	±	0,14	1,40	0,11	100,0	1 to 19	0.001 - 0.01
CH2		matrix	4,50	±	0,18	0,48	0,96	100,0	1 to 18	0.0008 - 0.02
CH3		matrix	4,52	±	0,18	1,30	0,17	97,5	2 to 19	0.0007 - 0.01
CH4		matrix	4,35	±	0,24	0,69	0,66	58,0	4 to 10	0.002 - 0.009
Eastern Wharton Basin Volcanic Province										
SO199-DR56-1	Basalt	plagioclase	105,3	±	2,0	1,2	0,29	74,4	6 to 9	0.0002 - 0.009
SO199 DR57-1	Basalt	plagioclase	107,1	±	4,1	1,90	0,09	69,5	8 to 13	0.00015-0.0005
SO199-DR58-1	basaltic Trachyandesite	plagioclase	94,9	±	0,4	1,4	0,20	85,6	13 to 20	0.00015-0.00025
SO199-DR58-2	basaltic Trachyandesite	plagioclase	94,3	±	0,3	0,04	0,97	50,5	17 to 19	0.00015-0.0002
SO199-DR59-3		plagioclase	96,6	±	0,4	1,40	0,22	89,5	10 to 15	0.0002-0.0009
SO199-DR65-1	Trachybasalt	plagioclase	103,6	±	0,7	0,7	0,60	93,5	6 to 10	0.00015 - 0.0003
SO199-DR66-5		plagioclase	111,8	±	6,5	1,70	0,09	59,8	11 to 19	0.0004 - 0.002
SO199-DR73-5		plagioclase	115,9	±	3,8	1,60	0,09	49,6	10 to 20	0.0002 - 0.0007
SO199-DR73-11C		K-feldpar	114,7	±	0,3	0,72	0,72	79,7	1 to12	0.00002 - 0.01
SO199-DR75-2		plagioclase	115,2	±	2,3	2,90	0,002	89,1	9 to 18	0.0002 - 0.001
SO199-DR79-3	Trachyte	K-feldpar	101,5	±	0,2	1,7	0,13	86,3	15 to 20	0.00003 - 0.00007
SO199-DR79-4	Trachyte	K-feldpar	101,8	±	0,3	1,7	0,16	80,5	13 to 16	0.00003 - 0.0001
Argo Basin Volcanic Province										
SO199-DR72-1	Basalt	plagioclase	136,2	±	1,7	1,9	0,11	80,6	6 to 10	0.00015 - 0.0002

Table 2: Sr-Nd-Pb-Hf Isotopes

Sample No	Lat °S	Long °E	Depth (mbsl)	Age (Ma)	±2σ (Ma)	87Sr/ 86Sr	±2σ	87Rb/ 86Sr	87Sr/ 86Sr_i	143Nd/ 144Nd	±2σ	εNd	147Sm/ 144Nd	143Nd/ 144Nd_i	εNd_t
Investigator Ridge															
SO199-DR2-3	7.013	98.107	4602	*62.1*											
SO199-DR2-4	7.013	98.107	4602	*62.1*		0.703475	5	0.174	0.703321	0.513026	2	7.57	0.226	0.512934	7.34
SO199-DR5-1	8.157	98.597	4357	*62.1*		0.703502	5	0.115	0.703400	0.513000	3	7.06	0.182	0.512926	7.17
SO199-DR6-2	9.041	98.074	4135	*62.1*		0.705150	59	0.203	0.704971	0.513069	2	8.41	0.249	0.512968	7.99
SO199-DR6-6	9.041	98.074	4135	*62.1*											
SO199-DR6-8	9.041	98.074	4135	*62.1*		0.705877	6	0.012	0.705867	0.512868	3	4.48	0.214	0.512781	4.35
SO199-DR8-1	9.953	98.067	4925	*62.1*		0.703304	5	0.156	0.703167	0.512947	3	6.03	0.145	0.512888	6.44
SO199-DR8-5	9.953	98.067	4925	**62.1**	**2.7**										
SO199-DR9-1	10.887	98.079	4700	*62.1*		0.703791	5	0.260	0.703562	0.512870	3	4.52	0.133	0.512816	5.02
SO199-DR10-1	10.988	98.130	4060	*74.6*											
SO199-DR10-2	10.988	98.130	4060	*74.6*											
SO199-DR10-9	10.988	98.130	4060	*74.6*											
SO199-DR10-15	10.988	98.130	4060	*74.6*											
SO199-DR10-16	10.988	98.130	4060	**74.6**	**2.5**										
SO199-DR11-1	11.938	98.192	3953	*90.6*		0.705449	5	0.127	0.705285	0.512757	3	2.32	0.158	0.512663	2.76
SO199-DR11-4	11.938	98.192	3953	**90.6**	**2.1**	0.705404	5	0.017	0.705382	0.512740	3	1.98	0.166	0.512641	2.33
SO199-DR23-1A	13.903	98.371	4203	*102.5*											
SO199-DR23-14	13.903	98.371	4203	*102.5*		0.704341	5	0.034	0.704291	0.512956	3	6.21	0.209	0.512817	6.06
SO199-DR23-15	13.903	98.371	4203	**102.5**	**2.9**	0.704853	5	0.023	0.704820	0.512959	4	6.26	0.202	0.512823	6.19
SO199-DR23-19	13.903	98.371	4203	*102.5*											
SO199-DR29-1	16.565	98.839	5262	*140*		0.703655	6	0.029	0.703597	0.512952	3	6.13	0.167	0.512800	6.13
SO199-DR30-1A	16.783	98.785	5060	**153.1**	**3.3**	0.704326	5	0.420	0.703411	0.512873	3	4.58	0.230	0.512642	3.92
SO199-DR30-6	16.783	98.785	5060	*153.1*											
SO199 DR31-1	17.585	99.117	5361												
Cocos-Keeling Volcanic Province															
SO199-DR13-1	11.906	96.651	2402	**56.0**	**0.2**	0.703661	6	0.218	0.703487	0.512846	3	4.06	0.120	0.512802	4.61
SO199-DR13-12C	11.906	96.651	2402	**55.6**	**0.2**										
SO199 DR16-1C	12.394	95.288	2883	**46.7**	**0.2**	0.703733	6	0.161	0.703626	0.512789	3	2.95	0.104	0.512758	3.50
SO199-DR16-2C	12.394	95.288	2883	*51.7*											
SO199-DR18-1	12.805	95.377	3549	*51.7*											
SO199-DR20-6	13.606	96.389	3140	*51.7*		0.704246	5	0.426	0.703933	0.512819	3	3.54	0.136	0.512773	3.94
Outsider Smt															
SO199-DR1-1	6.227	97.373	4036	*51.7*		0.704363	5	0.203	0.704214	0.512865	3	4.42	0.146	0.512815	4.75
SO199-DR1-10	6.227	97.373	4036	**53.4**	**0.3**										

Sample No	Lat °S	Long °E	Depth (mbsl)	Age (Ma)	±2σ (Ma)	87Sr/ 86Sr	±2σ	87Rb/ 86Sr	87Sr/ 86Sr_i	143Nd/ 144Nd	±2σ	εNd	147Sm/ 144Nd	143Nd/ 144Nd_i	εNd_t
Central Wharton Basin Volcanic Province															
SO199-DR35-1A	10.312	99.491	3084	**63.6**	**2.5**	0.703583	5	0.220	0.703384	0.512946	2	6.01	0.161	0.512879	6.31
SO199 DR36-1	10.352	99.500	2548	*75.9*											
SO199-DR40-1	10.765	101.812	4306	**70.4**	**0.3**	0.704301	5	0.113	0.704188	0.512712	3	1.44	0.122	0.512656	2.11
SO199-DR40-2	10.765	101.812	4306	**69.5**	**0.5**	0.704423	5	0.079	0.704344	0.512702	3	1.25	0.121	0.512647	1.92
SO199 DR40-3	10.765	101.812	4306	**70.1**	**0.4**										
SO199 DR41-1	10.759	102.176	3754	*75.9*											
SO199-DR41-3	10.759	102.176	3754	*75.9*											
SO199-DR42-1	11.030	102.304	3963	**71.6**	**0.5**										
SO199 DR42-3	11.030	102.304	3963	**70.9**	**0.5**	0.704623	6	0.243	0.704378	0.512668	3	0.59	0.125	0.512610	1.24
SO199 DR44-1	11.775	103.241	2525	**63.5**	**0.3**	0.704852	6	0.144	0.704722	0.512449	3	-3.68	0.109	0.512404	-2.97
SO199-DR45-1	11.663	103.534	3746	**64.9**	**0.1**	0.724821	6	16.097	0.709980	0.512204	3	-8.46	0.087	0.512168	-7.55
SO199 DR46-1	10.915	103.617	4361	*75.9*		0.704440	5	0.131	0.704299	0.512717	3	1.54	0.119	0.512658	2.29
SO199 DR48-1	11.457	104.488	2202	*75.9*											
SO199 DR48-2C	11.457	104.488	2202	*75.9*											
SO199-DR49-3	11.512	104.783	4582	**84.2**	**0.7**										
SO199-DR49-1	11.512	104.783	4582	**85**	**0.4**	0.705341	6	0.220	0.705075	0.512447	2	-3.73	0.110	0.512385	-2.79
SO199 DR49-8	11.512	104.783	4582	*75.9*		0.836678	7	38.320	0.795364	0.512329	2	-6.03	0.104	0.512277	-5.14
SO199 DR49-14	11.512	104.783	4582	*75.9*		0.796280	7	31.454	0.762369	0.512507	2	-2.55	0.096	0.512459	-1.58
SO199-DR50-1	11.331	104.783	3125	**82.1**	**1.5**										
SO199 DR50-2	11.331	104.783	3125	*75.9*		0.709496	6	3.236	0.706007	0.512405	3	-4.55	0.098	0.512356	-3.60
SO199-DR50-9C	11.331	104.783	3125	**81.1**	**0.2**										
SO199 DR52-1	10.908	104.534	2820	*75.9*											
SO199-DR84-1	13.036	103.875	3542	*75.9*											
SO199-DR84-2	13.036	103.875	3542	*75.9*											
SO199-DR87-1	14.120	102.172	3377	**95.6**	**1.4**										
SO199-DR87-3	14.120	102.172	3377	*75.9*											
SO199-DR87-19C	14.120	102.172	3377	**89.8**	**0.2**										
SO199-DR89-1	11.933	101.616	4290	*75.9*											
Christmas Island (Lower Volcanic Series)															
SO199 DR54-1	10.540	105.403	3626	*40.47*		0.704043	3	0.068	0.704004	0.512732	3	1.84	0.113	0.512703	2.28
SO199-DR55-1	10.514	105.474	1891	**40.1**	**0.2**	0.703837	5	0.089	0.703786	0.512829	3	3.73	0.115	0.512799	4.15
SO199-DR55-3	10.514	105.474	1891	**39.64**	**0.43**	0.703806	3	0.035	0.703786	0.512838	3	3.89	0.110	0.512809	4.33
CH5A				**41.08**	**0.13**	0.714025	3	12.020	0.707011	0.512698	3	1.16	0.098	0.512671	1.68
CH5B				*40.47*		0.713002	3	6.106	0.709492	0.512708	2	1.36	0.095	0.512683	1.89
CH6				*40.47*		0.709842	3	3.949	0.707572	0.512708	2	1.37	0.095	0.512683	1.90
CH8				*40.47*		0.704178	3	0.060	0.704143	0.512976	3	6.59	0.194	0.512925	6.61
CH9				**36.96**	**0.55**	0.703990	3	0.087	0.703944	0.512778	3	2.73	0.111	0.512751	3.13
CH10				*40.47*		0.703837	3	0.106	0.703776	0.512801	3	3.19	0.123	0.512769	3.57
CH11				**42.61**	**0.4**	0.704106	3	0.142	0.704021	0.512714	3	1.48	0.111	0.512683	1.95
CH12				*40.47*		0.704245	3	0.106	0.704184	0.512661	2	0.44	0.097	0.512635	0.95
CH13				**43.61**	**0.38**	0.704098	3	0.131	0.704017	0.512712	3	1.44	0.113	0.512680	1.90

Sample No	Lat °S	Long °E	Depth (mbsl)	Age (Ma)	±2σ (Ma)	87Sr/86Sr	±2σ	87Rb/86Sr	87Sr/86Sr_i	143Nd/144Nd	±2σ	εNd	147Sm/144Nd	143Nd/144Nd_i	εNd_t
Christmas Island (Upper Volcanic Series)															
CH1A				**4.31**	**0.14**	0.705432	2	0.116	0.705425	0.512506	3	-2.57	0.106	0.512503	-2.52
CH1B				*4.42*		0.705435	3	0.117	0.705427	0.512505	3	-2.59	0.105	0.512502	-2.54
CH2				**4.5**	**0.18**	0.705430	3	0.115	0.705423	0.512518	2	-2.34	0.103	0.512515	-2.29
CH3				**4.52**	**0.18**	0.705458	3	0.110	0.705450	0.512505	3	-2.59	0.104	0.512502	-2.54
CH4				**4.35**	**0.24**	0.705428	3	0.114	0.705421	0.512505	2	-2.60	0.101	0.512502	-2.55
CH7A				*4.42*		0.705521	3	0.080	0.705516	0.512472	3	-3.24	0.101	0.512469	-3.19
CH7B				*4.42*		0.705493	3	0.085	0.705488	0.512476	3	-3.15	0.104	0.512473	-3.10
Eastern Wharton Basin Volcanic Province															
SO199-DR56-1	11.263	106.555	3997	**105.3**	**2**	0.705232	6	0.045	0.705165	0.512374	3	-5.15	0.118	0.512293	-4.09
SO199-DR56-4	11.263	106.555	3997	*104.8*		0.705534	5	0.313	0.705067	0.512361	2	-5.40	0.117	0.512281	-4.33
SO199 DR56-6	11.263	106.555	3997	*104.8*		0.707911	6	1.714	0.705358	0.512426	3	-4.14	0.107	0.512352	-2.95
SO199 DR57-1	11.710	106.554	3501	**107.1**	**4.1**	0.704143	5	0.221	0.703807	0.512725	2	1.70	0.133	0.512632	2.57
SO199-DR58-1	11.737	106.880	2609	**94.87**	**0.41**	0.705606	5	0.225	0.705303	0.512346	3	-5.70	0.137	0.512261	-4.98
SO199-DR58-2	11.737	106.880	2609	**94.26**	**0.33**										
SO199 DR58-5	11.737	106.880	2609	*104.8*											
SO199 DR59-1	11.761	106.884	3173	*104.8*											
SO199-DR59-3	11.761	106.884	3173	**96.6**	**0.4**										
SO199 DR59-4	11.761	106.884	3173	*104.8*		0.705753	6	0.388	0.705175	0.512391	2	-4.81	0.110	0.512316	-3.65
SO199-DR62-1	12.457	106.650	3477	*104.8*		0.704080	6	0.204	0.703776	0.512851	3	4.16	0.137	0.512758	4.97
SO199-DR63-1	12.662	106.650	3388	*104.8*											
SO199-DR65-1	12.610	107.239	3952	**103.6**	**0.7**	0.704877	5	0.231	0.704537	0.512487	3	-2.94	0.138	0.512394	-2.16
SO199-DR66-1	12.230	107.826	3907	*104.8*		0.704097	6	0.227	0.703758	0.512686	3	0.94	0.147	0.512586	1.61
SO199 DR66-2	12.230	107.826	3907	*104.8*		0.703943	5	0.108	0.703782	0.512722	3	1.63	0.157	0.512614	2.17
SO199-DR66-5	12.230	107.826	3907	**111.8**	**6.5**										
SO199-DR73-1	14.230	108.496	4331	*104.8*											
SO199-DR73-5	14.230	108.496	4331	**115.9**	**3.8**										
SO199-DR73-11C	14.230	108.496	4331	**114.7**	**0.3**										
SO199-DR75-2	13.388	108.003	3639	**115.2**	**2.3**										
SO199-DR79-1	14.249	106.090	3787	**103.72**	**0.86**	0.705658	6	0.494	0.704929	0.512560	3	-1.52	0.128	0.512473	-0.62
SO199-DR79-3	14.249	106.090	3787	**101.5**	**0.2**	0.708796	6	2.389	0.705349	0.512555	3	-1.62	0.117	0.512477	-0.59
SO199-DR79-4	14.249	106.090	3787	**101.8**	**0.34**	0.707231	5	1.402	0.705203	0.512544	3	-1.84	0.117	0.512466	-0.81
SO199-DR80-1	13.274	105.225	3220	*104.8*											
SO199-DR81-1	13.360	105.168	4400	*104.8*											
SO199-DR82-1	13.607	105.187	3861	*104.8*											
Argo Basin Volcanic Province															
SO199-DR69-1	15.074	114.085	4020	*136.2*											
SO199-DR72-1	12.347	113.779	4398	**136.2**	**1.7**	0.704267	5	0.600	0.703105	0.512949	3	6.06	0.166	0.512800	6.59

Table 2: Sr-Nd-Pb-Hf Isotopes cont.

Sample No	206Pb/ 204Pb	±2σ	207Pb/ 204Pb	±2σ	208Pb/ 204Pb	±2σ	207Pb/ 206Pb	±2σ	208Pb/ 206Pb	±2σ	238U/ 204Pb	232Th/ 204Pb	206Pb/ 204Pb_i	207Pb/ 204Pb_i	208Pb/ 204Pb_i	207Pb/ 206Pb_i	208Pb/ 206Pb_i
Investigator Ridge																	
SO199-DR2-3																	
SO199-DR2-4	18.0023	19	15.4876	17	37.9008	43	0.86031	2	2.10533	7	7.25	9.43	17.93	15.48	37.87	0.86349	2.1119
SO199-DR5-1	18.4466	8	15.5252	9	38.4032	29	0.84163	2	2.08186	8	21.66	55.29	18.24	15.52	38.23	0.85076	2.0965
SO199-DR6-2	19.0318	21	15.5545	18	38.6448	48	0.81729	2	2.03054	5	41.58	42.45	18.63	15.54	38.51	0.83393	2.0674
SO199-DR6-6																	
SO199-DR6-8	17.8372	11	15.5279	10	37.9181	28	0.87053	2	2.12579	6	4.32	15.66	17.80	15.53	37.87	0.87247	2.1281
SO199-DR8-1	18.4987	12	15.5179	12	38.5080	36	0.83886	2	2.08167	8	22.46	72.06	18.28	15.51	38.29	0.84828	2.0943
SO199-DR8-5																	
SO199-DR9-1	19.0619	11	15.5926	10	39.3136	25	0.81800	1	2.06242	3	26.99	115.72	18.80	15.58	38.96	0.82871	2.0721
SO199-DR10-1																	
SO199-DR10-2																	
SO199-DR10-9																	
SO199-DR10-15																	
SO199-DR10-16																	
SO199-DR11-1	18.8809	20	15.6645	18	41.2094	53	0.82965	2	2.18259	9	10.13	117.77	18.74	15.66	40.68	0.83563	2.1711
SO199-DR11-4	17.6878	11	15.5420	11	37.8906	32	0.87868	2	2.14219	7	3.99	13.80	17.63	15.54	37.83	0.88134	2.1455
SO199-DR23-1A																	
SO199-DR23-14	17.9677	17	15.5191	15	37.9075	40	0.86372	2	2.10976	7	8.80	11.01	17.83	15.51	37.85	0.87018	2.1233
SO199-DR23-15	17.9170	30	15.5154	26	37.9051	66	0.86596	3	2.11559	10	7.45	14.38	17.80	15.51	37.83	0.87144	2.1257
SO199-DR23-19																	
SO199-DR29-1	18.6053	16	15.5423	15	38.7635	39	0.83537	2	2.08346	6	29.26	123.66	17.96	15.51	37.90	0.86349	2.1101
SO199-DR30-1A	18.4840	12	15.5479	10	38.6073	27	0.84115	1	2.08869	3	20.92	26.30	17.98	15.52	38.41	0.86330	2.1360
SO199-DR30-6																	
SO199 DR31-1																	
Cocos-Keeling Volcanic Province																	
SO199-DR13-1	19.2476	12	15.6027	11	39.7417	36	0.81063	2	2.06475	9	15.27	153.11	19.11	15.60	39.32	0.81595	2.0569
SO199-DR13-12C																	
SO199 DR16-1C	18.9765	12	15.5838	11	39.4895	29	0.82121	2	2.08096	6	15.40	128.47	18.86	15.58	39.19	0.82581	2.0776
SO199-DR16-2C																	
SO199-DR18-1																	
SO199-DR20-6	18.8384	18	15.5899	16	39.6043	48	0.82756	2	2.10231	10	4.23	162.59	18.80	15.59	39.19	0.82897	2.0840
Outsider Smt																	
SO199-DR1-1	18.5580	16	15.6329	17	38.9640	52	0.84238	3	2.09958	13	21.67	80.23	18.38	15.62	38.76	0.84994	2.1083
SO199-DR1-10																	

Sample No	206Pb/204Pb	±2σ	207Pb/204Pb	±2σ	208Pb/204Pb	±2σ	207Pb/206Pb	±2σ	208Pb/206Pb	±2σ	238U/204Pb	232Th/204Pb	206Pb/204Pb_i	207Pb/204Pb_i	208Pb/204Pb_i	207Pb/206Pb_i	208Pb/206Pb_i
Central Wharton Basin Volcanic Province																	
SO199-DR35-1A	18.8907	8	15.5857	7	39.1474	18	0.82504	1	2.07231	3	30.02	109.07	18.59	15.57	38.80	0.83749	2.0870
SO199 DR36-1																	
SO199-DR40-1	18.6055	7	15.6263	6	38.9374	15	0.83987	1	2.09279	2	29.23	102.44	18.28	15.61	38.58	0.85378	2.1100
SO199-DR40-2	18.5991	7	15.6272	5	38.9487	14	0.84021	1	2.09412	2	29.22	105.84	18.28	15.61	38.58	0.85395	2.1104
SO199 DR40-3																	
SO199 DR41-1																	
SO199-DR41-3																	
SO199-DR42-1																	
SO199 DR42-3	18.3828	8	15.6251	7	38.6193	21	0.84998	1	2.10083	5	23.60	78.22	18.12	15.61	38.34	0.86154	2.1159
SO199 DR44-1	17.9610	13	15.6165	15	38.4073	47	0.86946	2	2.13837	12	16.36	69.27	17.80	15.61	38.19	0.87695	2.1456
SO199-DR45-1	17.5894	14	15.6420	16	38.5412	50	0.88929	2	2.19115	12	6.20	109.72	17.53	15.64	38.19	0.89230	2.1789
SO199 DR46-1	18.3421	8	15.6290	9	38.5452	26	0.85209	2	2.10146	7	25.17	83.54	18.04	15.61	38.23	0.86538	2.1188
SO199 DR48-1																	
SO199 DR48-2C																	
SO199-DR49-3																	
SO199-DR49-1	17.9742	10	15.6559	10	38.4444	25	0.87102	1	2.13887	4	13.93	68.36	17.79	15.65	38.16	0.87958	2.1449
SO199 DR49-8	17.7578	10	15.6559	13	38.5262	44	0.88163	3	2.16953	14	3.55	92.62	17.72	15.65	38.18	0.88361	2.1550
SO199 DR49-14	18.0356	12	15.6656	14	38.5490	44	0.86859	3	2.13738	12	4.33	149.34	17.98	15.66	37.99	0.87093	2.1122
SO199-DR50-1																	
SO199 DR50-2	18.0613	11	15.6742	11	38.7054	33	0.86784	2	2.14300	7	10.96	55.29	17.93	15.67	38.50	0.87377	2.1469
SO199-DR50-9C																	
SO199 DR52-1																	
SO199-DR84-1																	
SO199-DR84-2																	
SO199-DR87-1																	
SO199-DR87-3																	
SO199-DR87-19C																	
SO199-DR89-1																	
Christmas Island (Lower Volcanic Series)																	
SO199 DR54-1	19.2806	12	15.6473	12	39.2136	35	0.81155	2	2.03383	8	34.34	89.17	19.06	15.64	39.03	0.82023	2.0475
SO199-DR55-1	19.5640	12	15.6475	11	39.5626	32	0.79981	1	2.02221	5	29.62	132.52	19.38	15.64	39.30	0.80699	2.0279
SO199-DR55-3	19.5623	9	15.6467	9	39.5674	27	0.79984	1	2.02263	6	47.07	173.39	19.27	15.63	39.23	0.81118	2.0354
CH5A	18.9214	9	15.6389	7	39.1070	18	0.82652	1	2.06681	2	54.85	255.04	18.57	15.62	38.59	0.84124	2.0779
CH5B	18.9103	9	15.6380	9	39.1007	29	0.82696	2	2.06769	8	48.38	249.98	18.61	15.62	38.60	0.83973	2.0746
CH6	18.9676	12	15.6435	13	39.1616	38	0.82475	2	2.06465	8	38.29	162.39	18.73	15.63	38.84	0.83477	2.0739
CH8	18.6627	7	15.6532	7	38.9456	24	0.83874	1	2.08681	6	4.01	12.43	18.64	15.65	38.92	0.83981	2.0883
CH9	18.8928	5	15.6061	5	38.9330	13	0.82604	1	2.06073	2	44.22	174.47	18.64	15.59	38.61	0.83667	2.0717
CH10	19.2070	6	15.6364	5	39.2457	12	0.81410	1	2.04330	2	129.78	388.90	18.39	15.60	38.47	0.84820	2.0917
CH11	18.9364	9	15.6390	7	39.1476	18	0.82587	1	2.06732	3	39.97	174.76	18.67	15.63	38.78	0.83693	2.0769
CH12	18.8051	7	15.6455	7	39.0356	19	0.83198	1	2.07580	3	35.51	162.85	18.58	15.63	38.71	0.84143	2.0832
CH13	18.9351	6	15.6399	6	39.1617	16	0.82598	1	2.06821	4	36.51	147.99	18.69	15.63	38.84	0.83631	2.0785

Sample No	206Pb/ 204Pb	±2σ	207Pb/ 204Pb	±2σ	208Pb/ 204Pb	±2σ	207Pb/ 206Pb	±2σ	208Pb/ 206Pb	±2σ	238U/ 204Pb	232Th/ 204Pb	206Pb/ 204Pb_i	207Pb/ 204Pb_i	208Pb/ 204Pb_i	207Pb/ 206Pb_i	208Pb/ 206Pb_i
Christmas Island (Upper Volcanic Series)																	
CH1A	17.8674	17	15.5450	15	38.0317	37	0.87002	2	2.12855	6	11.09	51.89	17.86	15.54	38.02	0.87036	2.1288
CH1B	17.8692	11	15.5467	13	38.0352	40	0.87003	3	2.12853	11	10.97	54.03	17.86	15.55	38.02	0.87037	2.1288
CH2	17.8683	11	15.5461	12	38.0320	37	0.87003	2	2.12846	9	11.32	54.37	17.86	15.55	38.02	0.87040	2.1287
CH3	17.8680	10	15.5458	11	38.0316	34	0.87004	2	2.12848	9	11.70	59.01	17.86	15.55	38.02	0.87042	2.1287
CH4	17.8690	8	15.5461	8	38.0333	24	0.87001	1	2.12846	6	12.12	56.35	17.86	15.55	38.02	0.87038	2.1288
CH7A	17.8498	9	15.5471	8	38.0410	21	0.87100	1	2.13118	4	11.62	56.69	17.84	15.55	38.03	0.87137	2.1314
CH7B	17.8545	14	15.5481	13	38.0543	32	0.87082	2	2.13136	5	12.25	63.30	17.85	15.55	38.04	0.87121	2.1316
Eastern Wharton Basin Volcanic Province																	
SO199-DR56-1	17.7950	7	15.5627	7	38.3717	16	0.87455	1	2.15632	2	35.52	49.77	17.21	15.53	38.11	0.90265	2.2145
SO199-DR56-4	17.5237	11	15.5454	11	38.1879	25	0.88711	1	2.17921	4	29.90	62.18	17.03	15.52	37.86	0.91126	2.2229
SO199 DR56-6	17.5843	15	15.5449	14	38.5763	34	0.88402	1	2.19379	3	3.11	110.54	17.53	15.54	38.00	0.88645	2.1674
SO199 DR57-1	18.5318	18	15.5689	17	39.0988	47	0.84012	2	2.10983	9	19.14	88.72	18.21	15.55	38.63	0.85406	2.1211
SO199-DR58-1	17.3150	8	15.5571	9	37.9010	25	0.89848	2	2.18892	7	13.58	47.81	17.11	15.55	37.68	0.90849	2.2015
SO199-DR58-2																	
SO199 DR58-5																	
SO199 DR59-1																	
SO199-DR59-3																	
SO199 DR59-4	18.0262	14	15.6169	17	38.4505	55	0.86634	3	2.13303	15	10.55	43.37	17.85	15.61	38.22	0.87427	2.1411
SO199-DR62-1	18.6649	6	15.5818	6	39.0976	15	0.83481	1	2.09471	3	19.86	81.47	18.34	15.57	38.67	0.84878	2.1088
SO199-DR63-1																	
SO199-DR65-1	17.3800	15	15.4872	14	38.0517	37	0.89109	2	2.18939	7	16.01	63.37	17.12	15.47	37.73	0.90386	2.2035
SO199-DR66-1	17.8933	8	15.5493	8	38.0842	18	0.86900	1	2.12840	3	26.20	58.01	17.46	15.53	37.78	0.88919	2.1635
SO199 DR66-2	17.7488	9	15.5373	10	38.0665	30	0.87540	2	2.14474	8	12.09	46.81	17.55	15.53	37.82	0.88475	2.1551
SO199-DR66-5																	
SO199-DR73-1																	
SO199-DR73-5																	
SO199-DR73-11C																	
SO199-DR75-2																	
SO199-DR79-1	17.5754	15	15.4970	14	38.3250	37	0.88175	2	2.18061	6	14.25	55.41	17.34	15.49	38.04	0.89286	2.1932
SO199-DR79-3	17.4463	7	15.4971	6	38.3576	15	0.88827	1	2.19861	2	3.72	94.11	17.39	15.49	37.88	0.89113	2.1788
SO199-DR79-4	17.4291	10	15.4947	11	38.3458	34	0.88902	2	2.20010	9	2.43	98.40	17.39	15.49	37.85	0.89088	2.1764
SO199-DR80-1																	
SO199-DR81-1																	
SO199-DR82-1																	
Argo Basin Volcanic Province																	
SO199-DR69-1																	
SO199-DR72-1	19.2896	15	15.6271	13	39.2162	30	0.81013	1	2.03302	4	63.60	125.58	17.93	15.56	38.37	0.86780	2.1397

Table 2: Sr-Nd-Pb-Hf Isotopes cont.

Sample No	176Hf/ 177Hf	±2σ	εHf	176Lu/ 177Hf	176Hf/ 177Hf_i	εHf_t
Investigator Ridge						
SO199-DR2-3						
SO199-DR2-4	0.283178	5	14.34	0.032	0.283139	14.37
SO199-DR5-1						
SO199-DR6-2	0.283538	5	27.10	0.079	0.283443	25.15
SO199-DR6-6						
SO199-DR6-8						
SO199-DR8-1						
SO199-DR8-5						
SO199-DR9-1	0.283018	3	8.71	0.012	0.283004	9.61
SO199-DR10-1						
SO199-DR10-2						
SO199-DR10-9						
SO199-DR10-15						
SO199-DR10-16						
SO199-DR11-1	0.283168	6	13.99	0.050	0.283079	12.92
SO199-DR11-4	0.283133	10	12.77	0.047	0.283050	11.90
SO199-DR23-1A						
SO199-DR23-14	0.283298	6	18.61	0.063	0.283173	16.52
SO199-DR23-15	0.283302	13	18.73	0.058	0.283187	17.02
SO199-DR23-19						
SO199-DR29-1	0.283230	5	16.21	0.027	0.283157	16.80
SO199-DR30-1A	0.283196	3	15.01	0.053	0.283038	12.89
SO199-DR30-6						
SO199 DR31-1						
Cocos-Keeling Volcanic Province						
SO199-DR13-1	0.283024	4	8.90	0.007	0.283016	9.89
SO199-DR13-12C						
SO199 DR16-1C						
SO199-DR16-2C						
SO199-DR18-1						
SO199-DR20-6	0.282992	5	7.78	0.007	0.282985	8.70
Outsider Smt						
SO199-DR1-1	0.283070	5	10.53	0.018	0.283052	11.07
SO199-DR1-10						

Sample No	176Hf/ 177Hf	±2σ	εHf	176Lu/ 177Hf	176Hf/ 177Hf_i	εHf_t
Central Wharton Basin Volcanic Province						
SO199-DR35-1A	0.283101	4	11.62	0.017	0.283079	12.31
SO199 DR36-1						
SO199-DR40-1	0.282863	3	3.21	0.008	0.282852	4.41
SO199-DR40-2	0.282870	3	3.45	0.009	0.282858	4.61
SO199 DR40-3						
SO199 DR41-1						
SO199-DR41-3						
SO199-DR42-1						
SO199 DR42-3	0.282801	6	1.02	0.008	0.282790	2.23
SO199 DR44-1	0.282624	3	-5.25	0.004	0.282619	-3.99
SO199-DR45-1	0.282466	3	-10.81	0.003	0.282462	-9.48
SO199 DR46-1	0.282775	3	0.10	0.011	0.282759	1.25
SO199 DR48-1						
SO199 DR48-2C						
SO199-DR49-3						
SO199-DR49-1	0.282563	3	-7.38	0.005	0.282555	-5.73
SO199 DR49-8	0.282462	4	-10.97	0.004	0.282456	-9.46
SO199 DR49-14	0.282666	5	-3.76	0.002	0.282662	-2.17
SO199-DR50-1						
SO199 DR50-2	0.282537	5	-8.31	0.003	0.282532	-6.76
SO199-DR50-9C						
SO199 DR52-1						
SO199-DR84-1						
SO199-DR84-2						
SO199-DR87-1						
SO199-DR87-3						
SO199-DR87-19C						
SO199-DR89-1						
Christmas Island (Lower Volcanic Series)						
SO199 DR54-1						
SO199-DR55-1	0.282931	3	5.63	0.003	0.282929	6.45
SO199-DR55-3						
CH5A						
CH5B						
CH6						
CH8						
CH9						
CH10						
CH11						
CH12						
CH13						

Sample No	176Hf/ 177Hf	±2σ	εHf	176Lu/ 177Hf	176Hf/ 177Hf_i	εHf_t
Christmas Island (Upper Volcanic Series)						
CH1A						
CH1B						
CH2						
CH3						
CH4						
CH7A						
CH7B						
Eastern Wharton Basin Volcanic Province						
SO199-DR56-1	0.282513	5	-9.15	0.008	0.282496	-7.37
SO199-DR56-4	0.282483	5	-10.23	0.013	0.282457	-8.77
SO199 DR56-6	0.282591	6	-6.42	0.006	0.282579	-4.46
SO199 DR57-1	0.282917	3	5.13	0.014	0.282888	6.53
SO199-DR58-1	0.282503	3	-9.52	0.009	0.282486	-7.95
SO199-DR58-2						
SO199 DR58-5						
SO199 DR59-1						
SO199-DR59-3						
SO199 DR59-4	0.282547	7	-7.94	0.011	0.282525	-6.36
SO199-DR62-1	0.282996	5	7.92	0.011	0.282973	9.48
SO199-DR63-1						
SO199-DR65-1	0.282674	6	-3.46	0.010	0.282655	-1.79
SO199-DR66-1	0.282874	4	3.62	0.016	0.282842	4.84
SO199 DR66-2	0.282871	5	3.52	0.014	0.282843	4.89
SO199-DR66-5						
SO199-DR73-1						
SO199-DR73-5						
SO199-DR73-11C						
SO199-DR75-2						
SO199-DR79-1	0.282773	3	0.04	0.011	0.282751	1.61
SO199-DR79-3	0.282787	3	0.51	0.008	0.282772	2.29
SO199-DR79-4	0.282781	4	0.31	0.006	0.282769	2.21
SO199-DR80-1						
SO199-DR81-1						
SO199-DR82-1						
Argo Basin Volcanic Province						
SO199-DR69-1						
SO199-DR72-1	0.283195	3	14.95	0.020	0.283142	16.18

Supplement_Table1: Major and Trace Elements

Sample No	SiO_2 (%)	TiO_2 (%)	Al_2O_3 (%)	Fe_2O_3 (%)	MnO (%)	MgO (%)	CaO (%)	Na_2O (%)	K_2O (%)	P_2O_5 (%)	H_2O (%)	CO_2 (%)	LOI (%)	Total (%)
Investigator Ridge														
SO199-DR2-3*	48.08	0.94	18.31	8.96	0.12	6.15	11.81	2.57	0.33	0.08	n.a.	n.a.	2.4	99.75
SO199-DR2-4	48.36	0.97	18.4	9.21	0.12	6.29	12.1	2.57	0.31	0.1	2.1	0.32	2.42	100.85
SO199-DR5-1	47.81	1.43	16.94	8.59	0.12	7.85	9.41	3.54	0.53	0.2	3.56	0.33	3.89	100.31
SO199-DR6-2	49.83	0.66	14.48	10.89	0.2	8.87	10.9	1.91	0.43	0.06	2.37	0.27	2.64	100.87
SO199-DR6-6*	36.77	2.04	13.00	10.94	0.25	21.12	3.92	0.73	0.13	0.25	n.a.	n.a.	10.4	99.55
SO199-DR6-8	40.17	0.25	12.98	4.12	0.15	19.53	9.21	2.16	0.22	0.02	9.42	0.04	9.46	98.27
SO199-DR8-1	45.62	1.78	16.28	9.94	0.14	10.33	6.25	3.26	1.07	0.34	4.9	0.71	5.61	100.62
SO199-DR8-5*	46.21	1.61	15.98	10.42	0.13	8.07	7.16	3.39	0.81	0.26	n.a.	n.a.	5.6	99.64
SO199-DR9-1	46.37	2.33	15.56	8.08	0.11	4.2	13.51	3.23	1.88	0.43	0.86	3.72	4.58	100.28
SO199-DR10-1	50.45	0.2	12.67	6.26	0.12	12.29	12.41	1.85	0.75	0.02	3.34	0.03	3.37	100.39
SO199-DR10-2*	50.27	0.29	16.22	4.27	0.10	10.80	13.22	2.21	0.21	0.01	n.a.	n.a.	2.0	99.60
SO199-DR10-9*	47.89	1.15	15.52	10.96	0.15	6.93	10.68	2.58	0.73	0.12	n.a.	n.a.	3.0	99.71
SO199-DR10-15*	47.42	1.42	16.25	12.89	0.11	4.46	9.54	2.47	1.31	0.19	n.a.	n.a.	3.7	99.76
SO199-DR10-16*	46.52	2.54	15.19	15.61	0.13	3.81	8.85	3.09	0.91	0.36	n.a.	n.a.	2.7	99.71
SO199-DR11-1	47.38	1.46	9.32	8.74	0.09	18.05	10.49	2.46	0.13	0.02	1.45	0.02	1.47	99.61
SO199-DR11-4	51.67	0.25	18.48	3.54	0.06	8.1	11.82	3.47	0.22	0.02	1.88	0.03	1.91	99.54
SO199-DR23-1A*	52.28	0.23	17.41	5.00	0.10	9.04	11.79	2.78	0.14	0.01	n.a.	n.a.	0.9	99.68
SO199-DR23-14	47.66	0.27	17.99	4.21	0.1	10.56	11.83	2.15	0.37	0.02	4.66	0.03	4.69	99.85
SO199-DR23-15	46.89	0.42	18.51	3.9	0.08	10.06	13.51	1.86	0.25	0.03	4.42	0.01	4.43	99.94
SO199-DR23-19	45.29	0.21	18.21	3.92	0.11	10.09	15.72	0.58	0.39	0.02	5.97	0.03	6.00	100.54
SO199-DR29-1	48.71	1.1	16.24	9.49	0.13	10.03	10.07	2.14	0.19	0.15	2.68	0.01	2.69	100.94
SO199-DR30-1A	45.14	0.96	17.18	13.08	0.19	9.94	7.16	1.92	1	0.1	3.8	0.05	3.85	100.52
SO199-DR30-6*	48.20	0.74	16.27	9.17	0.13	8.16	12.25	1.91	0.24	0.06	n.a.	n.a.	2.5	99.63
SO199 DR31-1	38.68	0.01<UG	0.54	13.27	0.12	33.53	0.09	0.37	0.04	0.04	14.01	0.13	14.14	100.82
Cocos-Keeling Volcanic Province														
SO199-DR13-1	54.6	1.62	18.74	7.79	0.1	1.89	5.17	5.22	2.65	0.63	1.39	0.03	1.42	99.83
SO199-DR13-12C*	55.64	1.39	17.54	6.78	0.09	1.60	5.02	5.63	3.33	0.66	n.a.	n.a.	2.0	99.68
SO199 DR16-1C	45.11	2.49	19.84	11.43	0.19	4.33	5.87	3.43	2.12	0.89	4.92	0.06	4.98	100.68
SO199-DR16-2C*	43.79	2.30	18.72	10.29	0.15	4.23	5.94	3.35	2.27	0.93	n.a.	n.a.	7.6	99.57
SO199-DR18-1*	46.49	2.10	17.46	12.15	0.21	2.75	5.98	3.67	1.22	0.98	n.a.	n.a.	6.7	99.71
SO199-DR20-6	58.69	0.66	17.44	8.19	0.11	0.83	2.55	5.74	3.68	0.15	1.53	0.03	1.56	99.6
Outsider Smt														
SO199-DR1-1	50.64	1.61	15.87	8.55	0.11	5.61	10.87	3.2	1.39	0.43	1.45	0.25	1.70	99.98
SO199-DR1-10*	49.45	1.58	15.92	8.41	0.11	5.60	11.00	3.07	1.20	0.49	n.a.	n.a.	2.9	99.73

Sample No	SiO_2 (%)	TiO_2 (%)	Al_2O_3 (%)	Fe_2O_3 (%)	MnO (%)	MgO (%)	CaO (%)	Na_2O (%)	K_2O (%)	P_2O_5 (%)	H_2O (%)	CO_2 (%)	LOI (%)	Total (%)
Central Wharton Basin Volcanic Province														
SO199-DR35-1A	48.51	2.49	14.97	13.94	0.16	4.34	10.14	3.32	0.95	0.45	1.25	0.05	1.30	100.57
SO199 DR36-1	19.85	2.5	8.43	10.72	0.15	2.16	24.68	1.79	0.75	14.62>OG	4.1	1.97	6.07	77.1
SO199-DR40-1	45.03	3.49	18.85	13.01	0.12	1.14	7.44	3.39	2.88	2.06>OG	2.19	0.17	2.36	97.71
SO199-DR40-2	43.62	3.58	19.46	13.65	0.09	1.58	7.75	3.23	1.86	2.01>OG	2.87	0.15	3.02	97.84
SO199 DR40-3	49.86	1.98	17.56	11.1	0.11	0.74	5.93	4.66	4.01	2.14>OG	1.54	0.07	1.61	97.56
SO199 DR41-1	45.17	3.37	16.66	12.2	0.22	1.98	8.46	3.63	2.35	2.50>OG	3	0.23	3.23	97.27
SO199-DR41-3*	41.90	3.17	15.22	11.18	0.42	1.94	9.45	3.44	2.35	3.41	n.a.	n.a.	7.1	99.58
SO199-DR42-1*	48.20	3.25	17.50	11.80	0.15	0.99	5.45	3.68	4.21	1.38	n.a.	n.a.	3.0	99.61
SO199 DR42-3	48.1	3.2	18.12	11.46	0.11	0.87	6.71	3.85	3.96	1.88>OG	1.81	0.11	1.92	98.3
SO199 DR44-1	48.09	3.01	17.33	11.78	0.12	3.01	6.89	4.02	2.88	0.99	2.11	0.26	2.37	100.49
SO199-DR45-1	62.2	0.29	17.72	5.17	0.17	0.27	1.43	6.02	6.14	0.1	0.27	0.01	0.28	99.79
SO199 DR46-1	47.35	2.36	19.59	12.59	0.08	1.33	6.82	3.66	2.3	1.03	3.05	0.1	3.15	100.26
SO199 DR48-1	39.69	2.96	15.7	10.2	0.21	0.8	12.45	3.32	3.28	5.40>OG	2.34	1.5	3.84	92.45
SO199 DR48-2C	40.93	2.81	15.68	9.57	0.08	1.31	13.53	3.36	2.54	2.26>OG	2.52	4.94	7.46	97.27
SO199-DR49-3*	48.35	3.13	16.91	9.51	0.08	3.25	5.86	3.75	2.06	1.04	n.a.	n.a.	5.7	99.64
SO199-DR49-1	52.38	3.1	17.09	8.47	0.08	1.8	6.04	4.17	4.16	1.35	1.12	0.07	1.19	99.83
SO199 DR49-8	61.24	0.32	17.28	6.95	0.09	0.18	1.07	6.2	5.95	0.09	0.69	0.02	0.71	100.08
SO199 DR49-14	63.2	0.36	17.59	4.51	0.07	0.31	1.22	6.37	6.16	0.08	0.4	0.01	0.41	100.28
SO199-DR50-1	44.94	0.84	13.59	4.48	0.08	1.11	15.15	3.39	5.09	0.77	0.74	9.07	9.81	99.25
SO199 DR50-2	59.03	0.68	18.76	5.09	0.1	1.04	1.98	4.9	6.48	0.21	2.06	0.04	2.10	100.37
SO199-DR50-9C*	55.19	1.36	18.80	5.63	0.05	0.88	3.46	4.17	6.11	0.51	n.a.	n.a.	3.4	99.56
SO199 DR52-1	46.72	2.89	18.25	9.06	0.14	1.7	8.88	3.56	2.49	1.80>OG	2.57	1.56	4.13	97.82
SO199-DR84-1*	47.49	4.44	14.30	13.39	0.15	3.89	9.08	3.41	0.85	0.53	n.a.	n.a.	2.2	99.73
SO199-DR84-2*	47.51	4.45	14.04	13.50	0.16	3.97	9.09	3.43	0.83	0.56	n.a.	n.a.	2.1	99.64
SO199-DR87-1	50.58	2.9	21.6	8.41	0.05	1.46	5.24	3.4	2.19	0.89	3.2	0.06	3.26	99.98
SO199-DR87-3*	48.37	2.73	19.47	9.38	0.05	1.51	4.69	3.22	2.30	0.74	n.a.	n.a.	7.3	99.76
SO199-DR87-19C*	65.26	0.21	16.24	3.72	0.09	0.15	0.17	6.19	6.58	0.06	n.a.	n.a.	1.1	99.77
SO199-DR89-1*	41.12	2.69	17.77	9.49	0.09	2.43	7.41	3.02	3.03	3.34	n.a.	n.a.	8.9	99.29
Christmas Island (Lower Volcanic Series)														
SO199 DR54-1	41.66	4.22>OG	16.01	14.1	0.31	1.36	9.05	3.66	2	3.30>OG	3.42	0.26	3.68	91.83
SO199-DR55-1	47.5	3.2	15.8	12.37	0.17	2.45	8.07	4.57	2.37	1.94>OG	1.06	0.1	1.16	97.66
SO199-DR55-3*	41.42	3.13	15.60	11.55	0.10	3.90	10.41	3.35	1.25	3.64	n.a.	n.a.	5.1	99.45
CH5A*	58.50	0.35	17.10	7.19	0.22	0.94	2.23	5.08	5.85	0.09	n.a.	n.a.	2.2	99.75
CH5B*	58.71	0.35	17.03	7.25	0.23	0.84	2.27	5.08	5.81	0.09	n.a.	n.a.	2.1	99.76
CH6*	58.90	0.26	17.25	6.77	0.18	0.40	2.25	5.33	5.67	0.05	n.a.	n.a.	2.7	99.76
CH8*	51.17	0.99	19.93	9.04	0.15	3.23	9.45	2.90	0.36	0.11	n.a.	n.a.	2.5	99.83
CH9*	43.08	3.51	11.52	13.01	0.16	10.49	9.19	2.25	1.95	1.00	n.a.	n.a.	3.2	99.36
CH10*	49.35	2.62	13.79	12.29	0.16	7.33	8.09	3.37	1.04	0.51	n.a.	n.a.	1.1	99.65
CH11*	46.28	3.16	12.35	12.42	0.16	9.95	8.92	2.69	1.52	0.52	n.a.	n.a.	1.5	99.47
CH12*	45.70	3.30	12.69	12.36	0.19	8.40	8.94	2.65	1.74	0.72	n.a.	n.a.	2.8	99.49
CH13*	46.46	3.24	12.64	12.22	0.16	8.97	9.23	2.74	1.58	0.54	n.a.	n.a.	1.7	99.48

Sample No	SiO_2 (%)	TiO_2 (%)	Al_2O_3 (%)	Fe_2O_3 (%)	MnO (%)	MgO (%)	CaO (%)	Na_2O (%)	K_2O (%)	P_2O_5 (%)	H_2O (%)	CO_2 (%)	LOI (%)	Total (%)
Christmas Island (Upper Volcanic Series)														
CH1A*	43.48	1.92	12.21	10.95	0.18	11.03	12.24	1.88	2.47	0.58	n.a.	n.a.	2.3	99.24
CH1B	43.06	1.93	12.22	10.97	0.18	11.25	12.39	1.79	2.40	0.55	n.a.	n.a.	2.5	99.24
CH2*	43.07	1.87	11.81	10.84	0.17	11.89	12.30	1.79	2.23	0.54	n.a.	n.a.	2.7	99.21
CH3*	43.35	1.89	11.94	10.98	0.18	11.76	12.28	1.79	2.17	0.53	n.a.	n.a.	2.3	99.17
CH4*	42.90	1.90	12.18	11.00	0.18	11.42	12.31	1.82	2.27	0.54	n.a.	n.a.	2.7	99.22
CH7A*	40.54	2.20	10.75	11.93	0.18	14.67	12.28	1.70	1.74	0.54	n.a.	n.a.	2.6	99.13
CH7B*	40.71	2.20	10.52	12.01	0.18	14.91	12.26	1.59	1.66	0.55	n.a.	n.a.	2.5	99.09
Eastern Wharton Basin Volcanic Province														
SO199-DR56-1	48.1	1.28	23.97	4.72	0.05	1.49	13.84	3.07	1.19	0.3	0.56	1.66	2.22	100.23
SO199-DR56-4	52.35	3.43	17.53	10.08	0.06	1.23	4.62	4.36	3.57	1.06	1.5	0.06	1.56	99.85
SO199 DR56-6	62.42	0.5	18.08	3.99	0.09	0.72	1.55	5.38	5.98	0.11	0.97	0.02	0.99	99.81
SO199 DR57-1	50.52	2.85	14.61	13.16	0.19	4.04	8.84	3.73	1.21	0.4	1.16	0.03	1.19	100.74
SO199-DR58-1	50.16	2.76	17.74	10.64	0.08	2.63	5.81	3.69	2.05	1.14	2.74	0.08	2.82	99.52
SO199-DR58-2	50.93	2.5	17.48	9.75	0.05	2.21	5.87	3.46	3.44	1.49>OG	2.29	0.12	2.41	98.1
SO199 DR58-5	49.89	1.72	17.67	9.29	0.05	1.09	6.37	3.82	4.43	2.52>OG	2.12	0.16	2.28	96.61
SO199 DR59-1	47.71	2.37	16.89	9.68	0.13	1.67	8.33	3.32	4.56	1.79>OG	2.03	1.68	3.71	98.37
SO199-DR59-3*	43.83	2.30	16.25	8.69	0.09	1.41	10.63	3.13	3.96	2.74	n.a.	n.a.	6.6	99.63
SO199 DR59-4	48.31	2.37	17.34	7.41	0.08	0.82	8.82	3.61	4.86	3.68>OG	1.49	0.24	1.73	95.35
SO199-DR62-1	46.56	3.01	18.94	14.39	0.1	1.82	6.74	3.49	1.4	0.5	2.83	0.06	2.89	99.84
SO199-DR63-1*	44.92	2.73	17.68	15.26	0.11	1.72	5.92	3.18	1.56	0.45	n.a.	n.a.	6.2	99.73
SO199-DR65-1	43.25	3.21	18	13.69	0.12	1.44	7.75	2.81	2.51	1.12	3.99	2.26	6.25	100.15
SO199-DR66-1	50.81	1.54	19.92	8.84	0.06	3.84	7.64	3.39	1.68	0.32	2.19	0.03	2.22	100.26
SO199 DR66-2	50.15	1.47	18.02	8.85	0.09	5.66	10.14	3.3	0.87	0.18	1.74	0.01	1.75	100.48
SO199-DR66-5*	50.62	1.63	15.96	9.80	0.13	4.99	10.62	3.03	0.78	0.21	n.a.	n.a.	2.0	99.77
SO199-DR73-1	49.86	2.82	15.56	14.79	0.08	2.35	4.16	3.49	3.06	0.91	3.15	0.08	3.23	100.31
SO199-DR73-5*	50.30	1.38	18.55	8.52	0.07	2.63	5.79	2.52	3.14	0.28	n.a.	n.a.	6.6	99.78
SO199-DR73-11C*	65.20	0.23	15.80	4.02	0.03	0.34	0.15	5.66	6.82	0.03	n.a.	n.a.	1.5	99.78
SO199-DR75-2*	46.03	3.43	13.18	16.62	0.19	4.39	8.05	2.25	1.13	0.29	n.a.	n.a.	4.1	99.66
SO199-DR79-1	48.7	2.99	17.51	9.78	0.12	1.46	7.89	3.63	3.42	1.27	1.83	1.62	3.45	100.22
SO199-DR79-3	62.26	0.43	17.97	4.61	0.1	0.54	1.68	5.22	6.14	0.09	1.05	0.02	1.07	100.11
SO199-DR79-4	61.12	0.49	18.08	5.51	0.08	0.68	1.73	5.08	5.7	0.17	1.33	0.03	1.36	100
SO199-DR80-1*	68.30	0.27	14.15	4.33	0.05	0.18	0.37	5.69	5.38	0.04	n.a.	n.a.	0.9	99.66
SO199-DR81-1*	54.81	1.93	16.89	8.07	0.05	0.74	3.19	4.56	5.68	0.99	n.a.	n.a.	2.8	99.71
SO199-DR82-1*	40.47	3.48	15.27	14.33	0.15	1.41	8.91	2.94	1.86	3.50	n.a.	n.a.	7.4	99.72
Argo Basin Volcanic Province														
SO199-DR69-1*	48.46	2.72	18.04	11.18	0.08	1.61	6.27	3.39	2.55	0.57	n.a.	n.a.	4.9	99.77
SO199-DR72-1	50.16	2.53	19	12.18	0.08	1.77	7.2	3.33	1.59	0.43	2.09	0.03	2.12	100.39

Supplement_Table1: Major and Trace Elements

Sample No	Co (ppm)	Cr (ppm)	Ni (ppm)	V (ppm)	Zn (ppm)	Ga (ppm)	Cs (ppm)	Rb (ppm)	Sr (ppm)	Ba (ppm)	Nb (ppm)	Ta (ppm)	Hf (ppm)	Zr (ppm)	Y (ppm)
Investigator Ridge															
SO199-DR2-3*	38	397	110	259	70	15.7	0.400	8.20	105	3	0.500	<0.1	1.50	53.1	23.8
SO199-DR2-4	35	378	116	245	116	20	0.432	5.98	99.5	5.64	0.697	0.061	1.51	52.4	22.6
SO199-DR5-1	45	216	167	219	113	24	0.435	7.21	182	48.1	6.06	0.377	2.65	107	28.6
SO199-DR6-2	48	100	117	276	54	16	0.064	3.53	50.4	25.4	1.01	0.076	0.59	15.9	18.6
SO199-DR6-6*	39	21	74	278	24	5.8	<0.1	1.50	14.4	12.0	12.3	0.900	4.50	206	39.2
SO199-DR6-8	27	534	268	147	32	8.0	0.010	1.54	358	33.0	0.489	0.044	0.233	6.61	6.85
SO199-DR8-1	44	273	207	190	76	20	0.422	14.7	273	115	16.5	1.01	3.38	162	23.20
SO199-DR8-5*	44	315	211	178	85	15	0.900	15.8	246	80	12.3	0.700	3.20	147	24.5
SO199-DR9-1	31	114	26	268	93	23	0.345	30.6	341	257	37.4	2.23	4.69	209	31.1
SO199-DR10-1	42	744	340	152	63	12	0.424	11.4	67.5	11.2	0.439	0.046	0.167	5.832	4.24
SO199-DR10-2*	29	835	229	141	25	8.5	<0.1	1.70	127	52	0.500	<0.1	0.400	13.5	7.10
SO199-DR10-9*	48	356	141	348	102	15	1.900	50.6	107	31	4.60	0.200	2.00	61.5	20.0
SO199-DR10-15*	30	301	71	347	124	18	0.400	16.7	123	30	6.80	0.500	3.20	113	29.3
SO199-DR10-16*	38	34	45	533	142	21	0.500	18.7	119	74	13.5	0.800	4.80	156	51.3
SO199-DR11-1	52	20	789	269	35	20	0.014	0.751	17.1	3.79	12.5	0.821	1.90	95.4	47.7
SO199-DR11-4	26	251	118	105	15	11	0.045	1.57	261	41.4	0.79	0.062	0.284	9.29	6.25
SO199-DR23-1A*	38	465	185	143	9	10	0.100	2.80	181	17	0.200	<0.1	0.300	5.5	6.60
SO199-DR23-14	28	431	250	126	44	12	0.099	3.19	268	17.9	0.47	0.041	0.212	5.89	6.32
SO199-DR23-15	30	527	186	127	33	16	0.067	1.79	230	13.5	1.39	0.100	0.250	7.06	7.01
SO199-DR23-19	23	467	328	105	72	17	0.083	5.57	21.2	11.0	0.528	0.060	0.218	6.89	6.43
SO199-DR29-1	47	277	277	191	94	20	0.070	1.55	154	34.1	7.96	0.514	1.35	53.3	18.2
SO199-DR30-1A	66	629	293	144	114	11	0.508	14.9	102	24.6	1.80	0.132	1.47	53.6	24.6
SO199-DR30-6*	47	766	171	244	59	13	0.300	4.70	78.0	8	1.10	<0.1	1.30	43.8	21.9
SO199 DR31-1	168	75	2049	67	240	bdl	0.011	0.478	10.3	2.85	0.681	0.019	0.078		0.377
Cocos-Keeling Volcanic Province															
SO199-DR13-1	7	bdl	2	73	144	27	0.941	32.1	425	601	103	5.85	11.0	514	44.4
SO199-DR13-12C*	6	bdl	bdl	64	107	28	0.800	50.7	384	575	96.7	6.20	11.5	413	46.0
SO199 DR16-1C	35	bdl	39	158	127	28	1.05	42.4	761	601	114	7.08	11.3	569	34.2
SO199-DR16-2C*	27	bdl	32	148	97	20	1.40	51.7	779	646	113	7.90	12.6	570	40.5
SO199-DR18-1*	14	bdl	24	128	192	27	0.500	17.4	387	303	63.2	3.80	9.50	386	70.0
SO199-DR20-6	LLD<UG	bdl	bdl	40	142	37	0.289	31.6	215	1256	88.5	5.44	17.8	728	65.3
Outsider Smt															
SO199-DR1-1	37	33	31	273	94	22	0.756	20.5	292	200	17.9	1.08	3.08	134	27.9
SO199-DR1-10*	33	41	31	285	84	18	0.800	20.4	319	197	18.6	1.00	3.20	131	29.8

Sample No	Co (ppm)	Cr (ppm)	Ni (ppm)	V (ppm)	Zn (ppm)	Ga (ppm)	Cs (ppm)	Rb (ppm)	Sr (ppm)	Ba (ppm)	Nb (ppm)	Ta (ppm)	Hf (ppm)	Zr (ppm)	Y (ppm)
Central Wharton Basin Volcanic Province															
SO199-DR35-1A	33	35	28	327	134	26	0.873	18.8	247	123	20.8	1.26	4.19	171	38.1
SO199 DR36-1	84	378	36	233	151	bdl									
SO199-DR40-1	28	37	34	298	137	29	0.617	35.1	897	567	62.6	3.84	6.98	308	38.2
SO199-DR40-2	27	45	34	285	147	28	0.912	28.0	1024	557	63.3	3.94	7.09	310	42.3
SO199 DR40-3	15	bdl	4	133	160	26	0.416	57.5	759	746	75.6	4.80	8.96	414	48.8
SO199 DR41-1	47	226	42	227	181	25	0.746	34.0	960	840	55.3	3.53	5.84	246	30.3
SO199-DR41-3*	37	178	105	231	180	23	0.500	31.1	1065	867	56.4	3.50	6.10	244	28.6
SO199-DR42-1*	22	62	41	332	136	26	0.700	56.5	678	581	56.6	3.40	7.30	299	41.0
SO199 DR42-3	28	54	22	288	145	30	0.639	56.1	669	545	54.6	3.29	6.71	298	34.0
SO199 DR44-1	37	111	75	182	170	29	0.849	47.7	960	832	69.5	4.01	8.39	378	27.1
SO199-DR45-1	bdl	bdl	13	bdl	109	39	0.214	124	22.4	47.9	152	9.83	21.5	823	28.8
SO199 DR46-1	26	395	79	226	122	25	0.725	31.9	706	480	46.7	2.71	5.10	228	37.4
SO199 DR48-1	47	144	77	219	127	19	0.374	43.5	990	929	51.7	3.12	6.04	255	114
SO199 DR48-2C	26	120	59	201	117	27	0.419	30.0	931	882	46.5	2.92	5.35	228	34.8
SO199-DR49-3*	29	62	21	155	177	23	2.50	38.1	643	587	50.9	3.10	8.10	325	33.6
SO199-DR49-1	21	36	11	165	113	26	0.626	58.4	769	704	72.5	4.22	10.0	454	31.2
SO199 DR49-8	bdl	bdl	bdl	39	189	47	0.674	194	14.8	15.1	210	11.1	35.1	1629	71.2
SO199 DR49-14	bdl	bdl	bdl	bdl	113	43	0.172	139	12.9	7.34	83.0	10.1	17.9	449	25.1
SO199-DR50-1	bdl	bdl	bdl	29	81	27	0.949	77.7	333	1168	54.7	3.43	9.27	401	36.7
SO199 DR50-2	bdl	bdl	bdl	bdl	112	34	1.06	115	103	126	135	7.36	22.1	1012	35.8
SO199-DR50-9C*	6	bdl	bdl	68	93	26	1.20	54.6	767	2165	69.9	4.10	11.3	461	19.4
SO199 DR52-1	41	125	38	157	161	24	0.624	32.8	1127	1193	62.9	3.94	7.29	318	30.0
SO199-DR84-1*	45	34	25	420	87	22	0.500	13.1	285	188	31.8	1.90	6.40	241	48.7
SO199-DR84-2*	53	34	21	413	93	21	0.500	12.9	283	178	31.1	2.20	6.20	241	47.9
SO199-DR87-1	24	67	11	341	150	26	0.766	30.2	428	301	34.5	2.47	5.48	221	37.3
SO199-DR87-3*	13	62	bdl	280	122	17	1.10	38.7	428	273	34.1	2.60	5.10	203	40.5
SO199-DR87-19C*	bdl	bdl	bdl	bdl	32	28	0.200	109	15.8	285	60.1	6.40	17.6	748	140
SO199-DR89-1*	16	253	62	196	116	16	1.30	54.6	2767	927	94.8	6.30	11.1	465	34.3
Christmas Island (Lower Volcanic Series)															
SO199 DR54-1	31	104	66	301	162	23	0.920	26.6	1131	470	60.8	4.31	8.36	351	130
SO199-DR55-1	37	105	80	225	173	33	0.208	32.8	1064	471	105	6.20	12.1	567	36.8
SO199-DR55-3*	27	103	69	198	191	23	0.500	15.1	1235	446	106	6.70	13.7	584	54.9
CH5A*	bdl	bdl	bdl	bdl	139	28	2.00	131	31.6	215	163	9.40	19.9	759	46.0
CH5B*	bdl	bdl	bdl	bdl	142	27	0.600	131	62.1	225	171	10.0	19.5	781	46.1
CH6*	bdl	bdl	bdl	bdl	162	30	<0.1	129	94.6	58.0	202	11.5	22.8	941	55.3
CH8*	20	bdl	bdl	271	43	18	1.10	6.90	331	109	1.70	0.200	1.60	46.5	19.5
CH9*	51	274	215	199	76	19	0.200	31.8	1053	561	73.7	4.30	6.50	259	27.5
CH10*	44	240	134	171	79	21	0.200	17.3	471	298	38.1	2.30	6.70	253	25.0
CH11*	53	315	240	235	74	19	0.300	29.5	602	403	55.3	3.40	6.70	258	25.6
CH12*	48	308	213	220	75	19	0.300	31.9	867	569	65.0	3.90	8.50	331	25.1
CH13*	50	301	233	224	74	19	0.100	28.8	638	396	56.9	3.30	6.50	253	25.2

Sample No	Co (ppm)	Cr (ppm)	Ni (ppm)	V (ppm)	Zn (ppm)	Ga (ppm)	Cs (ppm)	Rb (ppm)	Sr (ppm)	Ba (ppm)	Nb (ppm)	Ta (ppm)	Hf (ppm)	Zr (ppm)	Y (ppm)
Christmas Island (Upper Volcanic Series)															
CH1A*	44	664	141	340	69	15	0.900	53.0	1321	1275	54.7	3.30	6.10	251	22.7
CH1B	46	664	141	340	69	15	0.900	51.7	1277	1227	54.1	3.20	5.80	249	21.8
CH2*	47	719	156	331	62	14	0.800	49.1	1239	1192	51.7	3.20	6.10	244	21.5
CH3*	47	712	156	338	61	15	0.800	48.4	1268	1485	53.5	3.20	6.20	245	21.9
CH4*	46	678	149	327	69	15	0.700	49.9	1262	1304	51.5	2.90	5.30	240	20.9
CH7A*	53	1198	243	330	67	13	0.700	37.5	1364	1149	53.6	3.30	5.10	197	19.5
CH7B*	58	1252	264	326	68	13	0.600	36.8	1259	1263	53.7	3.00	5.00	193	19.2
Eastern Wharton Basin Volcanic Province															
SO199-DR56-1	27	bdl	11	125	49	27	0.191	11.5	748	302	18.5	1.09	2.70	116	12.7
SO199-DR56-4	18	bdl	6	212	141	29	0.522	56.1	518	777	55.5	3.35	8.54	373	60.7
SO199 DR56-6	bdl	bdl	bdl	11	113	34	0.072	51.2	86.4	1292	84.7	6.31	19.4	735	44.8
SO199 DR57-1	49	bdl	3	363	126	27	1.06	25.1	329	337	43.2	2.50	5.35	223	39.1
SO199-DR58-1	35	82	53	144	217	26	2.17	41.0	528	378	34.7	2.07	6.00	253	34.4
SO199-DR58-2	25	49	16	146	182	25	2.39	55.0	493	670	32.4	2.10	6.61	279	33.7
SO199 DR58-5	10	bdl	bdl	115	152	28	1.17	74.2	540	1316	77.0	4.78	10.4	447	45.9
SO199 DR59-1	18	18	10	170	144	27	4.65	115	548	996	62.3	3.92	8.04	341	64.7
SO199-DR59-3*	15	34	24	180	112	22	1.70	76.4	661	1011	66.6	3.70	8.70	356	86.1
SO199 DR59-4	14	bdl	bdl	152	118	23	0.823	85.8	640	1075	66.9	3.91	8.32	342	77.6
SO199-DR62-1	32	107	47	296	227	26	1.39	30.3	429	262	39.0	2.26	4.94	208	30.8
SO199-DR63-1*	21	21	26	320	205	22	1.20	33.5	411	180	32.8	2.00	4.70	190	33.7
SO199-DR65-1	33	113	40	276	157	31	0.889	34.7	434	325	29.8	1.85	5.98	253	37.7
SO199-DR66-1	27	204	53	96	215	23	1.53	29.5	375	145	13.0	0.77	2.88	121	26.6
SO199 DR66-2	32	255	49	191	163	19	0.956	13.5	362	143	12.5	0.738	2.76	116	19.9
SO199-DR66-5*	33	287	31	258	66	19	0.500	14.9	377	83.0	9.50	0.600	3.50	114	25.2
SO199-DR73-1	29	bdl	11	235	169	28	2.86	62.6	369	438	25.1	1.68	5.96	238	37.8
SO199-DR73-5*	20	103	36	97	76	18	1.30	45.7	360	243	12.9	1.00	3.20	122	23.0
SO199-DR73-11C*	0	bdl	bdl	<8	105	42	0.200	148	15.2	9	59.6	6.70	23.7	609	55.7
SO199-DR75-2*	42	21	bdl	434	118	21	0.600	19.7	281	154	27.6	1.80	6.70	265	37.4
SO199-DR79-1	28	80	38	157	136	28	3.31	78.6	460	394	33.5	2.12	5.62	252	39.2
SO199-DR79-3	bdl	bdl	bdl	12	119	38	0.094	46.7	56.5	403	52.6	3.76	18.5	845	50.6
SO199-DR79-4	bdl	bdl	bdl	15	123	37	0.194	42.0	86.7	624	53.3	3.48	16.7	792	48.8
SO199-DR80-1*	1	bdl	bdl	12	35	41	0.300	194.1	11.5	5	145	10.0	35.1	1486	63.3
SO199-DR81-1*	7	bdl	bdl	62	130	28	1.30	86.1	350	1078	69.6	4.60	13.5	486	53.2
SO199-DR82-1*	18	bdl	47	445	127	26	0.900	27.4	452	393	43.2	3.10	8.90	346	64.6
Argo Basin Volcanic Province															
SO199-DR69-1*	28	144	58	271	111	22	1.40	40.6	319	116	13.0	0.800	5.10	219	51.4
SO199-DR72-1	35	52	14	173	110	25	1.91	41.0	197	51.1	17.4	1.09	3.98	150	41.0

Supplement_Table1: Major and Trace Elements

Sample No	La (ppm)	Ce (ppm)	Pr (ppm)	Nd (ppm)	Sm (ppm)	Eu (ppm)	Gd (ppm)	Tb (ppm)	Dy (ppm)	Ho (ppm)	Er (ppm)	Tm (ppm)	Yb (ppm)	Lu (ppm)	Pb (ppm)	Th (ppm)	U (ppm)
Investigator Ridge																	
SO199-DR2-3*	2.30	5.90	1.11	5.70	2.20	0.860	3.37	0.630	4.21	0.920	2.61	0.400	2.41	0.370	0.400	<0.2	0.100
SO199-DR2-4	1.65	5.16	0.973	5.70	2.14	0.858	3.00	0.572	3.91	0.835	2.35	0.354	2.33	0.341	0.650	0.095	0.075
SO199-DR5-1	6.02	15.2	2.38	12.0	3.62	1.34	4.43	0.792	5.08	1.06	2.90	0.428	2.80	0.412	0.632	0.533	0.216
SO199-DR6-2	1.09	2.95	0.513	2.95	1.22	0.491	1.94	0.405	2.97	0.686	1.99	0.314	2.17	0.324	0.129	0.082	0.083
SO199-DR6-6*	9.50	29.5	4.23	19.5	5.30	1.61	6.27	1.11	6.88	1.47	4.36	0.620	4.15	0.630	1.40	0.900	0.300
SO199-DR6-8	0.85	2.43	0.404	2.20	0.782	0.444	1.07	0.196	1.30	0.271	0.739	0.106	0.68	0.097	0.382	0.093	0.026
SO199-DR8-1	13.7	30.8	3.98	17.4	4.17	1.51	4.51	0.731	4.38	0.864	2.34	0.341	2.24	0.325	1.25	1.37	0.441
SO199-DR8-5*	10.8	27.2	3.51	14.8	3.85	1.37	4.44	0.780	4.43	0.890	2.50	0.390	2.49	0.380	0.900	1.20	0.300
SO199-DR9-1	28.3	56.9	6.95	29.1	6.41	2.09	6.59	1.02	5.88	1.15	2.99	0.421	2.72	0.392	2.01	3.48	0.838
SO199-DR10-1	0.452	1.21	0.201	1.09	0.395	0.171	0.558	0.109	0.754	0.164	0.453	0.069	0.445	0.069	0.307	0.045	0.047
SO199-DR10-2*	1.00	2.80	0.420	2.20	0.750	0.460	1.17	0.210	1.29	0.280	0.700	0.110	0.690	0.110	0.100	<0.2	<0.1
SO199-DR10-9*	4.20	11.5	1.52	7.00	2.18	0.840	3.12	0.570	3.71	0.770	2.11	0.340	2.12	0.330	0.200	0.400	0.600
SO199-DR10-15*	7.90	15.1	2.50	11.3	3.58	1.26	4.74	0.820	5.39	1.08	3.18	0.500	3.06	0.470	0.900	0.700	0.500
SO199-DR10-16*	12.5	28.4	4.11	19.2	5.61	1.89	7.92	1.42	8.78	1.90	5.68	0.830	5.11	0.760	1.10	1.30	0.700
SO199-DR11-1	8.21	38.3	7.15	36.3	9.54	1.68	9.95	1.64	9.97	2.01	5.36	0.771	4.91	0.671	0.304	0.522	0.046
SO199-DR11-4	1.63	4.38	0.633	2.97	0.819	0.679	1.00	0.177	1.15	0.241	0.657	0.098	0.631	0.094	0.414	0.089	0.026
SO199-DR23-1A*	0.5	1.60	0.260	1.80	0.560	0.530	1.06	0.180	1.22	0.260	0.730	0.100	0.650	0.110	0.200	<0.2	<0.1
SO199-DR23-14	0.76	2.15	0.350	1.92	0.666	0.362	0.91	0.171	1.16	0.248	0.677	0.099	0.637	0.093	0.275	0.047	0.039
SO199-DR23-15	1.02	2.80	0.441	2.35	0.791	0.390	1.05	0.194	1.29	0.273	0.743	0.109	0.689	0.101	0.236	0.052	0.028
SO199-DR23-19	1.01	3.04	0.505	2.52	0.763	0.216	0.965	0.178	1.16	0.247	0.669	0.101	0.649	0.095	0.296	0.096	0.056
SO199-DR29-1	6.09	14.1	1.97	9.31	2.58	0.942	3.03	0.522	3.28	0.670	1.82	0.267	1.72	0.255	0.304	0.570	0.139
SO199-DR30-1A	1.76	5.91	0.872	4.79	1.83	0.716	2.73	0.600	4.50	1.04	3.14	0.518	3.61	0.550	0.404	0.161	0.133
SO199-DR30-6*	1.90	5.70	0.920	5.40	1.74	0.710	2.82	0.530	3.51	0.800	2.40	0.370	2.23	0.370	0.200	<0.2	0.100
SO199 DR31-1	0.136	0.662	0.032	0.127	0.046	0.014	0.055	0.011	0.078	0.017	0.051	0.011	0.085	0.015	2.01	0.023	0.565
Cocos-Keeling Volcanic Province																	
SO199-DR13-1	62.2	133	14.7	57.3	11.4	3.55	10.8	1.64	8.96	1.67	4.38	0.608	3.90	0.550	4.50	10.2	1.05
SO199-DR13-12C*	65.5	136	15.2	58.7	10.8	3.25	10.1	1.64	9.14	1.71	4.53	0.650	4.01	0.600	3.10	11.7	0.700
SO199 DR16-1C	88.8	133	15.1	54.4	9.44	2.82	8.68	1.22	6.43	1.19	3.18	0.460	3.02	0.449	9.50	18.2	2.26
SO199-DR16-2C*	106	142	18.7	66.4	11.0	3.24	8.81	1.41	7.43	1.37	3.67	0.550	3.54	0.530	7.50	21.0	2.90
SO199-DR18-1*	58.0	114	14.1	58.6	12.5	3.92	13.4	2.19	12.5	2.58	7.04	1.05	6.53	1.00	4.20	6.40	0.900
SO199-DR20-6	66.9	107	15.7	63.0	14.2	4.94	14.4	2.33	13.5	2.58	6.74	0.942	6.06	0.871	4.80	11.6	0.313
Outsider Smt																	
SO199-DR1-1	15.7	32.9	4.08	17.5	4.26	1.48	4.78	0.803	4.99	1.02	2.79	0.407	2.67	0.387	2.23	2.70	0.755
SO199-DR1-10*	16.2	34.6	4.32	18.1	4.13	1.46	4.77	0.860	5.13	1.05	2.99	0.430	2.78	0.410	1.60	3.10	0.900

Sample No	La (ppm)	Ce (ppm)	Pr (ppm)	Nd (ppm)	Sm (ppm)	Eu (ppm)	Gd (ppm)	Tb (ppm)	Dy (ppm)	Ho (ppm)	Er (ppm)	Tm (ppm)	Yb (ppm)	Lu (ppm)	Pb (ppm)	Th (ppm)	U (ppm)
Central Wharton Basin Volcanic Province																	
SO199-DR35-1A	15.5	34.7	4.74	22.0	5.86	2.01	6.77	1.14	7.01	1.41	3.77	0.547	3.52	0.508	1.10	1.80	0.512
SO199 DR36-1																	
SO199-DR40-1	51.1	102	12.5	51.8	10.5	3.48	9.91	1.41	7.45	1.34	3.38	0.452	2.81	0.398	3.32	5.13	1.51
SO199-DR40-2	54.7	102	13.1	54.3	10.9	3.66	10.4	1.49	7.92	1.45	3.68	0.495	3.08	0.438	3.25	5.20	1.48
SO199 DR40-3	76.0	144	18.4	73.8	13.8	4.41	12.7	1.73	9.00	1.65	4.20	0.552	3.43	0.495	4.68	6.72	1.78
SO199 DR41-1	44.0	84.0	10.2	42.2	9.09	3.09	8.56	1.21	6.26	1.11	2.70	0.352	2.10	0.293	3.43	4.56	1.65
SO199-DR41-3*	43.3	90.6	9.97	42.1	8.61	2.96	7.96	1.21	6.03	1.04	2.55	0.340	1.96	0.280	2.60	5.10	2.00
SO199-DR42-1*	48.3	97.1	11.7	47.2	9.67	3.28	8.90	1.36	7.51	1.36	3.84	0.530	3.04	0.470	3.40	4.50	1.40
SO199 DR42-3	43.3	90.2	10.8	44.9	9.31	3.14	8.86	1.28	6.83	1.26	3.19	0.434	2.70	0.384	3.61	4.29	1.34
SO199 DR44-1	61.5	123	14.2	55.9	10.1	3.32	9.03	1.21	5.90	1.00	2.41	0.299	1.77	0.239	4.87	5.17	1.26
SO199-DR45-1	124	249	23.0	75.2	10.8	0.854	8.79	1.20	5.90	1.08	2.98	0.440	3.01	0.449	13.3	22.4	1.31
SO199 DR46-1	46.4	68.1	9.50	37.9	7.52	2.55	7.61	1.11	6.21	1.20	3.16	0.438	2.74	0.395	3.38	4.30	1.34
SO199 DR48-1	81.6	92.3	14.6	61.2	12.1	3.89	13.2	1.87	11.1	2.37	6.63	0.922	5.88	0.925	15.6	4.21	2.39
SO199 DR48-2C	46.4	78.1	10.7	44.4	9.08	3.08	8.63	1.20	6.31	1.14	2.91	0.380	2.34	0.335	3.35	3.64	1.44
SO199-DR49-3*	41.2	89.5	10.3	43.7	8.76	2.91	8.20	1.25	6.44	1.22	3.26	0.420	2.58	0.370	3.80	4.20	1.20
SO199-DR49-1	60.0	122	14.3	56.4	10.3	3.22	9.10	1.25	6.31	1.13	2.84	0.375	2.36	0.332	5.85	6.12	1.29
SO199 DR49-8	154	258	32.3	117	20.2	1.07	17.1	2.52	13.6	2.60	7.17	1.05	6.97	1.02	14.0	19.9	0.789
SO199 DR49-14	132	201	30.5	109	17.5	0.559	12.7	1.60	6.88	1.08	2.64	0.331	2.12	0.313	6.82	15.6	0.466
SO199-DR50-1	62.7	102	13.0	49.1	8.49	2.62	7.71	1.09	5.94	1.17	3.22	0.459	3.00	0.453	7.67	5.34	0.808
SO199 DR50-2	94.9	184	19.7	69.6	11.3	2.00	9.55	1.36	7.09	1.31	3.55	0.511	3.34	0.485	14.50	12.2	2.50
SO199-DR50-9C*	50.6	115	12.4	46.9	8.01	3.94	5.90	0.890	4.45	0.73	1.86	0.250	1.44	0.200	3.70	6.90	0.400
SO199 DR52-1	54.1	106	12.7	51.3	10.0	3.34	8.92	1.22	6.20	1.10	2.74	0.355	2.20	0.307	4.60	5.33	1.27
SO199-DR84-1*	23.7	58.8	7.17	33.1	8.11	2.53	8.98	1.51	8.55	1.72	4.71	0.660	4.19	0.630	1.40	2.40	0.400
SO199-DR84-2*	23.6	59.1	7.15	31.4	7.82	2.60	8.88	1.55	8.47	1.72	4.59	0.690	4.02	0.620	1.30	2.80	0.400
SO199-DR87-1	38.5	70.2	9.75	40.5	8.40	2.76	8.24	1.23	6.95	1.33	3.49	0.500	3.17	0.467	1.74	3.86	2.09
SO199-DR87-3*	37.7	71.3	9.52	38.3	7.68	2.61	7.60	1.22	6.89	1.32	3.64	0.500	3.20	0.510	2.00	4.60	1.00
SO199-DR87-19C*	168.0	226	40.1	150	28.8	3.61	25.7	4.48	25.3	5.07	15.5	2.51	17.73	2.900	1.20	18.6	0.400
SO199-DR89-1*	83.9	161	16.3	57.8	9.08	2.92	7.19	1.09	5.49	1.05	2.83	0.410	2.57	0.410	7.70	14.6	2.80
Christmas Island (Lower Volcanic Series)																	
SO199 DR54-1	123	125	22.9	97.0	18.2	5.73	18.8	2.55	14.3	2.93	8.00	1.10	7.03	1.095	3.74	4.97	1.98
SO199-DR55-1	77.8	167	20.1	82.4	15.8	4.80	13.7	1.81	8.50	1.38	3.18	0.374	2.15	0.285	3.62	7.09	1.64
SO199-DR55-3*	90.2	180	22.3	89.8	16.4	5.21	14.2	2.04	9.65	1.65	4.10	0.550	3.02	0.440	3.20	8.20	2.30
CH5A*	109	231	23.6	85.0	13.9	2.85	10.3	1.75	9.05	1.66	4.41	0.620	3.78	0.550	4.00	15.3	3.40
CH5B*	112	235	24.3	90.9	14.3	2.87	10.5	1.83	9.42	1.69	4.56	0.640	3.86	0.560	4.40	16.5	3.30
CH6*	130	273	28.2	104	16.4	2.49	12.3	2.09	10.7	2.03	5.19	0.750	4.48	0.660	8.10	19.7	4.80
CH8*	3.50	10.0	1.44	7.40	2.38	0.89	3.01	0.550	3.18	0.700	2.02	0.300	1.93	0.300	1.60	0.300	0.100
CH9*	47.7	109	12.6	54.1	9.96	3.38	9.07	1.29	5.96	0.960	2.22	0.290	1.62	0.210	1.60	4.20	1.10
CH10*	26.5	59.3	7.02	31.5	6.45	2.19	6.35	0.990	5.05	0.910	2.28	0.300	1.81	0.250	0.500	2.90	1.00
CH11*	43.7	92.3	10.3	42.2	7.79	2.41	6.82	1.06	5.15	0.970	2.26	0.310	1.84	0.250	2.10	5.50	1.30
CH12*	54.5	119	13.0	50.9	8.21	2.69	6.69	1.06	4.84	0.890	2.18	0.310	1.89	0.250	2.90	7.10	1.60
CH13*	43.3	91.0	10.2	40.9	7.69	2.41	6.64	1.02	5.18	0.950	2.41	0.320	1.81	0.260	2.30	5.10	1.30

Sample No	La (ppm)	Ce (ppm)	Pr (ppm)	Nd (ppm)	Sm (ppm)	Eu (ppm)	Gd (ppm)	Tb (ppm)	Dy (ppm)	Ho (ppm)	Er (ppm)	Tm (ppm)	Yb (ppm)	Lu (ppm)	Pb (ppm)	Th (ppm)	U (ppm)
Christmas Island (Upper Volcanic Series)																	
CH1A*	56.0	123	13.6	54.1	9.52	2.87	6.93	1.01	4.75	0.770	1.85	0.250	1.47	0.220	9.60	7.70	1.70
CH1B	55.7	120	13.6	54.1	9.45	2.91	6.93	0.990	4.47	0.780	1.91	0.250	1.53	0.210	9.70	8.10	1.70
CH2*	54.0	121	13.3	53.0	9.08	2.75	6.61	0.960	4.44	0.730	1.81	0.250	1.37	0.220	9.40	7.90	1.70
CH3*	55.2	121	13.5	53.4	9.27	2.83	6.69	0.970	4.60	0.770	1.82	0.260	1.39	0.210	9.10	8.30	1.70
CH4*	53.7	117	13.1	54.8	9.16	2.75	6.86	0.950	4.38	0.760	1.81	0.250	1.44	0.200	9.30	8.10	1.80
CH7A*	54.4	115	13.0	52.7	8.83	2.68	6.36	0.920	4.16	0.710	1.78	0.230	1.28	0.180	9.70	8.50	1.80
CH7B*	53.7	116	13.0	51.2	8.84	2.65	6.27	0.910	4.16	0.690	1.61	0.230	1.25	0.180	9.20	9.00	1.80
Eastern Wharton Basin Volcanic Province																	
SO199-DR56-1	16.9	33.7	3.97	16.1	3.16	1.25	3.06	0.448	2.45	0.469	1.23	0.171	1.08	0.157	1.95	1.49	1.10
SO199-DR56-4	60.8	106	13.4	54.0	10.5	3.16	10.7	1.64	9.88	2.07	5.69	0.824	5.34	0.766	4.86	4.68	2.32
SO199 DR56-6	85.0	153	18.0	65.3	11.6	2.48	10.5	1.61	9.05	1.78	4.97	0.760	5.37	0.798	7.25	12.3	0.359
SO199 DR57-1	32.4	65.6	7.85	32.3	7.14	2.34	7.70	1.23	7.26	1.44	3.88	0.557	3.61	0.527	2.64	3.53	0.787
SO199-DR58-1	32.4	62.9	8.41	37.0	8.41	2.74	8.15	1.20	6.51	1.21	3.09	0.428	2.65	0.377	3.55	2.65	0.778
SO199-DR58-2	36.5	69.4	9.10	37.9	7.75	2.66	7.43	1.08	5.97	1.14	2.97	0.408	2.61	0.375	3.83	2.46	0.873
SO199 DR58-5	77.8	144	17.3	66.9	12.1	3.62	11.1	1.57	8.44	1.59	4.22	0.589	3.77	0.554	7.16	7.58	1.58
SO199 DR59-1	73.7	115	15.7	63.3	11.9	3.56	11.8	1.65	9.22	1.80	4.77	0.642	3.97	0.584	6.97	5.45	1.20
SO199-DR59-3*	91.5	121	16.6	65.7	12.0	3.63	12.2	1.84	9.85	2.06	5.88	0.830	4.69	0.750	6.80	6.20	1.50
SO199 DR59-4	97.4	120	16.4	66.1	12.1	3.59	12.3	1.69	9.36	1.89	5.04	0.685	4.31	0.643	8.68	5.76	1.45
SO199-DR62-1	26.6	51.5	6.75	28.2	6.41	2.14	6.69	1.06	6.11	1.18	3.10	0.438	2.78	0.394	2.29	2.80	0.706
SO199-DR63-1*	22.8	46.0	6.08	26.3	6.29	2.13	6.92	1.14	6.52	1.24	3.37	0.480	2.82	0.440	1.80	1.80	0.900
SO199-DR65-1	33.7	64.8	8.84	38.9	8.91	2.99	8.85	1.30	7.16	1.34	3.40	0.461	2.86	0.400	3.25	3.20	0.84
SO199-DR66-1	14.4	24.7	3.72	16.6	4.05	1.53	4.60	0.755	4.59	0.922	2.46	0.352	2.24	0.323	1.27	1.14	0.530
SO199 DR66-2	9.15	21.4	2.86	13.2	3.42	1.34	3.82	0.629	3.79	0.750	1.99	0.284	1.84	0.270	1.48	1.08	0.287
SO199-DR66-5*	8.30	21.5	2.89	14.4	4.04	1.62	4.93	0.830	4.58	0.910	2.71	0.370	2.21	0.340	0.900	0.800	0.400
SO199-DR73-1	33.9	68.5	9.03	37.8	8.29	2.62	8.24	1.25	7.21	1.38	3.63	0.505	3.21	0.463	4.15	4.33	0.711
SO199-DR73-5*	23.2	37.6	5.62	23.9	5.06	1.62	5.13	0.770	4.25	0.770	1.98	0.290	1.62	0.240	3.00	2.60	0.400
SO199-DR73-11C*	145	202	33.4	124	22.1	0.74	17.9	3.00	15.8	2.60	6.67	0.930	5.25	0.740	11.6	27.5	0.200
SO199-DR75-2*	19.9	55.0	6.62	28.2	7.57	2.48	8.40	1.38	7.66	1.46	4.04	0.600	3.57	0.520	2.30	2.40	0.400
SO199-DR79-1	37.7	66.3	8.66	36.1	7.69	2.51	7.83	1.18	6.66	1.30	3.41	0.476	3.01	0.434	3.91	3.35	0.890
SO199-DR79-3	75.7	127	18.3	70.2	13.6	2.31	12.2	1.90	10.8	2.07	5.80	0.885	6.28	0.970	6.20	9.03	0.369
SO199-DR79-4	76.9	112	18.0	69.2	13.5	2.82	12.5	1.91	10.5	1.98	5.20	0.737	4.79	0.695	5.32	8.11	0.207
SO199-DR80-1*	136	261	29.4	112	20.6	1.13	17.0	2.92	16.0	2.97	8.65	1.40	9.28	1.44	6.50	20.6	1.20
SO199-DR81-1*	75.7	158	16.8	66.4	12.7	3.58	11.4	1.85	10.0	2.02	5.56	0.810	4.91	0.740	4.10	9.20	1.40
SO199-DR82-1*	58.7	94.3	12.5	55.1	10.5	3.27	11.0	1.76	9.84	2.05	5.71	0.830	4.92	0.800	5.00	5.10	1.40
Argo Basin Volcanic Province																	
SO199-DR69-1*	11.9	30.7	4.68	22.9	6.63	2.47	8.61	1.50	9.07	1.91	5.48	0.780	4.95	0.740	0.900	0.700	0.700
SO199-DR72-1	13.7	30.4	4.37	20.5	5.67	1.99	6.81	1.18	7.43	1.52	4.08	0.596	3.80	0.556	0.626	1.17	0.613

Suppl File Table 2: Reproducibility of major and trace element data by XRF at IFM-GEOMAR

Oxide	Unit	Method	JA-2	JA-2	JA-2	Mean	Std. dev. (±1s)	Std. dev. (%)	JB-2	JB-2	JB-2	Mean	Std. dev. (±1s)	Std. dev. (%)
SiO_2	(%)	XRF	56.24	56.28	56.22	56.25	0.03	0.1	53.12	53.05	53.03	53.07	0.05	0.1
TiO_2	(%)	XRF	0.67	0.67	0.67	0.67	0.00	0.0	1.17	1.17	1.16	1.17	0.01	0.5
Al_2O_3	(%)	XRF	15.46	15.41	15.51	15.46	0.05	0.3	14.8	14.89	14.8	14.83	0.05	0.4
Fe_2O_3	(%)	XRF	6.38	6.37	6.38	6.38	0.01	0.1	14.44	14.47	14.41	14.44	0.03	0.2
MnO	(%)	XRF	0.11	0.11	0.11	0.11	0.00	0.0	0.21	0.21	0.21	0.21	0.00	0.0
MgO	(%)	XRF	8.06	8.04	8.04	8.05	0.01	0.1	4.76	4.8	4.79	4.78	0.02	0.4
CaO	(%)	XRF	6.26	6.27	6.23	6.25	0.02	0.3	9.91	9.9	9.84	9.88	0.04	0.4
Na_2O	(%)	XRF	3.05	3.05	3.24	3.11	0.11	3.5	2.15	2.19	2.34	2.23	0.10	4.5
K_2O	(%)	XRF	1.75	1.75	1.77	1.76	0.01	0.7	0.42	0.42	0.43	0.42	0.01	1.4
P_2O_5	(%)	XRF	0.15	0.16	0.16	0.16	0.01	3.7	0.1	0.1	0.1	0.10	0.00	0.0
Co	(ppm)	XRF	26	34	27	29	4.36	15.0	47	45	41	44	3.06	6.9
Cr	(ppm)	XRF	460	451	458	456	4.73	1.0	41	35	35	37	3.46	9.4
Ni	(ppm)	XRF	110	116	108	111	4.16	3.7	28	29	32	30	2.08	7.0
V	(ppm)	XRF	121	129	124	125	4.04	3.2	570	569	566	568	2.08	0.4
Zn	(ppm)	XRF	58	60	63	60	2.52	4.2	104	105	107	105	1.53	1.5
Ga	(ppm)	XRF	17	18	20	18	1.53	8.3	18	21	20	20	1.53	7.8
Rb	(ppm)	XRF	75	77	74	75	1.53	2.0	10	11	10	10	0.58	5.6
Ba	(ppm)	XRF	312	319	324	318	6.03	1.9	201	214	215	210	7.81	3.7
Sr	(ppm)	XRF	240	241	239	240	1.00	0.4	177	179	178	178	1.00	0.6
Y	(ppm)	XRF	5	4	4	4	0.58	13.3	21	21	21	21	0.00	0.0
Zr	(ppm)	XRF	87	92	86	88	3.21	3.6	40	41	43	41	1.53	3.7
LOI	(%)		n.a.	n.a.	n.a.				n.a.	n.a.	n.a.			
SUM	(%)		98.32	98.29	98.48	98.36	0.10	0.1	101.22	101.35	101.27	101.28	0.07	0.1

Suppl File Table 2: Reproducibility of major and trace element data by XRF at IFM-GEOMAR

Oxide	Unit	Method	JB-3	JB-3	JB-3	Mean	Std. dev. (±1s)	Std. dev. (%)	JR-1	JR-1	JR-1	Mean	Std. dev. (±1s)	Std. dev. (%)
SiO_2	(%)	XRF	50.82	50.75	51.08	50.88	0.17	0.3	75.02	75.03	74.72	74.92	0.18	0.2
TiO_2	(%)	XRF	1.41	1.4	1.4	1.40	0.01	0.4	0.11	0.11	0.11	0.11	0.00	0.0
Al_2O_3	(%)	XRF	17.31	17.3	17.45	17.35	0.08	0.5	12.74	12.79	12.72	12.75	0.04	0.3
Fe_2O_3	(%)	XRF	11.95	11.97	11.98	11.97	0.02	0.1	0.85	0.86	0.85	0.85	0.01	0.7
MnO	(%)	XRF	0.18	0.18	0.17	0.18	0.01	3.3	0.11	0.11	0.11	0.11	0.00	0.0
MgO	(%)	XRF	5.26	5.24	5.28	5.26	0.02	0.4	0.14	0.13	0.13	0.13	0.01	4.3
CaO	(%)	XRF	9.78	9.77	9.74	9.76	0.02	0.2	0.7	0.7	0.69	0.70	0.01	0.8
Na_2O	(%)	XRF	2.88	2.84	3.05	2.92	0.11	3.8	4.19	4.1	4.26	4.18	0.08	1.9
K_2O	(%)	XRF	0.78	0.77	0.78	0.78	0.01	0.7	4.46	4.46	4.45	4.46	0.01	0.1
P_2O_5	(%)	XRF	0.3	0.3	0.29	0.30	0.01	1.9	0.02	0.03	0.02	0.02	0.01	24.7
Co	(ppm)	XRF	43	45	43	44	1.15	2.6	6	8	8	7	1.15	15.7
Cr	(ppm)	XRF	64	66	69	66	2.52	3.8	bdl	bdl	bdl			
Ni	(ppm)	XRF	28	35	29	31	3.79	12.3	bdl	bdl	bdl			
V	(ppm)	XRF	366	374	380	373	7.02	1.9	bdl	bdl	bdl			
Zn	(ppm)	XRF	104	99	100	101	2.65	2.6	29	24	29	27	2.89	10.6
Ga	(ppm)	XRF	25	22	24	24	1.53	6.5	19	19	18	19	0.58	3.1
Rb	(ppm)	XRF	19	20	20	20	0.58	2.9	266	269	268	268	1.53	0.6
Ba	(ppm)	XRF	268	216	224	236	28.00	11.9	60	51	32	48	14.29	30.0
Sr	(ppm)	XRF	403	403	403	403	0.00	0.0	28	30	27	28	1.53	5.4
Y	(ppm)	XRF	19	20	19	19	0.58	3.0	10	9	9	9	0.58	6.2
Zr	(ppm)	XRF	82	80	85	82	2.52	3.1	82	85	84	84	1.53	1.8
LOI	(%)		n.a.	n.a.	n.a.				n.a.	n.a.	n.a.			
SUM	(%)		100.82	100.68	101.4	100.97	0.38	0.4	98.41	98.38	98.13	98.31	0.15	0.2

Suppl File Table 2: Reproducibility of major element data by ICP-OES at Acme Labs

Oxide	Unit	Analytical Code	Laboratory	BIR-1	BIR-1	Mean	Std. dev. (±1s)	Std. dev. (%)	SO-18 Acme	SO-18 Acme	SO-18 Acme	SO-18 Acme	Mean	Std. dev. (±1s)	Std. dev. (%)	BHVO-2	BCR-2	AGV-2
SiO_2	(%)	4A-4	Acme	46.81	46.96	46.89	0.11	0.2	58.07	58.24	58.16	58.17	58.16	0.07	0.1	49.52	53.53	58.96
TiO_2	(%)	4A-4	Acme	0.94	0.94	0.94	0.00	0.0	0.69	0.69	0.69	0.69	0.69	0.00	0.0	2.75	2.26	1.02
Al_2O_3	(%)	4A-4	Acme	15.56	15.49	15.53	0.05	0.3	14.07	14.05	14.15	14.16	14.11	0.06	0.4	13.56	13.70	17.05
Fe_2O_3	(%)	4A-4	Acme	11.15	11.13	11.14	0.01	0.1	7.64	7.59	7.54	7.53	7.58	0.05	0.7	12.26	13.75	6.61
MnO	(%)	4A-4	Acme	0.17	0.17	0.17	0.00	0.0	0.39	0.39	0.39	0.39	0.39	0.00	0.0	0.17	0.20	0.10
MgO	(%)	4A-4	Acme	9.78	9.71	9.75	0.05	0.5	3.35	3.35	3.35	3.35	3.35	0.00	0.0	7.38	3.65	1.78
CaO	(%)	4A-4	Acme	13.12	13.14	13.13	0.01	0.1	6.36	6.33	6.32	6.32	6.33	0.02	0.3	11.29	7.12	5.20
Na_2O	(%)	4A-4	Acme	1.77	1.77	1.77	0.00	0.0	3.70	3.66	3.68	3.69	3.68	0.02	0.5	2.20	3.09	4.10
K_2O	(%)	4A-4	Acme	0.02	0.02	0.02	0.00	0.0	2.15	2.14	2.15	2.16	2.15	0.01	0.4	0.52	1.79	2.90
P_2O_5	(%)	4A-4	Acme	0.02	0.02	0.02	0.00	0.0	0.82	0.82	0.81	0.81	0.82	0.01	0.7	0.27	0.34	0.46
Co	(ppm)			n.a.	n.a.				n.a.	n.a.	n.a.	n.a.				n.a.	n.a.	n.a.
Cr	(ppm)			n.a.	n.a.				n.a.	n.a.	n.a.	n.a.				n.a.	n.a.	n.a.
Ni	(ppm)			n.a.	n.a.				n.a.	n.a.	n.a.	n.a.				n.a.	n.a.	n.a.
V	(ppm)			n.a.	n.a.				n.a.	n.a.	n.a.	n.a.				n.a.	n.a.	n.a.
Zn	(ppm)			n.a.	n.a.				n.a.	n.a.	n.a.	n.a.				n.a.	n.a.	n.a.
Ga	(ppm)			n.a.	n.a.				n.a.	n.a.	n.a.	n.a.				n.a.	n.a.	n.a.
Rb	(ppm)			n.a.	n.a.				n.a.	n.a.	n.a.	n.a.				n.a.	n.a.	n.a.
Ba	(ppm)			n.a.	n.a.				n.a.	n.a.	n.a.	n.a.				n.a.	n.a.	n.a.
Sr	(ppm)			n.a.	n.a.				n.a.	n.a.	n.a.	n.a.				n.a.	n.a.	n.a.
Y	(ppm)			n.a.	n.a.				n.a.	n.a.	n.a.	n.a.				n.a.	n.a.	n.a.
Zr	(ppm)			n.a.	n.a.				n.a.	n.a.	n.a.	n.a.				n.a.	n.a.	n.a.
LOI	(%)	4A-4	Acme	0.3	0.3				1.9	1.9	1.9	1.9				0.3	0.2	1.5
SUM	(%)	4A-4	Acme	99.72	99.72	99.72	0.00	0.0	99.70	99.71	99.71	99.72	99.71	0.01	0.0	99.67	99.64	99.66

Suppl File Table 3: Reproducibility and accuracy of ICPMS trace element data for BIR-1

# Digest/ Element	#1 IfG Kiel	#2 IfG Kiel	#3 IfG Kiel	Mean IfG Kiel	Std. dev. (±1σ)	Std. dev. (%)	Ref. value[1]	Rel. dev. (%)	4A-4B Acme	4A-4B Acme	Mean Acme	Std. dev. (±1s)	Std. dev. (%)	Rel. dev. (%)
Li (ppm)	3.21	3.29	3.44	3.31	0.12	3.5	3.4	-2.5	n.a.	n.a.				
Sc (ppm)	44.2	44.0	43.4	43.9	0.4	0.9	44	-0.3	43	43	43.0	0.0	0.0	-2.3
V (ppm)	306	334	313	318	15	4.7	313	1.5	338	336	337	1.4	0.4	7.7
Cr (ppm)	369	398	383	383	15	3.8	382	0.4	n.a.	n.a.				
Co (ppm)	49.0	51.5	51.4	50.6	1.4	2.8	51.4	-1.5	52.3	52.1	52.2	0.1	0.3	1.6
Ni (ppm)	154	159	166	160	6	3.6	166	-3.9	169	167	168	1.4	0.8	1.2
Cu (ppm)	128	131	124	127	3	2.7	126	1.1	n.a.	n.a.				
Zn (ppm)	70.7	71.9	72.2	71.6	0.8	1.1	71	0.8	n.a.	n.a.				
Ga (ppm)	15.3	16.1	15.9	15.8	0.4	2.5	16	-1.5	14.4	14.0	14.2	0.3	2.0	-11.3
Rb (ppm)	0.196	0.190	0.210	0.199	0.010	5.1	0.212	-6.3	0.2	0.1	0.15	0.07	47.1	-29.2
Sr (ppm)	108	112	104	108	4	3.4	104	3.7	109	110.1	110	0.8	0.7	5.3
Y (ppm)	15.5	15.5	15.5	15.5	0.0	0.2	16	-3.0	14.2	14.4	14.3	0.1	1.0	-10.6
Zr* (ppm)	14.4	15.1	13.9	14.5	0.6	4.1	14	3.3	14.4	14.1	14.3	0.2	1.5	1.8
Nb* (ppm)	0.525	0.542	0.505	0.524	0.019	3.6	0.55	-4.8	0.8	0.6	0.7	0.1	20.2	27.3
Cs (ppm)	0.005	0.004	0.006	0.005	0.001	22.1	0.005	0.5	<0.1	<0.1				
Ba (ppm)	6.48	6.47	6.53	6.50	0.03	0.5	5.83	11.4	6	6	6.0	0.0	0.0	2.9
La (ppm)	0.596	0.614	0.600	0.603	0.009	1.5	0.62	-2.7	0.6	0.6	0.6	0.0	0.0	-3.2
Ce (ppm)	1.89	1.90	1.87	1.89	0.02	0.8	1.95	-3.2	2.0	1.9	2.0	0.1	3.6	0.0
Pr (ppm)	0.364	0.379	0.373	0.372	0.008	2.0	0.38	-2.2	0.34	0.33	0.3	0.0	2.1	-11.8
Nd (ppm)	2.42	2.44	2.39	2.42	0.02	0.9	2.5	-3.4	2.1	2.2	2.2	0.1	3.3	-14.0
Sm (ppm)	1.10	1.12	1.11	1.11	0.01	0.9	1.1	1.0	1.01	1.03	1.0	0.0	1.4	-7.3
Eu (ppm)	0.516	0.532	0.527	0.525	0.008	1.5	0.54	-2.8	0.47	0.51	0.5	0.0	5.8	-9.3
Gd (ppm)	1.75	1.80	1.78	1.77	0.02	1.2	1.85	-4.1	1.74	1.74	1.7	0.0	0.0	-5.9
Tb (ppm)	0.357	0.362	0.363	0.360	0.003	0.9	0.36	0.1	0.35	0.35	0.4	0.0	0.0	-2.8
Dy (ppm)	2.563	2.599	2.597	2.59	0.02	0.8	2.5	3.4	2.37	2.19	2.3	0.1	5.6	-8.8
Ho (ppm)	0.563	0.573	0.574	0.570	0.006	1.0	0.57	0.0	0.54	0.55	0.5	0.0	1.3	-4.4
Er (ppm)	1.602	1.620	1.634	1.62	0.02	1.0	1.7	-4.8	1.46	1.57	1.5	0.1	5.1	-10.9
Tm (ppm)	0.245	0.246	0.249	0.247	0.002	0.9	0.26	-5.0	0.25	0.25	0.3	0.0	0.0	-3.8
Yb (ppm)	1.63	1.64	1.65	1.64	0.01	0.7	1.65	-0.8	1.50	1.58	1.5	0.1	3.7	-6.7
Lu (ppm)	0.243	0.243	0.251	0.245	0.004	1.8	0.26	-5.6	0.23	0.24	0.2	0.0	3.0	-9.6
Hf* (ppm)	0.573	0.588	0.578	0.580	0.007	1.3	0.581	-0.2	0.6	0.6	0.6	0.0	0.0	3.3
Ta* (ppm)	0.046	0.044	0.053	0.048	0.005	9.5	0.035	35.8	0.1	<0.1	0.1			186
Pb (ppm)	2.89	3.17	2.80	2.95	0.19	6.4	3.08	-4.1	2.9	n.a.	2.9			-5.8
Th (ppm)	0.032	0.030	0.030	0.031	0.001	2.7	0.03	2.3	<0.2	<0.2				
U (ppm)	0.012	0.012	0.012	0.012	0.000	2.6	0.01	17.6	<0.1	<0.1				

* Reference values from Carsten Müncker (University Bonn) as these values are considered the most reliable

Suppl File Table 3: Reproducibility and accuracy of ICP-MS trace element data for BHVO-2

# Digest/ Element	#1 IfG Kiel	#2 IfG Kiel	#3 IfG Kiel	Mean	Std. dev. (±1s abs)	Std. dev. (±1s %)	Ref. value1	Rel. dev. (%)	4A-4B Acme	Rel. dev. (%)
Li (ppm)	4.52	4.56	4.80	4.63	0.15	3.3	4.6	0.6	n.a.	
Sc (ppm)	35.0	34.9	32.1	34.0	1.7	4.9	31.8	6.9	32	0.6
V (ppm)	323	325	319	322	3	1.0	317	1.6	327	3.2
Cr (ppm)	298	298	296	297	1	0.4	289	2.8	n.a.	
Co (ppm)	45.0	44.6	44.7	44.8	0.2	0.4	45	-0.5	43.3	-3.8
Ni (ppm)	119	118	118	118	0.4	0.4	119	-0.6	118	-0.8
Cu (ppm)	142	142	134	139	5	3.5	127	9.6	n.a.	
Zn (ppm)	109	117	109	112	4	4.0	103	8.5	n.a.	
Ga (ppm)	22.1	21.9	22.2	22.1	0.1	0.7	21.7	1.7	19.4	-10.6
Rb (ppm)	9.26	9.23	9.45	9.31	0.12	1.3	9.2	1.2	8.4	-8.7
Sr (ppm)	399	391	380	390	10	2.5	395	-1.3	397	0.4
Y (ppm)	25.8	25.7	25.9	25.8	0.1	0.4	25.5	1.2	23.5	-7.8
Zr (ppm)	173	173	165	170	5	2.8	174	-2.1	155	-10.9
Nb (ppm)	18.0	17.9	17.2	17.7	0.5	2.6	18	-1.8	17.0	-5.6
Cs (ppm)	0.110	0.101	0.099	0.103	0.006	6.0	0.11	-6.0	0.1	-9.1
Ba (ppm)	130	131	132	131	1	0.7	130	1.1	126	-3.1
La (ppm)	15.4	15.3	15.3	15.3	0.04	0.3	15.2	0.9	14.1	-7.2
Ce (ppm)	37.9	38.1	37.6	37.8	0.3	0.7	38	-0.4	37.6	-1.1
Pr (ppm)	5.34	5.31	5.38	5.35	0.03	0.6	5.3	0.9	4.96	-6.4
Nd (ppm)	25.0	24.8	24.9	24.9	0.1	0.5	25	-0.3	23.6	-5.6
Sm (ppm)	6.13	6.08	6.17	6.12	0.05	0.8	6.2	-1.2	5.63	-9.2
Eu (ppm)	2.07	2.07	2.08	2.07	0.01	0.4	2.06	0.7	1.88	-8.7
Gd (ppm)	6.26	6.24	6.31	6.27	0.04	0.6	6.3	-0.4	5.72	-9.2
Tb (ppm)	0.962	0.957	0.964	0.961	0.004	0.4	0.93	3.3	0.91	-2.2
Dy (ppm)	5.34	5.33	5.41	5.36	0.04	0.8	5.25	2.1	4.61	-12.2
Ho (ppm)	0.981	0.974	0.987	0.981	0.006	0.6	0.99	-0.9	0.90	-9.1
Er (ppm)	2.44	2.43	2.47	2.45	0.02	0.9	2.5	-2.2	2.33	-6.8
Tm (ppm)	0.326	0.326	0.330	0.327	0.002	0.6	0.34	-3.8	0.32	-5.9
Yb (ppm)	2.00	2.01	2.03	2.01	0.01	0.7	2.00	0.7	1.82	-9.0
Lu (ppm)	0.274	0.278	0.281	0.278	0.003	1.2	0.28	-0.8	0.26	-7.1
Hf (ppm)	4.34	4.36	4.35	4.35	0.01	0.2	4.2	3.5	4.4	4.8
Ta (ppm)	1.12	1.12	1.18	1.14	0.03	2.8	1.13	0.9	1.1	-2.7
Pb (ppm)	1.58	(2.68)	1.72	1.65	0.10	6.0	1.7	-2.8	0.8	-52.9
Th (ppm)	1.22	1.21	1.20	1.21	0.01	0.6	1.21	0.0	1.2	-0.8
U (ppm)	0.419	0.417	0.414	0.417	0.003	0.7	0.41	1.6	0.5	22.0

[1]Reference values after Govindaraju (1994) and USGS (http://minerals.cr.usgs.gov/geo_chem_stand/basaltbhvo1.html), except Pr and U concentrations that are from UCD (http://icpms.geology.ucdavis.edu/).

Reproducibility and accuracy of ICP-MS trace element data for BCR-2

#1 IfG Kiel	#2 IfG Kiel	Mean	Std. dev. (±1s abs)	Std. dev. (±1s %)	Ref. value[1]	Rel. dev. (%)	4A-4B Acme	Rel. dev. (%)
8.90	8.88	8.89	0.01	0.1	9	-1.3	n.a.	
36.6	36.4	36.5	0.1	0.4	33	10.6	34	3.0
420	416	418	3	0.7	416	0.5	443	6.5
19.9	20.1	20.0	0	0.6	18	11.0	n.a.	
37.3	36.9	37.1	0.3	0.8	37	0.2	37.9	2.4
12.1	12.0	12.1	0.1	1.0	12.0	0.6	<20	
21.4	21.1	21.3	0.3	1.3	21.0	1.2	n.a.	
137	135	136	1	0.8	127	7.1	n.a.	
22.8	22.5	22.6	0.2	1.1	23	-1.6	22.3	-3.0
47.5	46.8	47.2	0.5	1.0	47.00	0.3	44.6	-5.1
343	340	341	2	0.7	340.00	0.3	338	-0.7
35.6	34.7	35.2	0.6	1.8	37	-4.9	32.1	-13.2
188	184	186	3	1.4	186	0.2	174	-6.7
12.2	11.9	12.1	0.2	1.5	12.60	-4.3	11.9	-5.6
1.20	1.17	1.19	0.02	1.8	1.10	7.9	1.2	9.1
684	668	676	11	1.7	677	-0.2	663	-2.1
25.6	25.0	25.3	0.4	1.7	25	1.2	24.3	-2.8
54.2	53.3	53.8	0.6	1.1	53	1.4	54.7	3.2
6.92	6.77	6.84	0.11	1.6	6.75	1.4	6.56	-2.8
29.5	28.8	29.2	0.5	1.8	28.7	1.7	27.4	-4.5
6.70	6.57	6.64	0.09	1.3	6.60	0.5	6.12	-7.3
1.99	1.96	1.97	0.02	1.2	1.96	0.7	1.86	-5.1
6.92	6.80	6.86	0.08	1.2	6.80	0.9	6.25	-8.1
1.10	1.07	1.09	0.02	1.5	1.07	1.5	1.06	-0.9
6.47	6.39	6.43	0.05	0.8	6.41	0.3	5.81	-9.4
1.30	1.28	1.29	0.01	0.9	1.29	-0.1	1.29	0.0
3.52	3.47	3.49	0.04	1.1	3.66	-4.6	3.44	-6.0
0.514	0.511	0.512	0.002	0.3	0.54	-5.1	0.51	-5.6
3.41	3.33	3.37	0.06	1.7	3.40	-0.9	3.24	-4.7
0.502	0.495	0.498	0.005	1.1	0.51	-1.3	0.49	-3.0
4.89	4.79	4.84	0.07	1.4	4.85	-0.3	4.9	1.0
0.762	0.745	0.75	0.01	1.5	0.74	1.8	0.7	-5.4
10.3	10.2	10.2	0.1	0.5	11	-7.1	2.8	-74.5
5.98	5.90	5.94	0.05	0.9	5.90	0.7	6.1	3.4
1.70	1.67	1.68	0.02	1.2	1.69	-0.4	1.8	6.5

[1]Reference values after Govindaraju (1994) and USGS (http://minerals.cr.usgs.gov/geo_chem_stand/basaltbhvo1.html)

Suppl File Table 3:	Accuracy of ICPMS trace element data for AGV-2					Reproducibility of ICPMS trace element data for SO-18 Acme Standard						
# Digest/ Element	#1 IfG Kiel	Ref. value1	Rel. dev. (%)	4A-4B Acme	Rel. dev. (%)	4A-4B Acme	4A-4B Acme	4A-4B Acme	4A-4B Acme	Mean Acme	Std. dev. (±1s)	Std. dev. (%)
Li (ppm)	9.96	11	9.5	n.a.		n.a.	n.a.	n.a.	n.a.	n.a.		
Sc (ppm)	12.64	13	2.8	13	0.0	25	25	25	25	25.0	0.0	0.0
V (ppm)	117	120	2.3	120	0.0	205	205	223	217	213	9	4.2
Cr (ppm)	16.99			n.a.		n.a.	n.a.	n.a.	n.a.	n.a.		
Co (ppm)	15.23	16	4.8	15.1	-5.6	31.3	26.7	28.4	28.0	28.6	1.9	6.8
Ni (ppm)	17.51	19	7.9	<20		42	40	41	37	40	2	5.4
Cu (ppm)	51.40	53	3.0	n.a.		n.a.	n.a.	n.a.	n.a.	n.a.		
Zn (ppm)	88.76	86	-3.2	n.a.		n.a.	n.a.	n.a.	n.a.	n.a.		
Ga (ppm)	21.05	20	-5.2	17.3	-13.5	18.9	16.8	18.0	17.7	17.9	0.9	4.9
Rb (ppm)	69.85	68.6	-1.8	63.2	-7.9	28.0	27.5	29.0	28.5	28.3	0.645	2.3
Sr (ppm)	618	658	6.1	670.1	1.8	402.4	399.2	421.5	410.6	408	10	2.4
Y (ppm)	19.41	20	2.9	17.5	-12.5	31.1	30.7	32.6	31.7	31.5	0.8	2.6
Zr (ppm)	221	230	3.9	216.9	-5.7	283	281	300	292	289	8.7	3.0
Nb (ppm)	12.91	15	14.0	13.5	-10.0	20.7	20.7	21.5	21.4	21.1	0.435	2.1
Cs (ppm)	1.18	1.16	-1.4	1.0	-13.8	6.8	7.0	7.4	7.0	7.05	0.252	3.6
Ba (ppm)	1116	1140	2.1	1080	-5.3	503	509	534	521	517	13.72	2.7
La (ppm)	37.97	38	0.1	35.5	-6.6	12.0	11.8	12.7	12.2	12.2	0.386	3.2
Ce (ppm)	69.66	68	-2.4	68.9	1.3	27.1	27.1	29.7	28.2	28.0	1.23	4.4
Pr (ppm)	8.206	8.30	1.1	7.59	-8.6	3.34	3.27	3.49	3.37	3.37	0.092	2.7
Nd (ppm)	30.95	30	-3.2	28.3	-5.7	13.8	13.1	14.2	13.8	13.7	0.46	3.3
Sm (ppm)	5.56	5.70	2.5	5.10	-10.5	2.87	2.79	2.95	2.87	2.87	0.07	2.3
Eu (ppm)	1.52	1.54	1.1	1.42	-7.8	0.87	0.85	0.89	0.87	0.87	0.016	1.9
Gd (ppm)	4.89	4.69	-4.3	3.99	-14.9	2.91	2.81	3.04	2.90	2.92	0.09	3.2
Tb (ppm)	0.668	0.64	-4.4	0.63	-1.6	0.50	0.49	0.52	0.51	0.51	0.013	2.6
Dy (ppm)	3.54	3.60	1.6	3.11	-13.6	2.93	2.89	3.01	2.91	2.94	0.05	1.8
Ho (ppm)	0.667	0.71	6.0	0.62	-12.7	0.62	0.60	0.63	0.62	0.62	0.013	2.0
Er (ppm)	1.79	1.79	-0.2	1.69	-5.6	1.82	1.80	1.88	1.83	1.83	0.03	1.9
Tm (ppm)	0.251	0.26	3.5	0.25	-3.8	0.27	0.27	0.28	0.28	0.275	0.006	2.1
Yb (ppm)	1.64	1.60	-2.5	1.43	-10.6	1.77	1.72	1.80	1.78	1.77	0.03	1.9
Lu (ppm)	0.248	0.25	0.9	0.23	-8.0	0.27	0.26	0.28	0.27	0.27	0.008	3.0
Hf (ppm)	5.09	5.08	-0.1	5.3	4.3	9.6	9.3	10.1	9.7	9.7	0.330	3.4
Ta (ppm)	0.848	0.89	4.7	0.9	1.1	6.9	7.0	7.3	7.3	7.1	0.206	2.9
Pb (ppm)	12.65	13	2.7	4.3	-66.9	n.a.	n.a.	n.a.	n.a.	n.a.		
Th (ppm)	6.00	6.10	1.6	6.5	6.6	10.2	10.1	10.7	10.7	10.4	0.320	3.1
U (ppm)	1.83	1.88	2.9	1.9	1.1	16.4	16.2	17.3	16.9	16.7	0.497	3.0

[1]Reference values after Govindaraju (1994) and USGS (http://minerals.cr.usgs.gov/geo_chem_stand/basaltbhvo1.html)

Suppl File Table 4:

Reproducibility of ICP-MS trace element data based on sample replicates

Sample / Laboratory	SO199 DR6-2 (IfG-Kiel)	SO199 DR6-2 (IfG-Kiel)	Rel. dev.[1] (%)	SO199 DR56-4 (IfG-Kiel)	SO199 DR56-4 (IfG-Kiel)	Rel. dev.[1] (%)	SO199 DR2-4 (IfG-Kiel)	SO199 DR2-4 (IfG-Kiel)	Rel. dev.[1] (%)	SO199 DR66-1 (IfG-Kiel)	SO199 DR66-1 (IfG-Kiel)	Rel. dev.[1] (%)	SO199 DR55-1 (IfG-Kiel)	SO199 DR55-1 (IfG-Kiel)	Rel. dev.[1] (%)
Li (ppm)	9.56	9.67	1.1%	14.5	14.4	0.4%	35.7	35.0	1.9%	56.9	56.0	1.6%	7.71	7.67	0.5%
Sc (ppm)	46.8	45.7	2.3%	27.5	27.8	1.1%	42.4	41.6	1.9%	33.9	33.5	1.2%	14.8	14.8	0.4%
V (ppm)	284	287	0.8%	207	210	1.8%	254	250	1.7%	87.7	87.3	0.5%	228	227	0.4%
Cr (ppm)	114	115	1.1%	5.02	5.08	1.2%	408	408	0.2%	197	197	0.3%	119	121	1.9%
Co (ppm)	46.9	46.5	0.8%	22.4	22.4	0.1%	29.9	29.2	2.2%	25.7	25.3	1.9%	33.2	33.1	0.3%
Ni (ppm)	92.4	91.9	0.6%	16.7	16.7	0.1%	97.1	96.0	1.2%	53.7	53.2	0.9%	108	108	0.7%
Cu (ppm)	46.2	45.8	0.8%	29.7	29.4	0.9%	88.8	87.8	1.1%	75.3	75.0	0.4%	88.8	87.3	1.6%
Zn (ppm)	54.8	54.1	1.3%	142	143	0.7%	108	108	0.5%	198	199	0.2%	178	180	0.6%
Ga (ppm)	14.6	14.7	0.2%	25.5	25.5	0.1%	16.9	16.9	0.0%	18.3	18.4	0.7%	30.7	30.5	0.7%
Rb (ppm)	3.53	3.53	0.1%	56.1	55.8	0.5%	5.98	5.94	0.8%	29.5	29.5	0.2%	32.8	32.5	1.0%
Sr (ppm)	50.4	51.3	1.8%	518	525	1.3%	99.5	99.4	0.0%	375	373	0.4%	1064	1056	0.8%
Y (ppm)	18.6	18.7	0.2%	60.7	61.9	1.9%	22.6	22.4	0.9%	26.6	26.6	0.1%	36.8	36.6	0.7%
Zr (ppm)	15.9	16.0	0.6%	373	376	0.7%	52.4	52.4	0.0%	121	121	0.1%	567	561	1.0%
Nb (ppm)	1.01	0.989	1.9%	55.5	55.2	0.5%	0.697	0.678	2.8%	13.0	13.0	0.1%	105	104	1.2%
Cs (ppm)	0.064	0.065	1.9%	0.522	0.524	0.4%	0.432	0.427	1.0%	1.53	1.53	0.1%	0.208	0.206	0.7%
Ba (ppm)	25.4	25.4	0.0%	777	789	1.6%	5.64	5.53	2.0%	145	144	0.6%	471	468	0.8%
La (ppm)	1.09	1.09	0.3%	60.8	61.1	0.4%	1.647	1.628	1.2%	14.4	14.4	0.2%	77.8	77.0	1.1%
Ce (ppm)	2.95	2.95	0.1%	106	109	2.4%	5.16	5.11	1.0%	24.7	24.8	0.2%	167	166	0.5%
Pr (ppm)	0.513	0.515	0.3%	13.40	13.44	0.3%	0.973	0.963	1.0%	3.72	3.71	0.2%	20.1	19.9	0.8%
Nd (ppm)	2.95	2.96	0.4%	54.0	54.6	1.0%	5.70	5.63	1.1%	16.6	16.7	0.4%	82.4	81.7	0.8%
Sm (ppm)	1.22	1.22	0.0%	10.5	10.5	0.5%	2.14	2.12	1.1%	4.05	4.06	0.0%	15.8	15.6	1.3%
Eu (ppm)	0.491	0.496	1.1%	3.16	3.16	0.2%	0.858	0.856	0.2%	1.53	1.53	0.1%	4.80	4.76	0.9%
Gd (ppm)	1.94	1.92	0.7%	10.7	10.7	0.1%	3.00	2.97	1.0%	4.60	4.66	1.4%	13.7	13.6	0.8%
Tb (ppm)	0.405	0.404	0.4%	1.64	1.64	0.0%	0.572	0.566	1.1%	0.755	0.753	0.3%	1.81	1.79	1.1%
Dy (ppm)	2.97	2.99	0.5%	9.88	9.90	0.2%	3.91	3.88	0.9%	4.59	4.59	0.0%	8.50	8.43	0.9%
Ho (ppm)	0.686	0.680	0.8%	2.07	2.08	0.3%	0.835	0.824	1.3%	0.922	0.920	0.2%	1.38	1.38	0.3%
Er (ppm)	1.99	2.00	0.4%	5.69	5.72	0.4%	2.35	2.33	0.9%	2.46	2.47	0.2%	3.18	3.17	0.0%
Tm (ppm)	0.314	0.316	0.5%	0.824	0.826	0.2%	0.354	0.349	1.4%	0.352	0.354	0.6%	0.374	0.375	0.2%
Yb (ppm)	2.17	2.16	0.3%	5.34	5.34	0.1%	2.33	2.29	1.6%	2.24	2.25	0.5%	2.15	2.14	0.5%
Lu (ppm)	0.324	0.326	0.6%	0.766	0.759	0.9%	0.341	0.339	0.6%	0.323	0.327	1.2%	0.285	0.278	2.4%
Hf (ppm)	0.587	0.612	4.3%	8.54	8.50	0.5%	1.51	1.49	1.3%	2.88	2.88	0.1%	12.1	12.0	1.1%
Ta (ppm)	0.076	0.074	2.4%	3.35	3.35	0.1%	0.061	0.056	8.5%	0.774	0.767	0.8%	6.20	6.16	0.7%
Pb (ppm)	0.129	0.128	0.5%	4.86	4.86	0.0%	0.650	0.650	0.0%	1.27	1.28	1.1%	3.62	3.59	0.9%
Th (ppm)	0.082	0.081	1.9%	4.68	4.62	1.2%	0.095	0.097	2.4%	1.14	1.13	0.3%	7.09	6.97	1.7%
U (ppm)	0.083	0.083	0.1%	2.32	2.29	1.4%	0.075	0.072	4.0%	0.530	0.532	0.3%	1.64	1.62	1.2%

1: Calculated as the relative deviation from the arithmetic mean.

Suppl File Table 4: Reproducibility of ICP-MS trace element data based on sample replicates

Sample / Laboratory	SO199 DR23-19 (IfG-Kiel)	SO199 DR23-19 (IfG-Kiel)	Rel. dev.[1] (%)	SO199 DR52-1 (IfG-Kiel)	SO199 DR52-1 (IfG-Kiel)	Rel. dev.[1] (%)	SO199 DR81-1 (Acme)	SO199 DR81-1 (Acme)	Rel. dev.[1] (%)
Li (ppm)	81.0	81.4	0.5%	22.0	21.9	0.1%			
Sc (ppm)	29.7	29.9	0.7%	18.3	18.1	1.4%	13	12	7.7%
V (ppm)	108	107	0.7%	142	142	0.3%	62	63	1.6%
Cr (ppm)	529	534	0.9%	142	140	0.9%	n.a.	n.a.	
Co (ppm)	21.7	21.9	0.9%	33.7	34.1	1.4%	6.5	5.9	9.2%
Ni (ppm)	254	261	2.6%	56.0	56.2	0.3%	<20	<20	
Cu (ppm)	20.6	21.0	2.0%	124	123	1.0%	n.a.		
Zn (ppm)	73.3	74.7	1.8%	169	169	0.0%	n.a.		
Ga (ppm)	10.2	10.3	1.4%	24.5	24.3	0.7%	27.6	29.7	7.6%
Rb (ppm)	5.56	5.57	0.1%	32.9	32.8	0.3%	86.1	86.8	0.8%
Sr (ppm)	21.5	21.2	1.6%	1131	1127	0.4%	350.3	364.4	4.0%
Y (ppm)	6.39	6.43	0.7%	29.9	30.0	0.4%	53.2	54.3	2.1%
Zr (ppm)	6.14	6.89	12.2%	319	318	0.6%	485.9	507.3	4.4%
Nb (ppm)	0.653	0.528	19.1%	62.9	62.9	0.1%	69.6	71.0	2.0%
Cs (ppm)	0.084	0.083	1.0%	0.630	0.624	0.8%	1.3	1.3	0.0%
Ba (ppm)	11.3	11.0	2.8%	1199	1193	0.5%	1078	1121	4.0%
La (ppm)	1.02	1.01	0.1%	54.1	54.1	0.0%	75.7	78.4	3.6%
Ce (ppm)	3.09	3.04	1.3%	106	106	0.2%	157.9	162.4	2.8%
Pr (ppm)	0.501	0.505	0.9%	12.6	12.7	0.3%	16.76	17.21	2.7%
Nd (ppm)	2.50	2.52	0.7%	51.3	51.3	0.2%	66.4	67.8	2.1%
Sm (ppm)	0.772	0.763	1.2%	10.1	10.0	0.6%	12.67	12.81	1.1%
Eu (ppm)	0.208	0.216	3.7%	3.35	3.34	0.2%	3.58	3.70	3.4%
Gd (ppm)	0.949	0.965	1.7%	8.91	8.92	0.1%	11.36	11.43	0.6%
Tb (ppm)	0.174	0.178	2.0%	1.22	1.22	0.5%	1.85	1.87	1.1%
Dy (ppm)	1.16	1.16	0.6%	6.21	6.20	0.1%	10.04	10.44	4.0%
Ho (ppm)	0.244	0.247	1.3%	1.10	1.10	0.2%	2.02	1.99	1.5%
Er (ppm)	0.683	0.669	2.0%	2.74	2.74	0.1%	5.56	5.65	1.6%
Tm (ppm)	0.100	0.101	1.3%	0.359	0.355	1.0%	0.81	0.79	2.5%
Yb (ppm)	0.642	0.649	1.0%	2.21	2.20	0.4%	4.91	4.73	3.7%
Lu (ppm)	0.093	0.095	2.3%	0.311	0.307	1.4%	0.74	0.73	1.4%
Hf (ppm)	0.201	0.218	8.5%	7.35	7.29	0.8%	13.5	13.1	3.0%
Ta (ppm)	0.077	0.060	22.6%	3.96	3.94	0.6%	4.6	4.4	4.3%
Pb (ppm)	0.294	0.296	0.6%	4.61	4.60	0.3%	4.1	n.a.	
Th (ppm)	0.084	0.096	14.6%	5.35	5.33	0.4%	9.2	9.1	1.1%
U (ppm)	0.050	0.056	11.2%	1.29	1.27	1.3%	1.4	1.4	0.0%

1: Calculated as the relative deviation from the arithmetic mean.

Suppl. File Table 5: Agilent 7500cs ICPMS reproducibility evaluated from same dissolution (IfG-Kiel)

Sample	SO199 DR56-1	SO199 DR56-1	SO199 DR56-1	SO199 DR56-1	SO199 DR56-1	Std. dev. (±1s %)	SO199 DR23-19	SO199 DR23-19	SO199 DR23-19	SO199 DR23-19	SO199 DR23-19	SO199 DR23-19	Std. dev. (±1s %)
Li (ppm)	11.4	11.4	11.6	11.3	11.4	0.6	81.0	80.7	81.0	80.8	81.2	81.2	0.2
Sc (ppm)	13.4	13.6	13.6	13.6	13.7	0.7	29.7	29.8	29.8	32.0	32.7	32.1	4.1
V (ppm)	124	126	127	129	129	1.4	108	109	109	114	116	113	2.7
Cr (ppm)	14.1	14.3	14.4	14.4	14.5	1.0	529	545	541	570	576	573	3.3
Co (ppm)	24.2	24.4	24.3	24.3	24.2	0.3	21.7	21.9	21.8	22.7	23.3	22.9	2.7
Ni (ppm)	23.2	23.4	23.3	23.1	23.2	0.4	254	256	256	270	275	271	3.2
Cu (ppm)	30.4	30.4	30.5	30.2	30.3	0.4	20.6	20.6	20.7	21.4	21.9	21.5	2.4
Zn (ppm)	53.5	53.8	53.2	53.0	52.6	0.8	73.3	72.7	73.9	74.7	75.6	75.2	1.4
Ga (ppm)	22.3	22.3	22.3	22.0	22.0	0.7	10.2	10.2	10.3	10.4	10.5	10.4	1.3
Rb (ppm)	11.5	11.6	11.6	11.5	11.5	0.3	5.56	5.62	5.66	5.67	5.76	5.67	1.0
Sr (ppm)	748	757	766	756	762	0.8	21.5	22.1	22.1	21.7	21.8	21.5	1.1
Y (ppm)	12.7	12.8	12.8	12.6	12.6	0.7	6.39	6.39	6.46	6.43	6.49	6.39	0.6
Zr (ppm)	116	116	117	117	117	0.5	6.14	6.13	6.23	6.26	6.21	6.07	1.0
Nb (ppm)	18.5	18.5	18.5	18.4	18.4	0.3	0.653	0.578	0.623	0.541	0.548	0.534	7.6
Cs (ppb)	0.191	0.192	0.196	0.196	0.196	1.2	0.084	0.085	0.085	0.086	0.086	0.087	1.2
Ba (ppm)	302	307	309	309	311	1.0	11.3	11.9	11.8	11.6	11.6	11.5	1.7
La (ppm)	16.9	17.1	17.0	17.2	17.2	0.7	1.02	1.02	1.05	1.02	1.03	1.02	1.3
Ce (ppm)	33.7	33.9	34.1	34.0	34.2	0.5	3.09	3.08	3.14	3.07	3.11	3.08	0.8
Pr (ppm)	3.97	4.02	4.03	4.03	4.04	0.6	0.501	0.509	0.511	0.506	0.513	0.508	0.8
Nd (ppm)	16.1	16.2	16.3	16.3	16.4	0.6	2.50	2.51	2.56	2.54	2.55	2.52	0.9
Sm (ppm)	3.16	3.20	3.20	3.19	3.19	0.5	0.772	0.763	0.773	0.771	0.788	0.772	1.0
Eu (ppm)	1.25	1.26	1.26	1.25	1.26	0.4	0.208	0.208	0.211	0.211	0.212	0.212	0.8
Gd (ppm)	3.06	3.06	3.06	3.07	3.07	0.2	0.949	0.958	0.966	0.965	0.980	0.951	1.1
Tb (ppm)	0.448	0.452	0.452	0.453	0.453	0.4	0.174	0.175	0.175	0.176	0.177	0.176	0.5
Dy (ppm)	2.45	2.46	2.47	2.47	2.49	0.6	1.16	1.16	1.17	1.17	1.18	1.15	0.7
Ho (ppm)	0.469	0.473	0.468	0.470	0.474	0.5	0.244	0.242	0.245	0.243	0.247	0.242	0.7
Er (ppm)	1.23	1.24	1.23	1.22	1.23	0.4	0.683	0.669	0.675	0.669	0.675	0.669	0.7
Tm (ppm)	0.171	0.172	0.172	0.172	0.173	0.4	0.100	0.099	0.099	0.098	0.102	0.099	1.2
Yb (ppm)	1.08	1.08	1.08	1.08	1.08	0.2	0.642	0.636	0.645	0.650	0.643	0.627	1.1
Lu (ppm)	0.157	0.156	0.153	0.155	0.156	0.8	0.093	0.092	0.094	0.093	0.092	0.093	0.7
Hf (ppm)	2.70	2.71	2.69	2.71	2.71	0.3	0.201	0.195	0.202	0.208	0.212	0.207	2.8
Ta (ppm)	1.09	1.11	1.10	1.14	1.14	1.7	0.077	0.077	0.087	0.068	0.070	0.069	8.9
Pb (ppm)	1.95	1.96	1.95	1.94	1.95	0.3	0.294	0.272	0.282	0.274	0.282	0.278	2.6
Th (ppm)	1.49	1.50	1.48	1.49	1.50	0.4	0.084	0.084	0.085	0.082	0.084	0.081	1.5
U (ppm)	1.10	1.10	1.09	1.09	1.09	0.5	0.050	0.050	0.051	0.051	0.052	0.052	1.3

Anlage 3

Crustal ages along the Investigator Ridge and tectonic implications

Udo Barckhausen[1], Kaj Hoernle[2], Reinhard Werner[2], Folkmar Hauff[2], Paul van den Bogaard[2], Ana Gibbons[3]

1 BGR, Stilleweg 2, 30655 Hannover, Germany
2 IFM-GEOMAR, Wischhofstrasse 1-3, 24148 Kiel, Germany
3 University of Sydney, School of Geosciences, NSW 2006, Australia

Abstract

We present a study of crustal ages along the Investigator Ridge fracture zone in the Wharton Basin, Eastern Indian Ocean, based on the interpretation of new magnetic profiles and on Ar-Ar age dated rock samples which were dredged from the ridge during cruise SO-199 in 2008. The magnetic profiles were acquired on the east side of the Investigator Ridge and the crustal ages derived from the interpretation of these data and seem to contradict the ages of the rock samples in places. However, since it remains unknown on which side of the fracture zone the dredged rocks once formed, it is justifiable to assume that these rocks all represent material from the western side of the Investigator Ridge and hence reflect the crustal ages there. The crust at the southern end of the surveyed area at 17°S was formed in Jurassic times around 153 Ma according to magnetic data as well as rock ages. After ~150 Ma, in the model presented here the seafloor spreading to both sides of the Investigator Ridge took very different paths with steady and very slow spreading west of the ridge and ridge jumps east of it resulting in the offset of ~1000 km observed today across the fracture zone.

Introduction

The Investigator Ridge (IR) is a major tectonic feature in the Wharton Basin in the Eastern Indian Ocean. Its nature as a fracture zone has been recognized long ago (Liu et al., 1983), but since it also has a significant morphologic expression there has always been the question how much volcanism may have been involved in its formation. The crustal ages west of the IR are fairly well known from the analysis of east-west striking magnetic anomalies by Liu et al. (1983); Fig 1. Ages range from 79 Ma (Chron 33) at 19°S to 49 Ma at 2°S where the Ridge enters the subduction zone offshore Sumatra. This results in an average half spreading rate of ~60 mm/yr. Even though some of the anomaly identifications are uncertain, this is generally in good agreement with the findings farther west where party even higher spreading rates have been found (Liu et al., 1983). However, it has to be noted that south of 9.5°S a fracture zone exists only ~30 km west of the IR and that in this region the anomaly identifications of Liu et al. (1983) only apply to the area west of this unnamed fracture zone whereas we can only speculate about the crustal ages immediate west of the IR. Even less is known about crustal ages east of the IR. Anomaly 33 was identified at 9°S here which implies an extraordinary offset of roughly 1000 km along the IR. To the north, east-west striking anomalies 32, 31, and 30 were identified at spreading rates similar to those on the west side of the IR. In southern direction no further age determination was possible because anomaly 34 represents the so-called Cretaceous Normal Superchron which lasted from 118 to 83 Ma (Cande and Kent, 1995). The magnetic record only sets in again east of 107°E where southwest-

northeast striking anomalies of the M-series (older than 118 Ma) are present. This leaves a large area east of the IR blank where crustal ages can only be inferred from extrapolation so far.

New magnetic data

During a cruise with RV Sonne in 2008 the IR was systematically surveyed with multibeam bathymetry, collecting rock samples with a dredge approximately every 100 km, and magnetic profiling. One magnetic profile was positioned ~15 km east of the IR and extends over a distance of more than 1000 km from 8°S to 17.5°S parallel to the ridge. In the northern part of this profile, anomalies 33n and 33r can be identified in good agreement with the findings of Liu et al. (1983). South of anomaly 33r an anomaly pattern typical for the Chron 34 is observed with relatively high amplitude anomalies which cannot be correlated with any reversal timescale. An attempt to establish a correlation with magnetic data from the same time period in the Atlantic is underway in order to test the hypothesis that some correlatable patterns exist during the Cretaceous Normal Superchron (Dyment et al., 2009; Dyment, personal communication 2010). However, as long as no timescale for datable magnetic anomalies exists for the time period of the Cretaceous Normal Superchron, the new magnetic profile cannot provide crustal ages for the area east of the IR south of 11°S. Surprisingly, at the southern end of the profile south of 16°S the magnetic anomaly pattern seems to be correlatable with magnetic anomalies M22 through M25 attributing a Jurassic age to this part of the crust.

Constraints from Ar-Ar ages

At this point, ages derived from Ar-Ar dating of the rocks dredged in several locations along the IR become a critical link to the magnetic data. At dredge location DR30 16.78°S, 98.78°E) close to the IR one rock sample indeed gave an age of 153.1 ± 3.3 Ma (Hoernle et al., in prep.) which matches almost exactly the age of the tentatively identified anomaly M25 in this area according to the reversal timescale of Gradstein et al., 1994. The existence of crust that old in this position is unexpected in current plate tectonic models. Furthermore this finding raises some questions about possible spreading rates in this sector during the Late Jurassic and the Early Cretaceous which, given the distance to identified anomaly 33r at 11°S, must have been pretty low.
Four more reliable Ar-Ar ages could be determined from rock samples dredged along the IR at ca. 10°S, 11°S, 12°S, and 14°S (Fig. 2) with ages increasing constantly from 62 Ma at 10°S to 103 Ma at 14°S. At first glance these ages seem to fit very well with the expected increase in crustal ages from north to south. However, the ages are in disagreement with the identified magnetic anomalies at 10°S by more than 10 m.y. (62 Ma rock sample vs. 73 Ma magnetic anomaly), and spreading rates calculated from the rock sample ages are very low at ~10 mm/yr compared to established spreading rates west of the IR and also to spreading rates predicted by current plate tectonic models for the area east of the IR which are around 30 mm/yr (Gibbons, pers. comm. 2010).

Discussion

It becomes obvious that identified magnetic anomalies, plate tectonic models, and Ar-Ar ages of rock sample dredge from the IR do not match. So a discussion is

necessary how all the evidence for crustal ages and plate tectonic evolution of the Wharton Basin east of the IR fits together. We consider the rock sample ages to be very reliable since out of a large number of analyzed samples only those are taken into consideration here which meet highest quality criteria (Hoernle et al., in prep.). However, two uncertainties remain: first, it remains unknown to which side of the IR the rock samples actually belong which, given the assumed offset along the ridge, would make a huge difference in age. Second, the possibility cannot be excluded that the rocks dredged on exposed flanks of the IR were formed during volcanic events later than the formation of the oceanic crust even though the geochemistry of the rocks and the morphology of the ridge do not let this scenario seem very likely. The rock sample ages do not fit the identified magnetic anomalies on either side of the IR being too old for the western side and too young for the eastern side. As explained above, the tectonic situation is complicated by an unnamed fracture zone ~30 km west of the IR (Fig. 2) which leads to the fact that the crustal ages directly west of the IR are virtually unknown because no magnetic anomalies have been identified yet in the narrow strip between IR and this particular fracture zone. So it could be possible that all the rock samples come from the western side of the IR and define the crustal ages in this narrow strip of oceanic crust. In this interpretation the problem of the extremely low spreading rates which needs an explanation remains unsolved, however. On the other hand, assuming that part of the rock samples represents crust from the western side of the IR and another part comes from the eastern side of the IR does not help much in this case because at least two of the samples must belong to the same side (either west or east) and thus the low spreading rate problem persists.

Another possible explanation is that the identification of magnetic anomalies on the east side of the IR is completely wrong, a possibility which cannot be ruled out given the scarcity of data in much of the region and the fact that in large areas the crust definitely formed during the Cretaceous Normal Superchron and thus is not databale from magnetic anomalies. Therefore we tried to fit magnetic anomalies inbetween the new magnetic profile between 9°S and 11°S with a synthetic model that is in agreement with the ages of the respective rock samples. The result is clearly not convincing (Fig. 3). So to us it seems more likely that identifications of anomalies 33n and 33r are correct and the rock sample ages represent crustal ages west of the IR.

All the matters discussed above refer to the part of the IR located between 9°S and approximately 14°S. Things are different south of 15°S where a good match between a rock sample age on the western side of the IR and the age inferred from magnetic anomalies on the eastern side of the IR exists (Fig. 2). The question to be addressed here is how it is possible that crust of Jurassic age was found there in an area where plate tectonic models predict Cretaceous ages. Recent modelling shows that a relatively small piece of Jurassic crust which formed at the West Australian margin when (greater) India separated from it may have been captured by a backward jump of the spreading center (Gibbons, pers. communication, 2010). This could explain the existence of a sliver of Jurassic oceanic crust with a dimension of roughly 150 x 500 km in the vicinity of the southern IR. If this model is correct, then the trace of the ridge jump must still be present forming a structural boundary where an age gap separates the younger Cretaceous crust to the north from the Jurassic crust to the south.

The morphology of the IR shows indications for one or two ridge jumps in the area surveyed during cruise SO-199. At 16°S, just north of the area with the presumably Jurassic crust, a significant bend in the IR could be the remains of a ridge jump which must have occurred at ~150 Ma between Chrons M23 and M22 (Fig.4). The pattern

of the seafloor morphology east of the IR also changes at this position from clear NW-SE striking structures in the south to irregular structures north of the bend. At 11°S a step in the IR might also be connected to a later ridge jump and is associated with a notable change in the water depth east of the ridge (Fig.2). However, this must remain speculative as long as no exact crustal ages are known from this region.

Conclusions

The IR seems to have formed mainly by tectonic forces according to the Indian MORB type geochemistry of the rocks dredged from it (Hoernle et al., in prep.). The Ar-Ar ages of these rocks can best be explained when assuming that all the rock samples belong to the crust which formed west of the fracture zone. The morphology of the ridge with water depths on the western side being significantly lower than on the eastern side lets this interpretation seem plausible. In this case, a narrow zone between the IR and the unnamed fracture zone ~30km west of it (Fig. 2) would have partly accommodated the motion between very different seafloor spreading regimes west and east of the IR with a very slow but steady spreading rate. This situation must have persisted from some time before 153 Ma until ~58 Ma when the unnamed fracture zone fades out at Chron 26. The crust east of the IR has been affected by at least one but probably more jumps of the spreading axis. This is the only possible interpretation we have at the moment which solves the problem of seemingly contradicting ages derived from Ar-Ar ages of rock samples and from magnetic anomalies along parts of the IR and which at the same time allows for the extremely slow spreading rates which the age data require. A critical test for this hypothesis would be to obtain high quality magnetic profiles just west of the IR which could confirm or reject the low spreading rates in the narrow zone between the IR and the unnamed fracture zone ~30km west of it.

Acknowledgements

We wish to thank the captain, crew, and technical staff of cruise SO-199 for their support. This work was supported by the German Ministry of Education and Research (BMBF), Grant SO199-CHRISP. Figures were prepared with GMT public domain software (Wessel and Smith, 1998).

References

Cande, S.C. and D.V. Kent (1995), Revised calibration of the geomagnetic polarity timescale for the Late Cretaceous and Cenozoic, Journal of Geophysical Research, 100, 6093-6095, doi: 10.1029/94JB03098.

Dyment, J., Y. Gallet and E. Hoise (2009), First Complete High-Resolution Record of the Cretaceous Normal Superchron, American Geophysical Union Fall Meeting 2009, GP31A-05.

Gradstein, F. M., F. P. Agterberg, J. G. Ogg, J. Hardenbol, P. van Veen, J. Thierry, and Z. Huang (1994), A Mesozoic time scale, J. Geophys. Res., 99(B12), 24,051–24,074.

Heine, C., Müller, R.D. & Gaina, C. (2004), Reconstructing the lost Thetys Ocean basin: convergence history of the SE Asian margin and marine gateways, in *Continent-Ocean Interactions Within East Asian Marginal Seas*, editet by P. Clift, P. Wang, W. Kuhnt, and D. Hayes, AGU Geophys. Monograph Series 149, 37-54.

Liu, C.-L., Curray, J.R., and McDonald, J.M. (1983), New constraints on the tectonic evolution of the eastern Indian Ocean, Earth and Planet. Science Lett., 65, 331-342.

Figure captions

Figure 1. Identified magnetic lineations of the Wharton Basin from Liu et al., 1983. Numbers indicate magnetic Chrons, F.S.R. indicates the position of the fossil spreading ridge.

Figure 2. Magnetic anomalies of the survey area shown as wiggles along the shiptracks. Black: data from cruise SO-199, grey: data from Geodas database. Underlain is the color coded bathymetrie along the tracks of cruise SO-199. Dotted lines indicate fracture zones, red stars are the locations of where rock samples were dredged from the Investigator Ridge. Numbers in italics next to the stars are Ar-Ar ages of the rock samples, other numbers are identified magnetic lineations.

Figure 3. Northern part of the magnetic profile along the Investigator Ridge (SO199-205) compared to synthetic line calculated from a reversal timescale. The model was built to fit rock sample ages with magnetic anomalies at the same latitude. The model fit is poor and hence we conclude that the rocks dredged from the Investigator Ridge do not represent the oceanic crust east of the ridge.

Figure 4. Bathymetric map of the southernmost part of the survey area with superimposed magnetic anomalies shown as wiggle traces along the shiptracks. Dotted lines indicate fracture zones, the red star shows a rock sample locations with the age in Million years in italics next to it. Black lines are identified magnetic lineations with Chrons next to them.

Figure 1

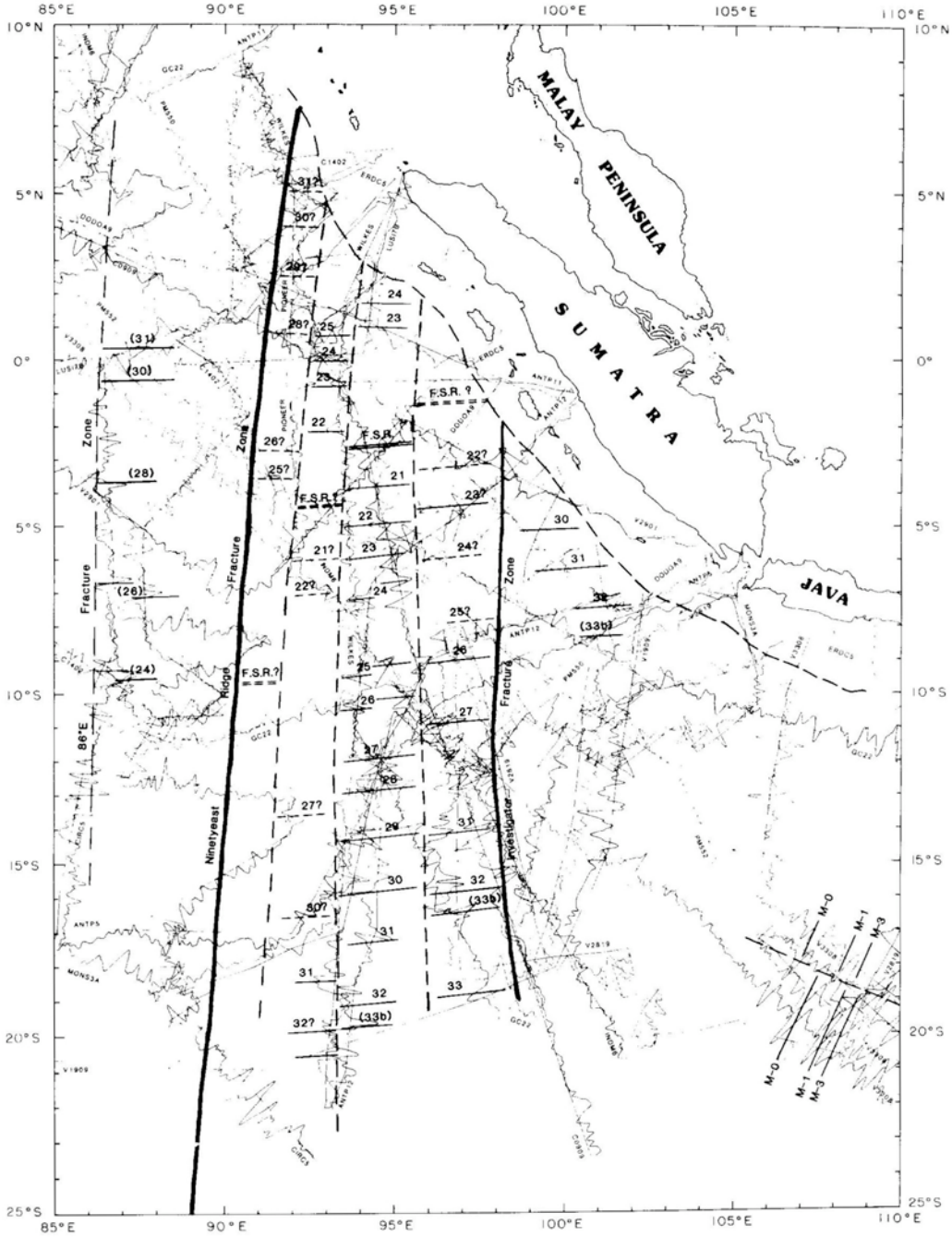
85°E
90°E
95°E
100°E
105°E
110°E
10°N
5°N
0°
5°S
10°S
15°S
20°S
25°S
MALAY PENINSULA
SUMATRA
JAVA
Ninetyeast Ridge Fracture Zone
Investigator Fracture Zone
86°E Fracture Zone
F.S.R.
F.S.R.?
M-0
M-1
M-3

Figure 2

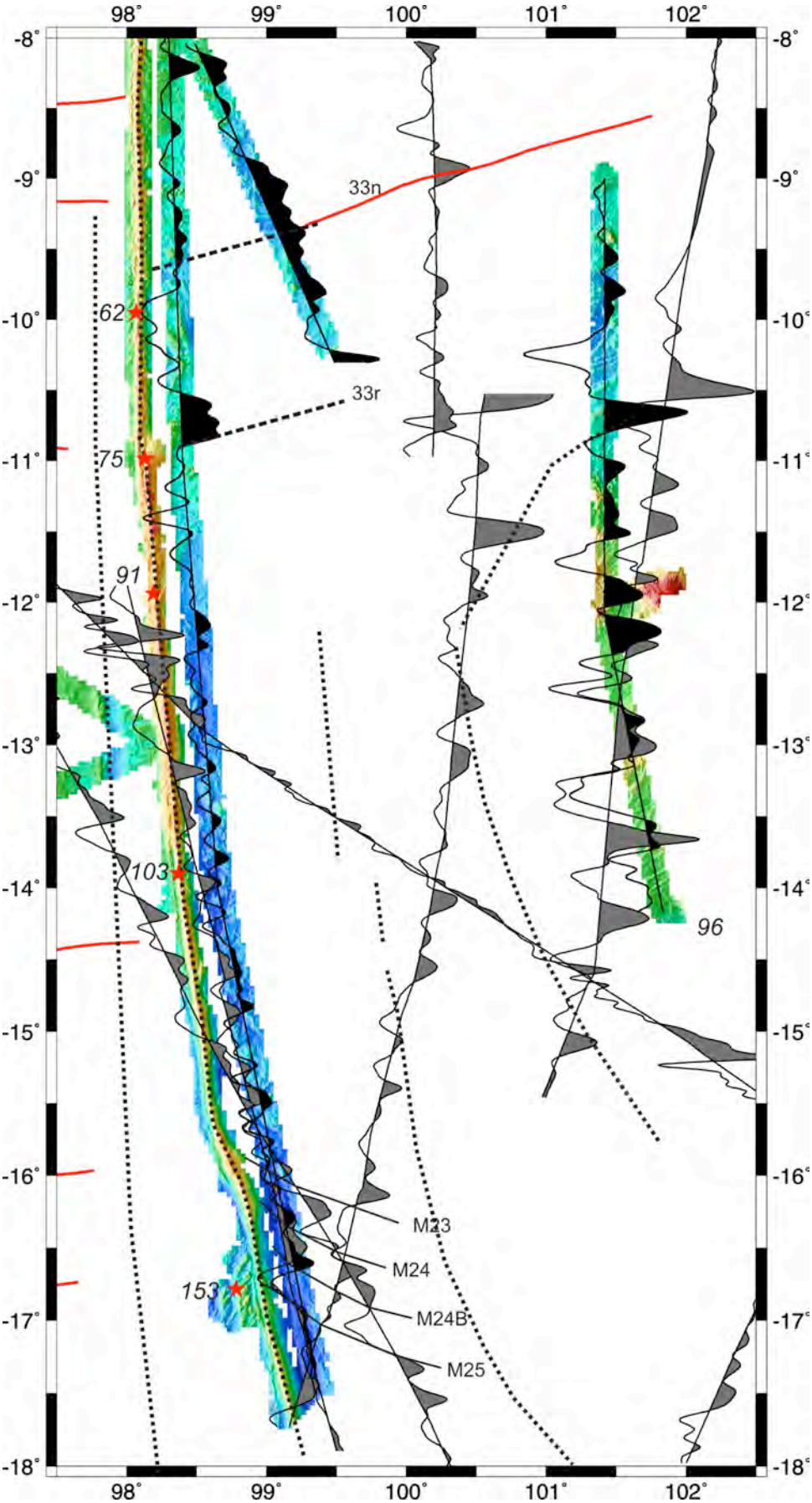
98°
99°
100°
101°
102°
-8°
-9°
-10°
-11°
-12°
-13°
-14°
-15°
-16°
-17°
-18°
33n
33r
62
75
91
103
153
96
M23
M24
M24B
M25

Figure 3

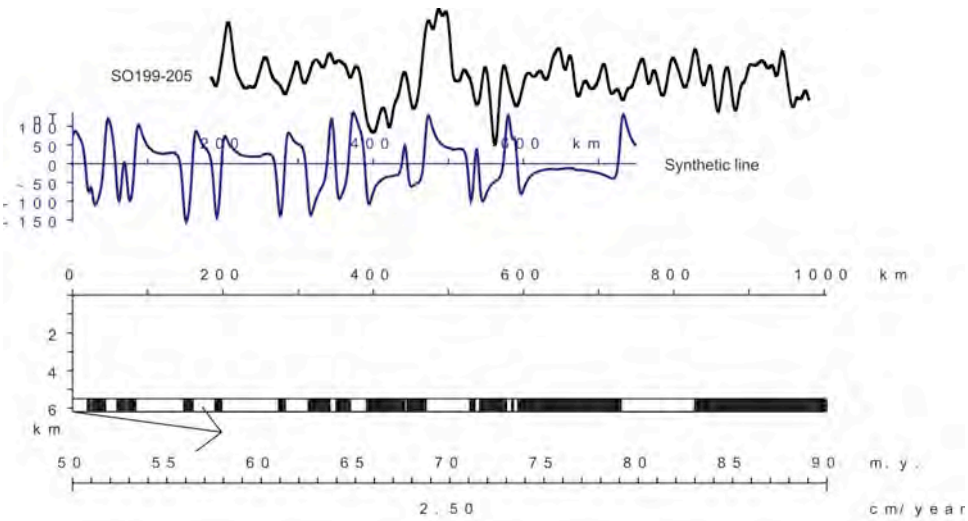

Figure 4

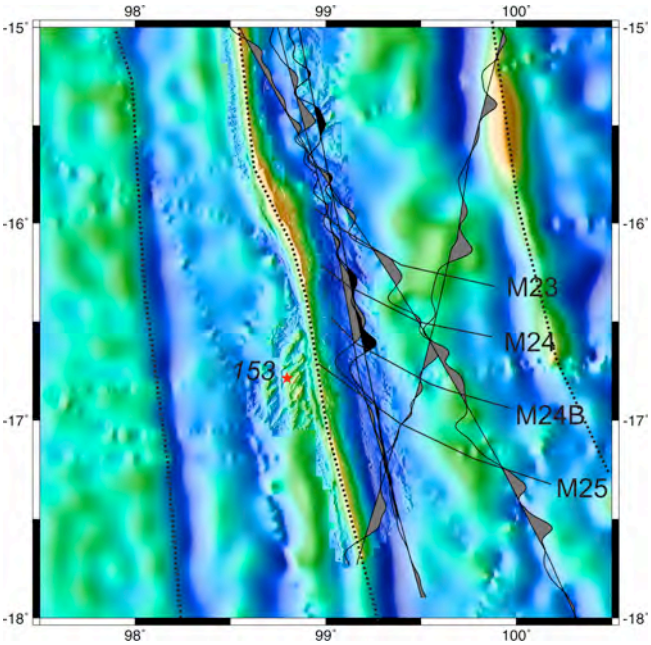

Anlage 4

Semnoderes paucispinosus sp. nov. (Kinorhyncha, Cyclorhagida) from the deep sea around Christmas Island, Indian Ocean

Birger Neuhaus [1]

Address:

[1] Museum für Naturkunde Berlin
Invalidenstr. 43
D-10115 Berlin
Germany
Tel.: +49 (0)30-2093 8525
e-mail: birger.neuhaus@mfn-berlin.de

Corresponding author: Birger Neuhaus

Number of Figures: 3

Number of Tables: 3

Running head: ***Semnoderes paucispinosus*** sp. nov. from deep-sea Indian Ocean

Keywords. Kinorhyncha, Cyclorhagida, ***Semnoderes paucispinosus*** sp. n., deep sea, Indian Ocean

Abstract. During the deep-sea expedition SO 199 with R/V Sonne four specimens of a new species of ***Semnoderes*** (Kinorhyncha, Cyclorhagida) were recovered from depth of 3,100-4,600 m around Christmas Island, Indian Ocean. The single female and the three specimens of undetermined sex were examined with a light microscope equipped with differential interference contrast. ***Semnoderes paucispinosus*** sp. nov. agrees with all its congeners ***S. armiger***, ***S. pacificus*** and ***S. ponticus*** in the existence of a first trunk segment clamshell-like anteriorly and ring-like posteriorly, of a middorsal spine in segments 1-11, of a midterminal spine, of a lateroventral acicular spine in segments 3-9 and 11 (lateroterminal spine) and in a lateral accessory position in segment 11 (lateroterminal accessory spine). ***Semnoderes paucispinosus*** sp. nov. is distinguished from all its congeners by the lack of any cuspidate spines, the lack of a lateroventral acicular spine in segment 2, the existence of a short, tube-like spine with a blunt tip lateroventrally in segments 5 and 11 and of an acicular spine in a sublateral instead of a lateroventral position in segment 10. The three individuals of undetermined sex may be male specimens with still not developed gonads, juvenile specimens with characters not known for postembryonic stages yet or sub-adult specimens so far unknown for Kinorhyncha.

Introduction

The meiobenthic Kinorhyncha have been reported from the intertidal (Higgins 1986; Neuhaus 1993; Sørensen 2008; Zelinka 1928) to the deep sea down to more than 5,000 m depth (Gutzmann et al. 2004; Meadows et al. 1994). Very few species of Kinorhyncha from the deep sea below 500 m depth have been identified to species level, namely ***Antygomonas oreas*** Bauer-Nebelsick, 1996, ***Campyloderes*** cf. ***vanhoeffeni*** Zelinka, 1913, ***Fissuroderes higginsi*** Neuhaus in Neuhaus & Blasche, 2006, ***F. novaezealandiae*** Neuhaus in Neuhaus & Blasche, 2006, ***F. papai*** Neuhaus in Neuhaus & Blasche, 2006, ***F. rangi*** Neuhaus in Neuhaus & Blasche, 2006 and ***Polacanthoderes martinezi*** Sørensen, 2008 (Bauer-Nebelsick 1996; Neuhaus 2004; Neuhaus & Blasche 2006; Sørensen 2008; Zelinka 1913).

From the East Indian Ocean only three kinorhynch species are known, ***Echinoderes andamanensis*** Higgins & Rao, 1979, ***E. ehlersi*** Zelinka, 1913 and ***Cateria gerlachi*** Higgins, 1968 from the Andaman Islands (Higgins & Rao 1979). The Indonesian archipelago and the waterbodies northwest of Australia are virtually ***terra incognita*** concerning Kinorhyncha identified to species level.

Species of ***Semnoderes*** have been reported from isolated spots around the world. ***Semnoderes armiger*** Zelinka, 1928 occurs in European waters, namely in the Gulf of Trieste, Mediterranean Sea (Zelinka 1928), at the West coast of Sweden (Nyholm 1947; Sørensen et al. 2009) and in the Atlantic Ocean off Scotland (McIntyre 1962, 1964). The second European species, ***S. ponticus*** Bacescu & Bacescu, 1956, has been found only along the Romanian coast of the Black Sea (Bacescu 1968; Bacescu & Bacescu 1956). ***Semnoderes pacificus*** Higgins, 1967 seems to appear in widely distant places such as the coast of New Caledonia and the Pacific coast of California (Higgins 1967) as well as the Atlantic coast of Panama (Sørensen 2006). A comparison between species of ***Semnoderes*** turns out to be limited: all descriptions of new species of ***Semnoderes*** are based on few specimens, type material of ***S. armiger*** and probably ***S. ponticus*** does not seem to exist and specimens of ***S. pacificus*** were mounted laterally which is unfavourable for light microscopical investigations (Bacescu 1968; Higgins 1967; Zelinka 1928).

This study is part of a series on species of Kinorhyncha from the deep sea collected mainly by the German research vessels R/V Sonne, R/V Meteor and R/V Polarstern. These papers intend to describe new species, compare the fauna of the deep sea with that of the continental shelves and elucidate the phylogenetic relationships both within the Kinorhyncha and of the Kinorhyncha to their closest relatives Loricifera and Priapulida.

Material and Methods

Specimens were collected by R/V Sonne during the deep-sea expedition SO 199 to the Indian Ocean (Fig. 1) with a geological chain bag dredge and with a TV-multicorer (Werner et al. 2009). Sediment sampled by four sediment trap tubes (length: 21 cm, diameter: 4 cm) inside the geological chain bag dredges was fixed immediately in cold 6% formaldehyde buffered with buffer tablets for haematology (Merck # 1.09468.10100, pH 7.2). After at least one day of fixation at 4-8° C, the sediment was washed carefully with plenty of tap water on a 40 µm-sieve and centrifuged (THERMO Heraeus Multifuge 3s) three times for 5 minutes with three to four times the amount of Levasil 200A/40% at 4,000 rpm in order to quantitatively extract the meiofauna. After rinsing with tap water on a 40 µm-sieve, specimens were stored in 75% ethanol. From the TV-multicorer, only the upper 5 cm of sediment in each core (inner core diameter: 9.5 cm) were taken and fixed in cold 6% formaldehyde. This material was later washed with tap water on a 40 µm-sieve, centrifuged for meiofauna and finally stored in 75% ethanol. All four specimens of the new species were mounted later as glycerin-paraffin slides on Cobb-aluminium slides (Hooper 1979) and sealed with glyceel according to the recipee of Bates (1997).

Kinorhynchs were observed with a Zeiss Axioskop 50 microscope equipped with differential interference contrast after Nomarski, with objectives Plan-Neofluar 40x/0,75, 63/0.90 Korr. and 100/1,30 Oil. Specimens were documented with a camera lucida. Photographs were taken with a digital camera Zeiss AxioCam MRc5 on a Zeiss Axioplan 2 with a motorized z-focus and an objective Planapo 63x/1,30. The images were digitally improved with Corel Photo Paint V.11, and mounted with the help of Corel Draw. Measurements were made with a camera lucida. Because of the thin cuticle and often deep indentation of cuticle midventrally, segment borders were sometimes difficult to observe. Segment length was measured both midventrally and laterally whenever possible. Otherwise, the terminology of the description and the way measurements were conducted follow Higgins (1983) as emmended by Bauer-Nebelsick (1996), Pardos et al. (1998) and Sørensen and Pardos (2008). Numbering of trunk segments follows Neuhaus and Higgins (2002: p. 621) for the reasons stated there.

List of abbreviations

ac	acicular spine with spinose tip
AM	followed by catalogue number of Australian Museum, Sydney
cu	bottle-shaped cuspidate spine, inflated basally with narrower distal part

DR	sediment trap in geological chain bag dredge for rocks, refers to station
fgo	female gonad
fr	fringe
go	gonopore
la	lateral accessory
lat	lateral
ld	laterodorsal
le	left side
lm	longitudinal muscle
ltas	(length of) lateral terminal accessory spine
lts	(length of) lateral terminal spine
lv	lateroventral
lvi	more inner position of lateroventral spine
lvo	more outer position of lateroventral spine
lv5	(length of) lateroventral spine of segment 5
md	middorsal
md1	(length of) middorsal spine of segment 1
ml	midlateral
mts	(length of) midterminal spine
mu	muscles attaching to mts and lts
MUC	multicorer, refers to station
mv	midventral
mvm	medioventromedial
n. a.	data not available
NMNH	followed by catalogue number of National Museum of Natural History, Washington, D.C., Smithsonian Institution
om	oblique muscle
oos	outer oral style
pa	papilla
pc	pachycyclus
pd	paradorsal
ps	primary scalid
ri	right side
s1	(length of) trunk segment 1
sd	subdorsal
sl	sublateral
SO 199	deep-sea expedition with R/V Sonne no. 199
sp	spinoscalid
ssp	sensory spot
st	sternal plate
sw5	standard width at posterior margin of segment 5
TL	total length, may be measured midventrally (mv) or laterally (lat)
tp	tergal plate
tr	trichoscalid
tu	short, tube-like spine
vl	ventrolateral
vm	ventromedial
ZMB	followed by catalogue number of Museum für Naturkunde Berlin (former Zoological Museum Berlin)

Results

***Semnoderes paucispinosus* sp. nov.** (Tabs. 1, 2; Figs 2-3)

Material examined. Holotype. Female (SO 199, dredge station DR 58, from11°44.20' S, 106°52.78' E to 11°44.38' S, 106°53.32' E, 3,609-3,113 m depth; 29.8.2008; seamount

belonging to seamount group southeast of Christmas Island, northwest facing steep slope, steepest on lower slope; specimen # 5, dorsoventral mount)(Fig. 1). **Paratypes.** Three specimens of undetermined sex, paratype 1 (SO 199, dredge station DR 40, from10°45.92' S, 101°48.73' E to 10°45.90' S, 101°49.26' E, 4,306-3,791 m depth; 23.8.2008; ridge, west facing slope beneath small cone of the northwest-southeast orientated ridge; specimen # 2, dorsoventral mount) and paratypes 2 and 3 (SO 199, multicorer station MUC 53, 10°37.21' S, 105°17.63' E, 4,688 m depth; 28.8.2008; abyssal plain off southwest corner of Christmas Island; specimen # 3, slightly oblique dorsoventral mount; specimen # 4, lateral mount)(Fig. 1).

Deposition of material. The female holotype is deposited at the Australian Museum, Sydney and catalogued under the number AM XYZ. The remaining specimens are stored at the Museum für Naturkunde Berlin in the “worm” collection and catalogued in the “Generalkatalog freilebende Würmer” under the number ZMB Vermes 113xx.

Etymology. The prefix “pauci-” is derived from Latin “paucus” = few; the sufix “-spinosus” is derived from Latin “spinosus” = spinous, and refers in the new species to the lack of lateroventral spines in the anterior two segments and the entire lack of cuspidate spines.

Diagnosis. First trunk segment clamshell-like anteriorly and ring-like posteriorly; very short, tube-like, blunt spine ventrolaterally in segments 5 and 11, acicular spine lateroventrally in segments 3-9 and 11, in lateral accessory position in segment 11 and sublaterally in segment 10; no cuspidate spine; papilla ventromedially in segment 9; sensory spot ventromedially in segments 2-9, in a sublateral area of segments 4-10, in a midlateral area of segments 1-10, subdorsally in segment 1, paradorsally in segments 3-9 and twice in segment 11; paradorsal sensory spots of segment 11 elongated and on cone-like base.

Female holotype (Figs 2B-H, K, L, 3A, B)

The following description is based on the holotypic female with its head protruded and mounted dorsoventrally. Several images of additional specimens (Figs 2A, J, M, 3C, D) demonstrate the described anatomical situation better than images of the holotype alone would. Also in order to avoid unneccessary duplication of text, such images are, therefore, included here.

Head. The head carries several rows of spinoscalids (Fig. 2D). The first ring exhibits 10 primary scalids with a broader base covered by about 4 long bristles and an elongate part with a blunt tip (Fig. 2B, D). All remaining spinoscalids show a spinose tip. The 14

trichoscalids originate from the introvert just above the placids with no trichoscalids above the placids neighbouring the midventral placid.

The 9 outer oral styles consist of two elements with a pointed tip (Fig. 2D). A basal cuticular plate shows about half a dozen long bristles. A weir of cuticular rods borders the mouth opening frontally. The pear-shaped pharyngeal bulb consists of an inner epithelium with numerous nuclei and an outer layer of alternating circular and radial muscle cells.

Neck. The neck region is characterized by 16 weakly sclerotized placids. The midventral (Fig. 2B) and middorsal placid (Fig. 2C) are considerably longer and slimmer than the remaining placids, which show a more triangular shape. The surface of the cuticle is smooth. Several circular muscles extend below the placids.

Trunk. The trunk is externally divided into 11 segments. The first trunk segment cuticle is clamshell-like anteriorly and ring-like posteriorly (Fig. 2A, C). Therefore, the anterior part of the first segment acts as a closing mechanism, when the head is retracted (Fig. 2A). The cuticle of the remaining segments seems to possess a dorsal tergal plate and two ventral sternal plates (Fig. 2B, K). Lateral articulations are weak in segments 2-11 and barely recognizable in segments 2 and 11. The sternal plates of segments 1 and 2 bulge caudally in the midventral area.

The anterior margin of the first trunk segment shows a smooth margin (Fig. 2A, C). The cuticle appears slightly transparent in the glycerine mount indicating a weakly sclerotized cuticle. At the anterior margin of each segment, the cuticle thickens towards the interior of the animal and forms a slightly stronger sclerotized pachycyclus to which the longitudinal muscles attach (Figs 2C, 3B). At the posterior end of each segment, the cuticle overlapping the subsequent segment terminates in a clearly recognizable pectinate fringe consisting of regularly arranged, longitudinal areas of thinner and thicker cuticle giving the cuticle a striped appearance (Figs 2G, 3D). The pectinate fringe appears serrated posteriorly with the teeth of the sternal plates beeing shorter, much smaller and more regularly arranged than those of the tergal plates.

The surface of the cuticle of all trunk segments is covered by irregularly distributed, triangular, minute cuticular scales. The surface of the cuticle is smooth otherwise. All spines reveal even smaller scales on their surface. Two rows of even finer scales are arrangend as a secondary fringe in a wave-like pattern in the anterior sternal and tergal cuticle of segments 2-10.

Lateral of the elongated sensory spots just above the midterminal spine, the tergal plate of segment 11 reveals on both sides one row of short cuticular pedicels which branch at their tip

into very fine, short, spine-like extensions (Fig. 3A, D). More ventrally of these two rows of pedicels, one row of long cuticular bristles borders the tergal plate.

One pair of gonopores occurrs ventrolaterally at the posterior border of segment 10 as two strongly sclerotized oval cuticular rings (Fig. 2F, G, K, L).

One papilla appears ventromedially in segment 9 (Tab. 1) and shows a sclerotized cuticular ring around the papilla (Fig. 2F, G). One short papilla without sclerotized ring is also located in a lateral accessory position in segment 8 (Fig. 2G; Tab. 1).

A sensory spot is found ventromedially in segments 2-9, lateroventrally in segment 11, paradorsally in segments 1 and 6-9 (slightly more laterally in segment 1), sublaterally in segments 4, 6, 7, 9 and 10 (in a slightly more lateral accessory position in segments 9 and 10), midlaterally in segments 1, 2, 9 and 10, subdorsally in segments 1, 9 and 10 and paradorsally in segments 3-9 (possibly also in segment 2) as well as twice in segment 11, one next to the middorsal spine and the other just above the midterminal spine (Figs 2F, 3A-D; Tab. 1). Each sensory spot appears on the surface of the body cuticle as two pores surrounded by a distinct oval field of cuticle where often cuticular micropapillae can be resolved with the light microscope. Usually, a cuticular tube can be recognized to extend from each pore into the epidermis. A sensory spot with three pores occurs exclusively subdorsally in segment 1. The paradorsal sensory spots of segment 11 differ from all remaining sensory spots in that they are elongated and located on a cone-shaped base. They may rise up to 14 µm above the body surface (Fig. 3A-D).

Lateral oblique and dorsal and ventral longitudinal muscles attach to the posterior margin of the pachycyclus of the sternal and tergal plates of each segment and extend to the anterior margin of the pachycyclus of the subsequent segment (Figs 2B, C, L, 3B). Two to four strands of the lateral oblique muscles extend between subsequent tergal plates and one strand runs from the tergal plate to the lateral articulation of the sternal plate of the subsequent segment (Fig. 2B).

Spines. An acicular spine is found lateroventrally in segments 3-9 and 11 (laterotermial spine), in a lateral accessory position in segment 11 (laterotermial accessory spine) and sublaterally in segment 10 (Figs 2A, E-M, 3A-D; Tab. 2). A tube-like, very short spine with a blunt tip exists ventrolaterally in segments 5 and 11 (Figs 2E, H, 3C; Tab. 2). Next to and laterally of the blunt, ventrolateral spine in segment 11, a slightly shorter cone-like process occurs (Fig. 2H, J). Each of the segments 1-10 shows a single, acicular middorsal spine whereas segment 11 exhibits two middorsal spines, one of them usually called the midterminal spine (Tab. 2). A strong triangular longitudinal muscle extends posteroventrally from a strongly sclerotized area (= apodeme) of the outer lateral edge of each lateral terminal

spine each to the lateral margin of segment 11 and to the midterminal spine (Figs 2H, L, M). A third muscle connects the apodemes of the two laterotermnal spines with each other.

Specimens of undetermined sex

In the following, only those characters are mentioned for the three paratypes that differ from the holotypic female or which are not visible in the female.

All three paratypic specimens do not reveal clear female or male inner or outer sexual organs such as gonopores, eggs, sperm or different spine patterns which often appear on segment 10. The paratypic specimens do not reveal characters typical for juvenile stages such as less distinct segmental borders and different appearance of sensory spots. Specimen # 2 seems to possess a gonad that may or may not contain developing eggs but does not have gonopores.

None of the paratypic specimens reveals a short papilla in a lateral accessory position in segment 8 and medioventrally in segment 9 (Tab. 1). An elongated, tube-like structure ventrolaterally in segment 11 of specimen # 2 may represent either a modified sensory spot or a modified papilla. Only specimen # 3 shows a sublateral papilla in segment 9. However, the lateral accessory and sublateral positions of specimen # 2 are not visible in the light microscope. Sensory spots with three pores occur exclusively on the tergal plate in segments 1, 9 and 10 (Tab. 1). Specimens disagree only slightly from the female and from each other in the pattern of sensory spots (Tab. 1).

Discussion

Diagnostic characters of species of *Semnoderes*

All four specimens of ***Semnoderes paucispinosus*** sp. nov. are regarded as belonging to one and the same species based on the identical spine pattern (Tab. 2), cuticular structures of the body surface and overall pattern of sensory spots (Tab. 1). Occasionally, sensory spots and papillae may not be recognizable because of unsuitable mount, e.g., the lateral accessory and sublateral positions are not visible in specimen # 2 or folds and dirt may mask potential organs. Observations of other kinorhynch species such as ***Pycnophyes dentatus*** Reinhard, 1881, ***P. kielensis*** Zelinka, 1928***, Paracentrophyes praedictus*** Higgins, 1983***, Antygomonas incomitata*** Nebelsick, 1990 and ***Campyloderes*** cf. ***vanhoeffeni*** indicate some individual variation in the position of sensory spots, papillae and gland cell outlets which may even lead to asymmetrical patterns within a given specimen (Nebelsick 1990; Neuhaus 1993, 1995; Neuhaus and Sørensen, unpublished observations).

Such variation becomes obvious in ***S. paucispinosus*** sp. nov. in the distribution of sensory spots around a midlateral line and around a sublateral line, respectively: the sensory organs

occupy positions from more laterodorsally to more subdorsally in segments 1-10 or from a more lateral accessory position to more sublaterally (Tab. 1). From these observations it is postulated that the ground pattern of ***S. paucispinosus*** sp. nov. comprises sensory spots at least in the following positions: ventromedially in segments 2-9, in a sublateral area of segments 4-10, in a midlateral area of segments 1-10, subdorsally in segment 1 and paradorsally in segments 3-9 and twice in segment 11; paradorsal sensory spots of segment 11 are elongated.

Among the three congeneric species of ***Semnoderes paucispinosus*** sp. nov., namely ***S. armiger***, ***S. pacificus*** and ***S. ponticus***, only for the first species more detailed morphological information is avavailable from specimens collected in the Mediterranean Sea (Zelinka 1928) and fom the West coast of Sweden (Sørensen et al. 2009). The original description of ***S. ponticus*** remains extremely vague and brief (Bacescu & Bacescu 1956), but a later drawing of Bacescu (1968: Tab. 1, Fig. 7) offers slightly more detail; from this illustration it is assumed that the lateroventral spine in segment 4 may be cuspidate. This character is therefore noted with a question mark in Tab. 3. Limited information is also available for ***S. pacificus***, because the two adult specimens were mounted laterally (Higgins 1967). Whereas in ***S. paucispinosus*** sp. nov. the exact position of lateral spines can be easily observed, such information on the congeners is not fully available (Bacescu 1968; Bacescu & Bacescu 1956; Higgins 1967; Sørensen et al. 2009; Zelinka 1928; this paper). In Tab. 3, positions are therefore circumscribed as lateroventral inner and outer position which may ignore that three lateral positions may exist, namely a lateral accessory, lateroventral and ventrolateral position as realized, e.g., in segment 8 of ***Antygomonas incomitata*** (see Nebelsick 1990).

Semnoderes paucispinosus sp. nov. agrees with all its congeners ***S. armiger***, ***S. pacificus*** and ***S. ponticus*** in the existence of a first trunk segment clamshell-like anteriorly and ring-like posteriorly, of a middorsal spine in segments 1-11, of a midterminal spine, of a lateroventral acicular spine in segments 3-9 and 11 (laterotermial spine) and in a lateral accessory position in segment 11 (laterotermial accessory spine) (Tab. 3). ***Semnoderes paucispinosus*** sp. nov. is distinguished from all its congeners by the lack of any cuspidate spines, the lack of a lateroventral acicular spine in segment 2, the existence of a short, tube-like spine with a blunt tip lateroventrally in segments 5 and 11 and of an acicular spine in a sublateral instead of a lateroventral position in segment 10 (Bacescu 1968; Bacescu & Bacescu 1956; Higgins 1967; Sørensen et al. 2009; Zelinka 1928; this paper; Tab. 3). However, because of the very faint nature of the tube-like spines, these may have been overlooked in other species of ***Semnoderes***.

Semnoderes pacificus and ***S. ponticus*** agree in the existence of a very small lateroventral acicular spine in segment 1, but disagree in the lack of a cuspidate lateroventral spine in segment 2 and the existence of a cuspidate lateroventral spine in segment 6 in ***S. ponticus***

(see Bacescu 1968; Bacescu & Bacescu 1956; Higgins 1967; Tab. 3). Contrary to ***S. armiger*** and ***S. pacificus***, ***S. paucispinosus*** sp. nov. and ***S. ponticus*** both lack a lateroventral acicular spine in segment 2; the latter two species can be distinguished from each other by the existence of a very small acicular lateroventral spine in segment 1, of a lateroventral acicular spine in segment 2, of a lateroventral cuspidate (?) spine in segments 4, 6, 8 and 9 in ***S. ponticus*** and the lack of these characters in ***S. paucispinosus*** sp. nov. (see Bacescu 1968; Bacescu & Bacescu 1956; Higgins 1967; Sørensen et al. 2009; Zelinka 1928; this paper; Tab. 3). In opposition to ***S. pacificus*** and ***S. paucispinosus*** sp. nov., ***S. armiger*** and ***S. ponticus*** both reveal a lateroventral cuspidate spine in segment 6; the latter two species can be separated from each other by the existence of a very small lateroventral spine in segment 1 and of a lateroventral cuspidate (?) spine in segment 4 as well as the lack of a lateroventral cuspidate spine in segment 2 (see Bacescu 1968; Bacescu & Bacescu 1956; Higgins 1967; Sørensen et al. 2009; Zelinka 1928; this paper; Tab. 3).

Comparison with other species of Kinorhyncha

For few species of Kinorhyncha it has been well documented that adult specimens may moult into a second adult stage, namely one female ***Antygomonas oreas***, two female and one male ***Zelinkaderes floridensis*** Higgins, 1990 and two female ***Centroderes*** sp. from Newfoundland have been found moulting into females (Bauer-Nebelsick 1996: Fig. 25; Higgins 1990: Fig. 65; Neuhaus, Higgins, Pardos and Sørensen, unpublished results). Both the exuvia and the hatching specimen of all females mentioned above reveal gonopores with a sclerotized cuticular ring. These observations suggest that moulting of an adult stages into a second adult stage may be more widespread at least among Cyclorhagida with a thin cuticle than assumed previously. Kinorhynch species with a thin cuticle have been assumed to have preserved an original character within Kinorhyncha (Neuhaus 1995; Neuhaus & Higgins 2002).

In ***Semnoderes paucispinosus*** sp. nov., the female specimen clearly shows gonopores with a sclerotized cuticular ring and gonads with eggs while the three specimens of undetermined sex do not possess gonopores, eggs or sperm. However, these three specimens reveal well developed cuticular structures such as clear borders of cuticular sternal and tergal plates, numerous minute cuticular scales and a well expressed pectinate fringe with short teeth. Such characters are typical of the adult but not of the juvenile stage (Neuhaus 1993, 1995; Sørensen et al. 2010). Until more specimens will become available, it remains uncertain whether these three specimens represent either young male specimens with sperm developing at a later time, or the last juvenile stage with characters hithertoo unknown for juvenile stages or a sub-adult stage in between the last juvenile stage and the adult stage with clear male or female characteristics. A subadult stage in the postembryonic

development is known as a postlarva in the close relative of the Kinorhyncha, the Loricifera (Heiner 2004; Heiner & Neuhaus 2007; Kristensen et al. 2007). To complicate matters even further, such a postlarva may be reduced secondarily within the Loricifera in pliciloricid and urnaloricid species (Gad 2005; Heiner & Kristensen 2005, 2009).

Acknowledgements

The author greatly appreciates superb support by Captain Lutz Mallon and his crew of R/V Sonne in collecting sediment during the cruise SO 199 in which the author also participated. Special thanks are also due to the chief scientists Drs Kaj Hoernle and Reinhard Werner, as well as to the shipboard scientific party for consistent help and advice during the cruise. My thanks go to Prof. Kaj Hoernle and Dr Folkmar Hauff (University, IFM-GEOMAR, both Kiel) for inviting the author to participate in the expedition with R/V Sonne. I also gratefully acknowledge support and advice by Kristine Kämpf, Dr Carsten Lüter, Karin Meschter, Alexandra Roth, Antje Schwiering, and Ronald Seidel, Museum für Naturkunde Berlin. I am grateful for stimulating and scholastic discussions with Dr Robert P. Higgins, Asheville, USA and Prof. Dr. Fernando Pardos, Madrid, Spain during the preparation of the manuscript. Specimens of Kinorhyncha have been kindly provided by Cheryl Bright, National Museum of Natural History, Smithsonian Institution, Washington, D.C. The Government of Australia is acknowledged for its permission to work in its territorial waters. Discounted purchase of a large-volume centrifuge for a previous expedition from Thermo Electron Corporation is gratefully acknowledged. I wish to express my sincere gratitude to the German Ministry of Education and Research (BMBF) for funding the expedition SO 199.

References

Bacescu, M. (1968): [Class kinorhynch. Determination of fauna of the Black and Azou Seas.] Naukova Dumka 1: 237-250. [in Russian]

Bacescu, M. & E. Bacescu (1956): Kinorhynchii – reprezentanti ai unei clase de animale, noua pentru fauna Romineasca. Comm. Acad. R. P. R. 6 (4): 543-548.

Bates, J. W. (1997): The slide-sealing compound "glyceel". J. Nematol. 29: 565-566.

Bauer-Nebelsick, M. (1996): ***Antygomonas oreas*** sp. nov., a new deep sea kinorhynch from the Pacific Ocean (Kinorhyncha: Cyclorhagida). Ann. Naturhist. Mus. Wien 98 B: 5-22.

Gad, G. (2005): Successive reduction of the last instar larva of Loricifera, as evidenced by two new species of ***Pliciloricus*** from the Great Meteor Seamount (Atlantic Ocean). Zool. Anz. 243: 239-271.

Gutzmann, E., Martínez Arbizu, P., Rose, A. & G. Veit-Köhler (2004): Meiofauna communities along an abyssal depth gradient in the Drake Passage. Deep-Sea Res. II: 1617-1628.

Heiner, I. (2004) ***Armorloricus kristenseni*** (Nanaloricidae, Loricifera), a new species from the Faroe Bank (North Atlantic). Helgol. Mar. Res. 58: 192-205.

Heiner, I. & R. M. Kristensen (2005): Two new species of the genus ***Pliciloricus*** (Loricifera, Pliciloricidae) from the Faroe Bank, North Atlantic. Zool. Anz. 243: 121-138.

Heiner, I. & R. M. Kristensen (2009): ***Urnaloricus gadi*** nov. gen. et nov. sp. (Loricifera, Urnaloricidae nov. fam.), an aberrant Loricifera with a viviparous pedogenetic life cycle. J. Morphol. 270: 129-153.

Heiner, I. & B. Neuhaus (2007): Loricifera from the deep sea at the Galápagos spreading center, with a description of ***Spinoloricus turbatio*** gen. et sp. nov. (Nanaloricidae). Helgol. Mar. Res. 61: 167–182.

Higgins, R. P. (1967): The Kinorhyncha of New-Caledonia. Expédition Française sur les Recifs coralliens de la Nouvelle-Calédonie. Paris, Fondation Singer-Polignac 2: 75-90.

Higgins, R. P. (1983). The Atlantic barrier reef ecosystem at Carrie Bow Cay, Belize, 2: Kinorhyncha. Smithson. Contrib. Mar. Sci. 18: 1-131.

Higgins, R. P. (1986): A new species of ***Echinoderes*** (Kinorhyncha: Cyclorhagida) from a coarse-sand California beach. Trans. Am. Microsc. Soc. 105: 266-273.

Higgins, R. P. (1990): Zelinkaderidae, a new family of cyclorhagid Kinorhyncha. Smithson. Contrib. Zool. 500: 1-26.

Higgins, R. P. & G. C. Rao (1979): Kinorhynchs from the Andaman Islands. Zool. J. Linnean Soc. 67: 75-85.

Hooper, D. J. (1979): Handling, fixing and mounting nematodes. In: J. F. Southey (ed.), laboratory methods for work with plant and soil nematodes. Ministry of Agriculture, Fisheries and Food, Technical bulletin 2. Her Majesty's Stationary Office, London, pp. 39-54.

Kristensen, R. M., Heiner, I. & R. P. Higgins (2007): Morphology and life cycle of a new loriciferan from the Atlantic coast of Florida with an emended diagnosis and life cycle of Nanaloricidae (Loricifera). Inv. Biol. 126: 120-137.

Meadows, P. S., Reichelt, A. C., Meadows, A. & J. S. Waterworth (1994): Microbial and meiofaunal abundance, redox potential, pH and shear strength profiles in deep sea Pacific sediments. J. Geol. Soc. 151: 377-390.

McIntyre, A. D. (1962): The class Kinorhyncha (Echinoderida) in British waters. J. Mar. Biol. Ass. U. K. 42: 503-509.

McIntyre, A. D. (1964): Meiobenthos of sub-littoral muds. J. Mar. Biol. Ass. U. K. 44: 665-674.

Nebelsick, M. (1990): ***Antygomonas incomitata*** gen. et sp. nov. (Cyclorhagida, Kinorhyncha) and its phylogenetic relationships. Zool. Scripta 19: 143-152.

Neuhaus, B. (1993): Postembryonic development of ***Pycnophyes kielensis*** and ***P. dentatus*** (Kinorhyncha) from the North Sea. Microfauna Marina 8, 163-193.

Neuhaus B. (1995): Postembryonic development of ***Paracentrophyes praedictus*** (Homalorhagida): neoteny questionable among the Kinorhyncha. Zool. Scripta 24: 179-192

Neuhaus, B. (2004): Description of ***Campyloderes*** cf. ***vanhoeffeni*** (Kinorhyncha, Cyclorhagida) from the Central American East Pacific deep sea with a review of the genus. Meiofauna Marina 13: 3-20.

Neuhaus, B. & T. Blasche (2006): ***Fissuroderes***, a new genus of Kinorhyncha (Cyclorhagida) from the deep sea and continental shelf of New Zealand and from the continental shelf of Costa Rica. Zool. Anz. 245: 19-52.

Neuhaus, B. & R. P. Higgins (2002): Ultrastructure, biology, and phylogenetic relationships of Kinorhyncha. Integ. Comp. Biol. 42: 619-632.

Nyholm, K.-G. (1947): Studies in the Echinoderida. Ark. Zool. 39A, 14: 1-36.

Pardos, F., Higgins, R. P. & J. Benito (1998): Two new ***Echinoderes*** (Kinorhyncha, Cyclorhagida) from Spain, including a reevaluation of kinorhynch taxonomic characters. Zool. Anz. 237: 195-208.

Sørensen, M. V. (2006): New kinorhynchs from Panama, with a discussion of some phylogenetically significant cuticular structures. Meiofauna Marina 15: 51–77.

Sørensen, M. V. (2008): A new kinorhynch genus from the Antarctic deep sea and a new species of ***Cephalorhyncha*** from Hawai (Kinorhyncha: Cyclorhagida: Echinoderidae). Org. Div. Evol. 8: 230-232.

Sørensen, M. V., Accogli, G. & J. G. Hansen (2010): Postembryonic development of ***Antygomonas incomitata*** (Kinorhyncha: Cyclorhagida). J. Morphol. 271: 863-882.

Sørensen, M. V., Heiner, I. & J. G. Hansen (2009): A comparative morphological study of the kinorhynch genera ***Antygomonas*** and ***Semnoderes*** (Kinorhyncha: Cyclorhagida). Helgol. Mar. Res. 63: 129–147.

Sørensen, M. V. & F. Pardos (2008): Kinorhynch systematics and biology – an introduction to the study of kinorhynchs, inclusive identification keys to the genera. Meiofauna Marina 16: 21-73.

Werner, R., Hauff, F. & K. Hoernle (eds)(2009): RV Sonne Fahrtbericht / Cruise Report SO199 CHRISP. IFM-GEOMAR Report 25: 1-206.

Zelinka, C. (1913). Die Echinoderen der Deutschen Südpolar-Expedition 1901- 1903. Deutsche Südpolar-Expedition XIV, Zoologie VI: 419-437.

Zelinka, K. (1928): Monographie der Echinodera. Leipzig, Verlag W. Engelmann, Leipzig.

Figure Legends

Fig. 1. Map of study area of deep-sea expedition SO 199. Numbers next to white dots refer to sample stations mentioned in the text. Map processed with GMT on board R/V Sonne by WTD for IFM-GEOMAR, Kiel.

Fig. 2 A-L. ***Semnoderes paucispinosus*** sp. nov., DIC photographs of holotypic female (**B-H**, **K**, **L**) and specimens of undetermined sex # 3 (**A**) and #2 (**J**, **M**). **A-C**, **E.** Ventral (**A**, **B**, **E**) and dorsal view (**C**) of anterior segments showing clamshell-like first segment if head is retracted (**A**) or protruded (**B**, **C**) as well as ventrolateral, blunt, tube-like spine in segment 5 (**E**). Arrows mark midventral (**B**) and middorsal placid (**C**). **D.** Ventral view of protruded head with mouth cone and scalids. **F**, **G.** Ventral view of posterior segments 8-11 with papillae in lateral accessory position in segment 8 and ventromedially in segment 9 at different focal levels. Arrows in **F** mark sensory spots in a lateral accessory position and ventromedially in segment 9. **H**, **J.** Ventral view of ventrolateral tube-like spine (double-arrow in **H**) and cone-like process (double-arrow in **H**, arrowheads in **J**) in segment 11 of two specimens. **K**, **L.** Ventral view of posterior segments 8-11 documenting gonopores and longitudinal muscles at different focal levels. **M.** Longitudinal muscles of laterotermial accessory spine connecting with tergal cuticle and midterminal spine. Scale bar in **E** 100 µm, valid for all photographs.

Fig. 3. A-D. ***Semnoderes paucispinosus*** sp. nov., DIC photographs of holotypic female (**A**, **B**) and specimen of undetermined sex # 4 (**C**, **D**). **A**, **B.** Dorsal view of posterior segments 9-11 showing two pairs of paradorsal sensory spots in segment 11 and row of pedicels (arrow in **A**) at different focal level. **C**, **D.** Left (**C**) and right (**D**) view of posterior segments 9-11 with two pairs of paradorsal sensory spots in segment 11, tube-like ventrolateral process in segment 1 (**C**) and row of pedicels (arrow in **D**) at different focal level. Scale bar in **C** 100 µm, valid for all photographs.

Tab. 1. Position of sensory spots and papillae in specimens of ***Semnoderes paucispinosus*** sp. nov. Characters with an intermediate position between reference positions are underlined and listed under the more dorsal position. Sensory spots with two pores except if mentioned otherwise (3).

Position Segment	mvm	vm	vl	lv	la	sl	ml	ld	sd	pd	md
Semnoderes sp. nov., AM # 5, holotypic ♀											
1							ssp		ssp (3)		
2		ssp					ssp			ssp ?	
3		ssp					ssp			ssp	
4		ssp				ssp	ssp			ssp	
5		ssp								ssp	
6		ssp				ssp				ssp	
7		ssp				ssp				ssp	
8		ssp			pa			ssp		ssp	
9		ssp ; pa				ssp	ssp (3)		ssp (3)	ssp	
10						ssp	ssp (3)		ssp (3)		
11					ssp					ssp ; ssp	
Semnoderes sp. nov., ZMB # 2, paratype											
1		ssp					ssp (3)		ssp (3)		
2				n. a.							
3		ssp		n. a.			ssp			ssp ?	
4		ssp		n. a.			ssp			ssp	
5				n. a.			ssp			ssp	
6		ssp		n. a.			ssp			ssp	
7		ssp		n. a.			ssp			n. a.	
8		ssp		n. a.			ssp			ssp	
9		ssp		n. a.			ssp (3)			ssp	
10				n. a.			ssp (3)				
11			ssp/pa							ssp ; ssp	
Semnoderes sp. nov., ZMB # 3, paratype											
1		ssp					ssp (3)		ssp (3)		
2		ssp?					ssp				
3		ssp				ssp	ssp			ssp	
4		ssp				ssp	ssp			ssp	
5		ssp ?				ssp ?	ssp			ssp ?	
6		ssp				ssp	ssp			ssp	
7		ssp				ssp		ssp		ssp ?	
8		ssp				ssp		ssp		ssp	
9		ssp				ssp (3); pa		ssp (3)		ssp	
10									ssp (3)		
11					ssp					ssp ; ssp	
Semnoderes sp. nov., ZMB # 4, paratype											
1		ssp					ssp (3)		ssp (3)		
2		n. a.				ssp					
3		n. a.					ssp			ssp	
4		n. a.					ssp			ssp	
5		n. a.					ssp			ssp ?	
6		n. a.				ssp	ssp			ssp	
7		ssp				ssp	ssp			ssp	
8		ssp				ssp	ssp			ssp	
9		ssp				ssp (3)		ssp (3)		ssp	
10						ssp (3)		ssp (3)			
11					pa					ssp ; ssp	

Tab. 2. *Semnoderes paucispinosus* sp. nov., morphological data of holotypic female and paratypic specimens (measurements in µm).

Specimen / **Character**	AM # 5, holotypic ♀ (dorsoventral mount)	ZMB # 2, paratype (dorsoventral mount)	ZMB # 3, paratype (dorsoventral mount)	ZMB # 4, paratype (lateral mount)
TL $_{mv / lat}$	357 / 388	402 / 439	435 / 504	n. a. / 359
s1 $_{mv / lat}$	42 / 60	/ 67	/ 75	n. a. / 69
s2 $_{mv / lat}$	n. a. / 12	30 / 21	26 / 33	n. a. / 30-31
s3 $_{mv / lat}$	32 / 26	34 / 40	32 / 37	n. a. / 36-40
s4 $_{mv / lat}$	30 / 30	33 / 42	37 / 40	n. a. / 41-44
s5 $_{mv / lat}$	36 / 31	37 / 46	40 / 43	n. a. / 43-45
s6 $_{mv / lat}$	43 / 41	46 / 42	40 / 45	n. a. / 45-51
s7 $_{mv / lat}$	46 / 44	42 / 46	43 / 44	n. a. / 52-55
s8 $_{mv / lat}$	46 / 47	47 / 51	46 / 49	n. a. / 52-55
s9 $_{mv / lat}$	53 / 56	46 / n. a.	48 / 49	n. a. / 52-54
s10 $_{mv / lat}$	34 / 40	34 / n. a.	37 / 41	n. a. / 38-46
s11 $_{lat}$	34	30	34	44-47
sw3	61	80	81	n. a.
sw4	74	96	94	n. a.
sw5	85	n. a.	101	n. a.
sw6	89	107	113	n. a.
sw7	97	106	113	n. a.
sw8	96	106	116	n. a.
sw9	85	97	101	n. a.
md1	27	33	28	30
md2	32	42	38	36
md3	36	55	48	43
md4	42	51	55	51
md5	43	59	64	57
md6	51	64	65	62
md7	51	64	59	67
md8	56	65	74	78
md9	63	85	85	88
md10	53	76	85	75
md11	371	290	341	329
mts	525	478	527	498
lv3 $_{le / ri}$	36 / 37	43 / 42	40 / 38	36 / 40
lv4 $_{le / ri}$	40 / 41	45 / 42	44 / 46	46 / 46
lv5 $_{le / ri}$	44 / 41	51 / 48	48 / 48	46 / 48
vl5 $_{le / ri}$	6 / 8	10 / 10	11 / 10	8 / 10
lv6 $_{le / ri}$	44 / 46	59 / 55	53 / 56	53 / 54
lv7 $_{le / ri}$	47 / 49	61 / 55	59 / 56	56 / 56
lv8 $_{le / ri}$	50 / 53	n. a. / 66	69 / 67	69 / 68
lv9 $_{le / ri}$	63 / 59	broken / 78	77 / 79	83 / 81
sl10 $_{le / ri}$	46 / 50	56 / 60	60 / 64	63 / 59
vl11 $_{le / ri}$	7 / n. a.	8 / 8	n. a. / n. a.	5 / n. a.
lts $_{le / ri}$	82 / 85	98 / 96	97 / 105	97 / 97
ltas $_{le / ri}$	124 / 124	190 / 186	182 / 181	182 / 186

Tab. 3. Comparison of selected characters of known species of ***Semnoderes***. + / — = character present / not present. Note that acicular and cuspidate spines of ***S. ponticus*** are just mentioned but not ordered according to their (unknown) correct lateral position. Autapomorphic characters are marked in bold and underlayn with grey background.

Species	***S. paucispinosus*** sp. nov.	***S. armiger*** Zelinka, 1928	***S. armiger*** Zelinka, 1928	***S. pacificus*** Higgins, 1967	***S. ponticus*** Bacescu & Bacescu, 1956
Location	Christmas Island, ndian Ocean	Gulf of Trieste, Mediterranean Sea	West coast, Sweden	New Caledonia	Romanian coast, Black Sea
Source of data	this paper	Zelinka 1928	Sørensen et al. 2009	Higgins 1967	Bacescu & Bacescu 1956; Bacescu 1968
specimens studied	1 ♀ / 3 specimens of unknown sex	1 ♀, 4 ♂	12 adults	1 ♂ / 1 ♀	?
Character					
TL_{lat}	388 / 359-504 µm	310-350 µm	372-500 µm	452 / 486 µm	450 µm
lateral spines: s1	—	—	—	10 / 10 µm	very small
s2	—	lvo: cu, ~ 25 µm	lv: cu, ~ 25 µm	lvo: cu, 27 / 27 µm	small
	—	lvi: ac, n. a.	vl: ac, ~ 12 µm	lvi: ac, 10 / 10 µm	—
s3	lv: ac, ~ 36 / 36-43 µm	lv: ac, 36 µm	lv: ac, ~ 36 µm	lv: ac, 28 / 28 µm	ac: small
s4	lv: ac, ~ 40 / 42-46 µm	lv: ac, ~ 41 µm	lv: ac, ~ 39 µm	lv: ac, 28 / 28 µm	ac
	—	—	—	—	**cu ?**
s5	lv: ac, ~ 42 / 46-51 µm	lvo: ac, 43 µm	lvo: ac, ~ 44 µm	lvo: ac, 28 / 30 µm	ac
	vl: **tu, ~ 7 / 8-11 µm**	lvi: cu, ~ 25 µm	lvi: cu, ~ 28 µm	lvi: cu, 28 / 30 µm	cu
s6	—	lvo: cu, ~ 25 µm	lvo: cu, ~ 28 µm	—	cu
	lv: ac, ~ 45 / 53-59 µm	lvi: ac, ~ 44 µm	lvi: ac, ~ 48 µm	lv: ac, 28 / 35 µm	ac
s7	lv: ac, ~ 48 / 55-61 µm	lv: ac, ~ 48 µm	lv: ac, ~ 51 µm	lv: ac, 28 / 35 µm	ac
s8	—	lvo: cu, ~ 25 µm	lvo: cu, ~ 28 µm	lvo: cu, 26 /33 µm	cu
	lv: ac, ~ 51 / 66-69 µm	lvi: ac, 50 µm	lvi: ac, ~ 50 µm	lvi: ac, 26 / 33 µm	ac
s9	lv: ac, ~ 61 / 77-83 µm	lvo: ac, ~ 51 µm	lvo: ac, ~ 54 µm	lvo: ac, 29 / 33 µm	ac
	—	lvi: cu, ~ 25 µm	lvi: cu, ~ 31 µm	lvi: cu, 29 / 33 µm	cu
s10	**sl**: ac, ~ 48 / 56-64 µm	lv: ac, ~ 52 µm	lv: ac, ~ 57 µm	lv: ac, 33 / 53 µm	ac
s11	vl: **tu, ~ 7 / 5-8 µm**	—	—	—	—
	lts: ac, ~ 83 / 96-105 µm	lts: ac, 79-93 µm	lts: ac, 73-103 µm	lts: ac, 56 / 45 µm	lts: ac
	ltas: ac, 124 / 181-190 µm	ltas: ac, 130-154 µm	ltas: ac, 121-153 µm	ltas: ac, 120 / 126 µm	ltas: ac
sw5	85 / 101 µm	93 µm	56 µm	n. a.	n. a.
sw7	97 / 59-67 µm	100 µm	n. a.	n. a.	n. a.
md1-9	+	+	+	+	+
md10	53 / 75-85 µm	70 / 34 µm	59-80 µm	74 / 78 µm	+
md11	371 / 290-341 µm	175 / 189 µm	133-199 µm	79 µm / broken	+
mts	525 / 478-527 µm	430-546 µm	466-644 µm	420 µm / broken	520 µm
papillae	♀: la 8 and vm 9; 1 specimen: sl 9	n. a.	♀: vl 8 and vm 9	n. a.	n. a.

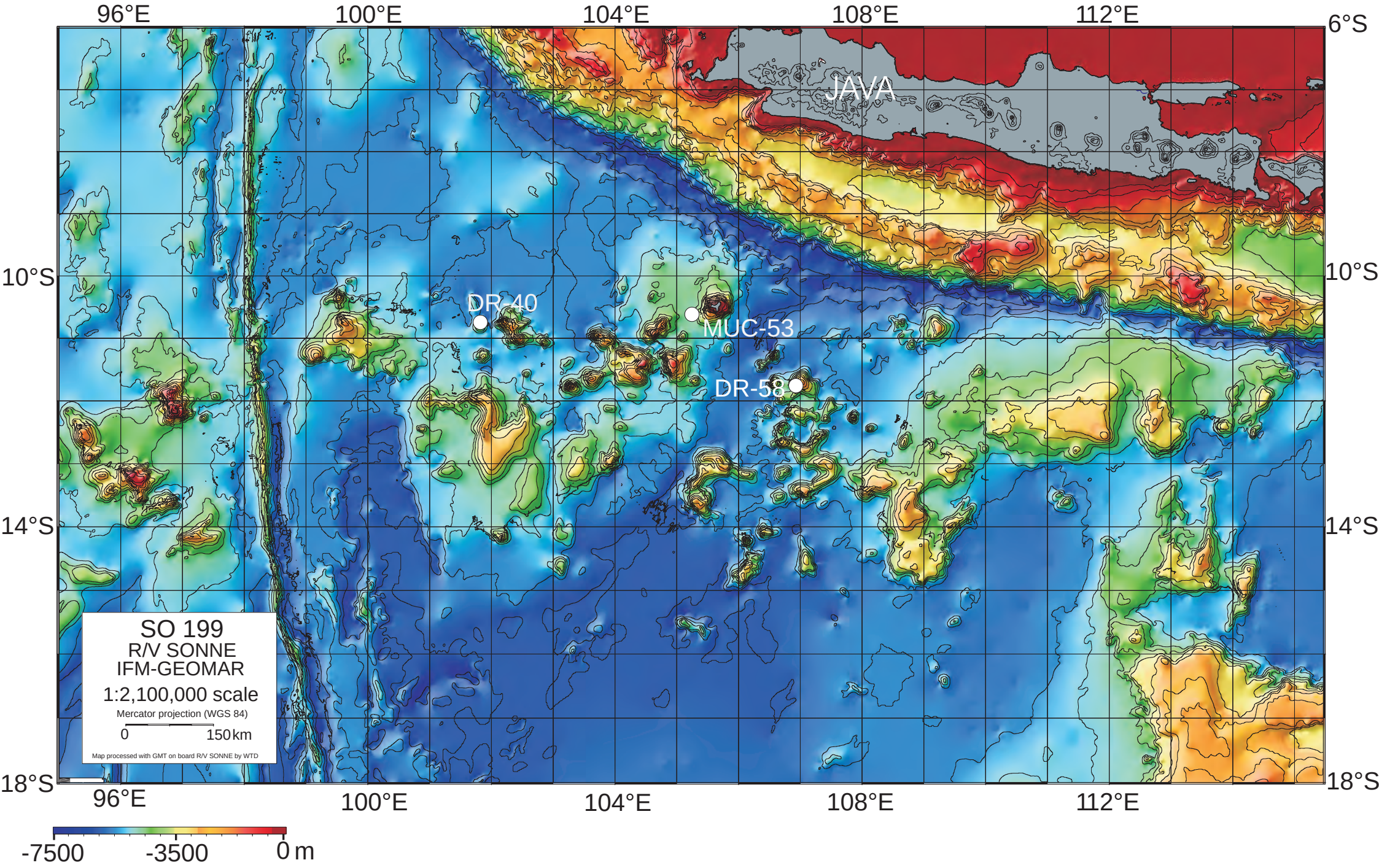

Semnoderes paucispinosus sp. nov.: **Fig. 1.**

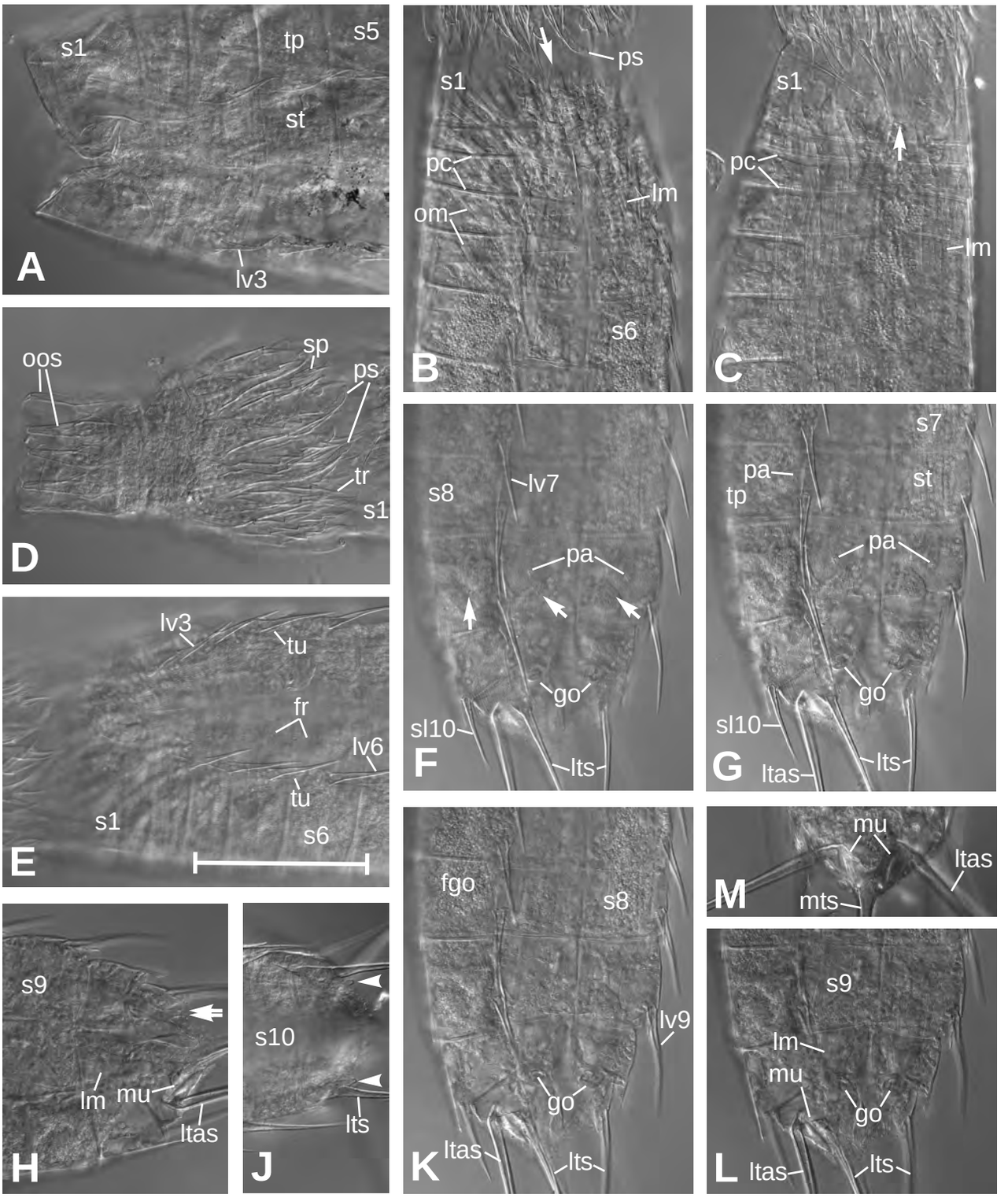

Semnoderes paucispinosus sp. nov:
Fig. 2 A-M.

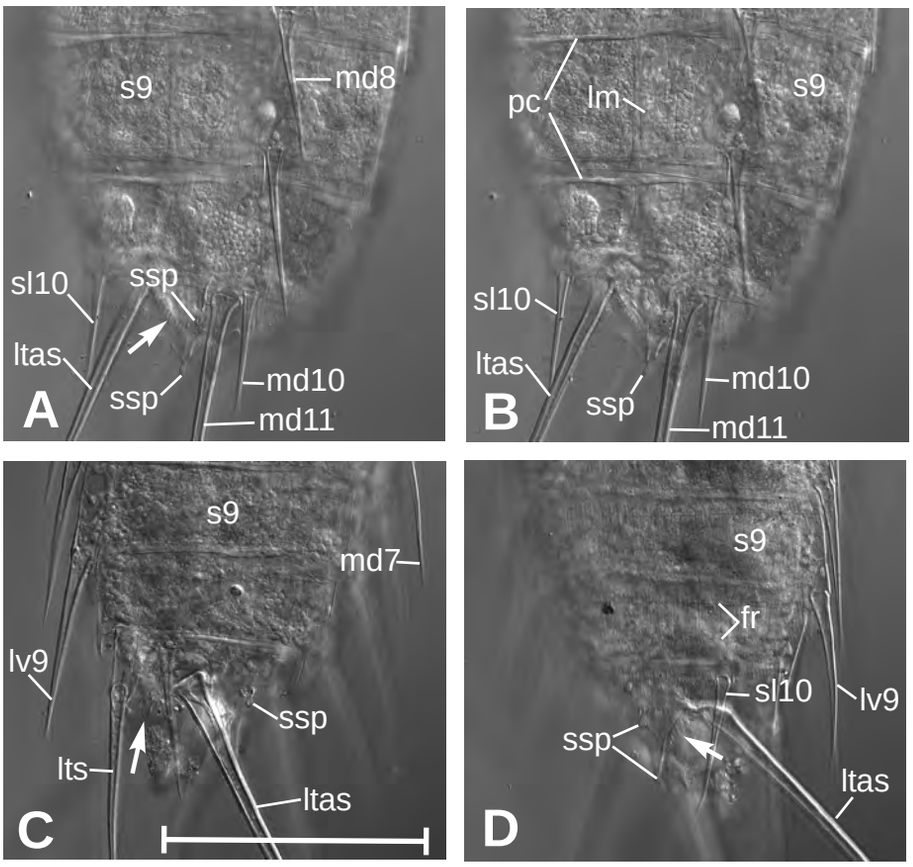

Semnoderes paucispinosus sp. nov: Fig. 3 A-D.

Anlage 5

BSH · Neptunallee 5 · 18057 Rostock

Dr. Reinhard Werner
IFM-GEOMAR
Wischhofstr. 1-3
24148 Kiel

BUNDESAMT FÜR
SEESCHIFFFAHRT
UND
HYDROGRAPHIE

Dienstsitz Rostock

Bathymetriedaten der Reisen SO199/1, SO199/2, SO201/1B, SO208 - Datenabgabe an das BSH

Datum
14.10.2010

Durchwahl
+ 49 (0) 381 4563 - 604

Aktenzeichen
(bitte bei Antwort angeben)
3127 / 2010 N1130

Sehr geehrter Herr Dr. Werner,

vielen Dank für die Abgabe der bathymetrischen Daten der Reisen SO199/1, SO199/2, SO201/1B und SO208 an das Bathymetrische Datenzentrum im BSH. Bitte nehmen Sie dieses Anschreiben zum Nachweis gegenüber dem Projektträger Forschungszentrum Jülich zu Ihren Unterlagen.

Mit freundlichen Grüßen,

Volkmar Leimer

Neptunallee 5
18057 Rostock
Tel.: + 49 (0) 381 4563 – 5
Fax: + 49 (0) 381 4563 – 948
posteingang@bsh.de
www.bsh.de

Bankverbindung:
Bundeskasse Kiel
zugunsten BSH
Deutsche Bundesbank
BLZ 210 000 00
Kto.-Nr. 210 010 30

IBAN:
DE42 2100 0000 0021 0010 30
BIC: MARKDEF1210

Von: datenmanagement@ifm-geomar.de
Betreff: Re: SO199_Stationsliste_fuer_Pangaea
Datum: 13. Januar 2011 12:58:25 MEZ
An: rwerner@ifm-geomar.de, khoernle@ifm-geomar.de

Sehr geehrte Fahrtleiter,

die Stationen der Fahrt SO199 sind importiert und sichtbar unter https://portal.ifm-geomar.de/group/ifm-geomar/metadata.
Bitte die Angaben kontrollieren und gegebenenfalls korrigieren.

Die Stationen sind ebenfalls in PANGAEA importiert:
http://www.pangaea.de/ddi?retr=events/Sonne/SO199.retr&conf=events/CruiseReportHTML.conf&format=html

Viele Grüße, Hela Mehrtens

--
-Datenmanagement-
Carsten Schirnick, Pina Springer, Dirk Fleischer, Hela Mehrtens

Leibniz-Institut für Meereswissenschaften (IFM-GEOMAR)

Büro Westufer: Raum 063
Büro Ostufer: 8D/213

Tel: +49 431 600 4025
E-Mail: datenmanagement@ifm-geomar.de